# DESIGN AND SYNTHESIS OF TERPYRIDINE BASED METALLO-SUPRAMOLECULAR ARCHITECTURES

A Dissertation

Presented to

The Graduate Faculty of The University of Akron

In Partial Fulfillment

of the Requirements for the Degree

Doctor of Philosophy

James M. Ludlow III

December, 2015

DESIGN AND SYNTHESIS OF TERPYRIDINE BASED

METALLO-SUPRAMOLECULAR

ARCHITECTURES

James M. Ludlow III

Dissertation

Approved:

_____
Advisor
Dr. George R. Newkome

_____
Committee Member
Dr. Chrys Wesedmiotis

_____
Committee Member
Dr. Stephen Z. D. Cheng

_____
Committee Member
Dr. Abraham Joy

_____
Committee Member
Dr. Claire A. Tessier

Accepted:

_____
Department Chair
Dr. Coleen Pugh

_____
Dean of the College
Dr. Eric J. Amis

_____
Dean of the Graduate School
Dr. Chand Midha

_____
Date

ABSTRACT

In the field of metallo-supramolecular chemistry, the *N*-heteroaromatic ligand, [2,2':6',2"] terpyridine (tpy), has received considerable attention due in part to its ability to coordinate with a wide variety of transition metals; this has enabled a range of bonding strengths, properties, and molecular architectures. A variety of strategies have been employed with <tpy-$M^{II}$-tpy>-based architectures including the use of triangle-based frameworks, flexible ligands, and harnessing of additional non-covalent forces to enhance self-assembly. To achieve three-dimensional architectures, new strategies include use of *meta*-substitution, multi-planar vertices, flexible vertices, and by restricting availability of planar conformations *via* precoordination or predesigned steric hindrance. There is also increasing focus on interconversions between supramolecular structures in response to reaction conditions and on hierarchical self-assembly.

Flexible, multitopic ligands can introduce new structural possibilities, allowing for intramolecular interactions and more adaptive systems to arise. When the semi-flexible 1,2-*bis*[4'-(4-ethynylphenyl)-2,2':6',2"-terpyridyl]-*o*-carborane is self-assembled under kinetic control, *via* formation of $Fe^{II}$ complexes, the main cyclic product is triangular (trimer). However, under thermodynamic control, using labile transition metals, *e.g.* $Zn^{II}$, the cyclic trimer is in dynamic equilibrium with a cyclic dimer, and with adequate entropic driving force the cyclic dimer is obtained exclusively.

The combination of flexible crown ethers possessing a trio of rigid, $60^{\circ}$ ligands allows for construction of a 3D structure (tetrahedron) under thermodynamic control.

Formation of the tetrahedron is facilitated by intramolecular, π-π interactions. Structural confirmation utilized 1D and 2D NMR, and electrospray ionization mass spectrometry coupled with travelling wave ion mobility (ESI-TWIM-MS). $^{19}F$ NMR experiments support presence of guest host interactions between anions and the supramolecular cavity.

One step synthesis of the first homoleptic <tpy-$Os^{II}$-tpy> metallomacrocycle was reported and characterized *via* NMR, ESI-MS, TWIM-MS, and UV-vis alongside its $Fe^{II}$ and $Ru^{II}$ analogues. Gradient tandem-MS was used to derive center-of-mass collision energies and revealed unexpectedly that the order of stability of the <tpy-$M^{II}$-tpy> complexes was $M^{II}$ = Ru > Os > Fe.

Toward hierarchical ordering of supramolecular materials, the effect of molecular geometry and amphiphilicity on the ability of self-assembled metallosupramolecular macrocycles to self-order was studied. Conversion of <tpy-$M^{II}$-tpy> macrocycles into directional amphiphiles enhanced ordering characteristics, enabling the formation of nanoscale structures.

DEDICATION

To Ety, Preston, and Mom

# ACKNOWLEDGMENTS

I would like to thank Professor George R. Newkome for the opportunity to work in his group and to benefit from his knowledge of chemistry and scientific research. I also appreciate the help and support of Dr. Charles N. Moorefield. I would like to thank my committee members: Professor Chrys Wesdemiotis, Professor Stephen Z. D. Cheng, Professor Abraham Joy, and Professor Claire A. Tessier for their time and suggestions. Thank you also to my fellow group members and colleagues for their valuable assistance in this research. Mass spectrometry was conducted by Kai Guo and Zaihong Guo; transmission electron microscopy by Dr. M. J. Saunders, electron diffraction by Mingjun Huang, atomic force microscopy by Gustavo Guzman; and diffusion-ordered spectroscopy by Chun Gao. Dr. Nicholas Johnson and Benjamin Thome assisted with variable temperature NMR. I appreciate the support of family and friends, most notably my grandmothers, Jane and Helen, my wife, Ety, and my son Preston for all the joy he brings.

TABLE OF CONTENTS

Page

LIST OF TABLES

LIST OF FIGURES

LIST OF SCHEMES

# CHAPTER I

# RECENT PROGRESS IN TERPYRIDINE-BASED METALLO-SUPRAMOLECULAR ARCHITECTURES

## 1.1 Introduction

If modern synthetic chemistry has a muse, it is almost certainly Mother Nature. When her secrets are revealed, it always stirs the imaginations and flasks of chemists around the globe. The concept of covalent macromolecules arose in large part, from the study of natural polymers, such as: starch, cellulose, and rubber.[1] An entire industry and a changed world have resulted from those insights. Around the time that Staudinger was being awarded the Nobel Prize for the macromolecular hypothesis,[2] the work of Watson, Crick, Franklin, and Wilkins[3, 4] highlighted the importance of non-covalent interactions including hydrogen bonding in structure and function of biological macromolecular systems, such as DNA. In a more recent example, thanks to advances in the fields of electron microscopy, spectroscopy, and crystallography, we are now gleaning insight into the molecular and supramolecular structures of photosystem[5] and the plethora of non-covalent interactions at play in the organization of the proteins, pigments, and biocatalysts that enable the process of photosynthesis.

The use of non-covalent interactions in chemical synthesis is known a supramolecular chemistry.[6] The genesis of this field resides within the crown ether work

of Pederson[7] followed by Cram[8] and Lehn[9] in the areas of guest-host and metal-ligand assemblies, respectively. A variety of forces has been employed within supramolecular chemistry including hydrogen bonding[10-12] and hydrophobic/hydrophilic.[13-17] Metal-ligand coordination driven self-assembly or metallosupramolecular chemistry has been utilized to construct a wide variety of structures by groups such as Lehn,[18-21] Fujita,[22-25] Stang,[26-29] Schmittel,[30-32] and Newkome.[33-36] The tridentate *N*-heteroaromatic ligand [2,2':6,2"]terpyridine (tpy) has been prominently featured in this arena. It was first reported[37] by Morgan and Burstall almost a century ago. Since then the one-step Kröhnke synthesis[38] from aromatic aldehydes gave access to a more efficient synthesis of terpyridine containing building blocks. More recently, the use of Suzuki[39] and Sonogashira[40] coupling methods has enabled facile synthesis of multitopic ligands[41] using a wider variety of core/vertex reagents including adamantane,[42] anthracene,[43] spirane,[44] and cavitands.[45] A pair of terpyridines coordinated with an appropriate transition metal generates a pseudo-octahedral coordination complex[46] with predictable geometry, allowing formation of predesigned structures.[47] This methodology has been termed the directional bonding approach.[48] Such ligands have been used to synthesize more elaborate architectures and develop new strategies. Examples of these structures include metallodendrimers,[49-52] macrocycles,[34, 36, 53-55] racks,[56, 57] and grids,[58-60] and cages.[61-63] Mass spectrometry (MS) has improved to replace single-crystal X-ray and today it plays an essential role in structural and chemical characterization of suprametallomolecular strucutures[64] *via* the soft ionization techniques electrospray ionization (ESI)[65] and matrix-assisted laser desorption ionization (MALDI)[66, 67] in tandem with travelling wave ion mobility (TWIM). A variety of applications has been

envisioned for terpyridine-based materials[68] in the areas of solar energy,[69-71] light emitting diodes (LEDs),[72-74] catalysis,[75-78] optoelectronics,[79, 80] sensors,[81-84] and life science applications, such as DNA binding and anti-cancer therapies.[85,86, 87] Accordingly, there has been strong emphasis upon transitioning toward the material sciences with a recent focus on moving from discreet supramolecular assemblies toward higher order structures or materials.[88]

This introductory chapter will review recent progress in the areas of terpyridine-based suprametallomolecular macrocycles, 3D structures, supramolecular interconversions, hierarchical self-assembly toward materials, and monolayer molecular sheet structures.

## 1.2 Macrocycles

An emerging theme is the use of 60° angles to construct new architectures. The structural and kinetic favorability of triangular-based systems has been harnessed, through use of multitopic 60°-based ligands to introduce a rigid framework upon which large and intricate architectures can be built.

Lu *et al.* elegantly demonstrated the utility of 60°-based systems to produce high yielding, uniform, predictable architectures with a multicomponent system (Figure 1.1). The 1:1:2 combination of *ortho* (60°) ligand **1** with *meta* (120°), ligand **2** *bis*terpyridines, with $Zn^{II}$ or $Cd^{II}$ gave a mixture of triangle **4**, rhombus **5**, and polygons of 120° directionality; however, replacement of the 120° ligand with a *tris* ligand **3** quantitatively gave the desired bridged rhombus **6**.[89] Thus, the utilization of a fully triangular-based structure provided a noteworthy synthetic enhancement.

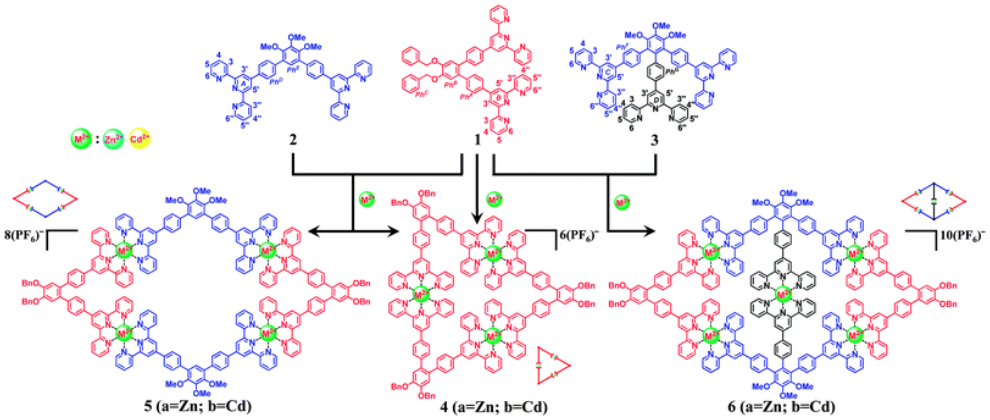


Figure 1.1 – Synthesis of rhomboid **5**, triangle **4**, and bridged rhomboid **6** from a combination of directional ligands **1**, **2**, and **3**.

Wang *et al.* demonstrated the use of 60°-based geometry to build a larger, 2D structure with a multicomponent coordination-driven self-assembly of the first terpyridine-based, shape-persistent, giant two-dimensional $D_{6h}$ supramacromolecular spoked wheel (Figure 1.2). Mixing a core hexa*kis*ligand **7**, with the aformentioned *tris* ligand **3**, and $Zn^{II}$ or $Cd^{II}$ ions in a stoichiometric ratio (1:6:12) permitted the selective generation of a highly symmetric spoked wheel **8** in 94% isolated yield *via* geometric and thermodynamic control. The products were characterized by a combination of TWIM-MS and NMR techniques together with transmission electron microscopy (TEM), which agreed with molecular modeling.[90]

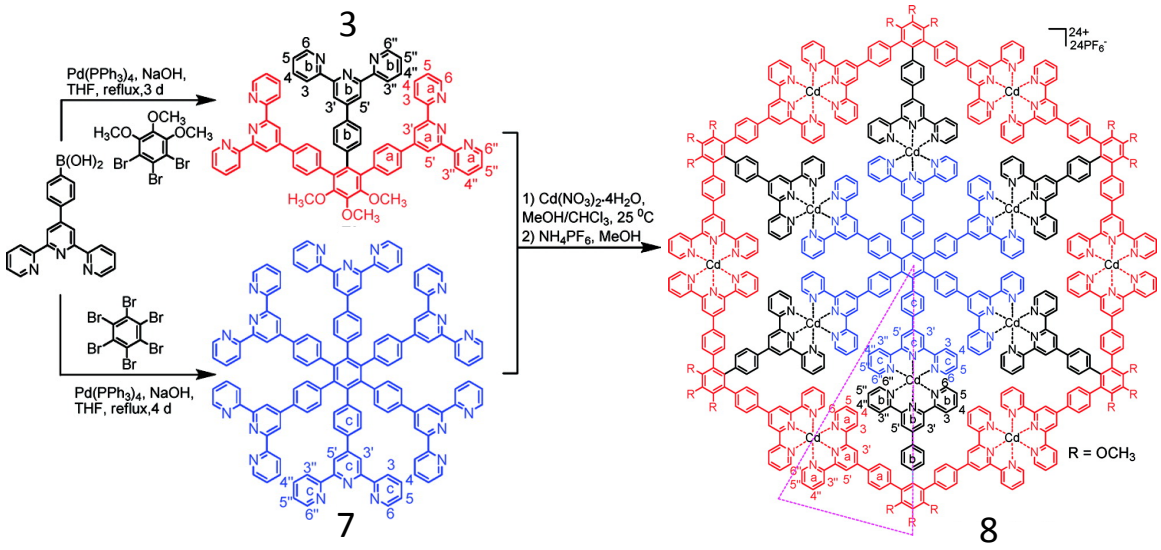


Figure 1.2 – Synthesis of *tris*ligand **3** and hexa*kis*ligand **7** *via* Suzuki coupling and their subsequent, multicomponent self-assembly into a spoked wheel **8** under thermodynamic control with $Cd^{II}$. [Modified with permission of the American Chemical Society: *J. Am. Chem. Soc.* **2011**, *133*, 11450-11453]

<Tpy-$M^{II}$-tpy>-based fractal architectures have been previously reported using a stepwise approach[34] with non-labile metals. More recently, using a multicomponent approach under thermodynamic control, a first-generation Sierpiński triangle mimic was self-assembled by Sarkar *et al*. with <tpy-$Cd^{II}$-tpy> connectivity. The *bis* ligand **9** was used with tetra*kis*ligand **10**, also with 60° directionality, synthesized *via* Suzuki cross-coupling, and $Cd^{II}$ at a stoichiometric ratio of 1:1:3. Near quantitative yield of **11** was achieved and characterization was accomplished by NMR, TWIM-MS, and TEM.[91]

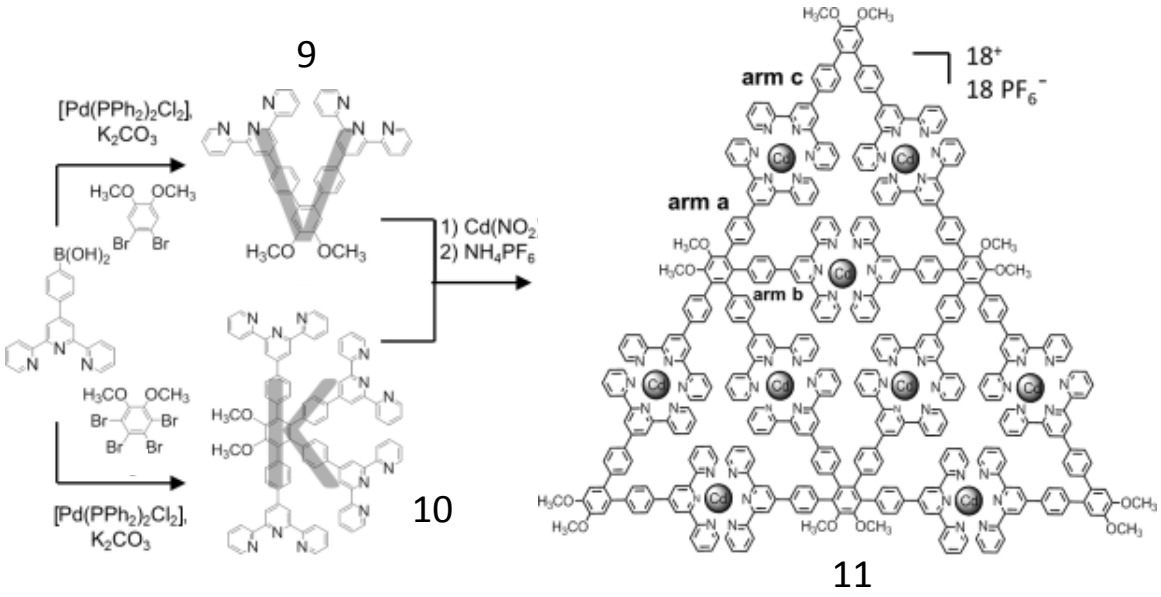


Figure 1.3 – Synthesis of *bis*ligand **9** and tetra*kis*ligand **10** *via* Suzuki coupling and their subsequent multicomponent assembly to a Sierpinski triangle **11** using $Cd^{II}$. [Modified with permission of Wiley: *Angew. Chem. Int. Ed.,* **2014***, 53,* 12182-12185.]

Precoordination strategies have been previously used to make <tpy-$M^{II}$-tpy>-based hexameric structures.[92, 93] Triangular geometry was also employed by Schultz *et al*. in stepwise assembly of two novel heterometallic, macromolecular constitutional isomers *via* this approach. The 60° ligand **12** was used to precoordinate a non-labile <tpy-$Ru^{II}$-tpy> bond within dimer **13**. Used in combination with the appropriate tetra*kis*ligand **14** or **15** and labile <tpy-$Zn^{II}$-tpy> connectivity, both the molecular bowtie **16** as well as butterfly **17** were synthesized. Precoordination of the dimer **13** restricted possible outcomes, preventing formation of triangular side product, to give the desired structures in high yield. The isomers were characterized by ESI-MS, TWIM-MS, and NMR. As shown in Figure 1.4, these structural isomers have remarkably different experimental collision cross sections, as determined by TWIM at low charge state (4+),

but negligible difference at higher charge states (5+ to 7+) indicating different sizes and shapes at high charge states. It needs to be noted that these constitutional isomers, and the *bis*rhombus are substructures of the aforementioned spoked wheel architecture.[35]

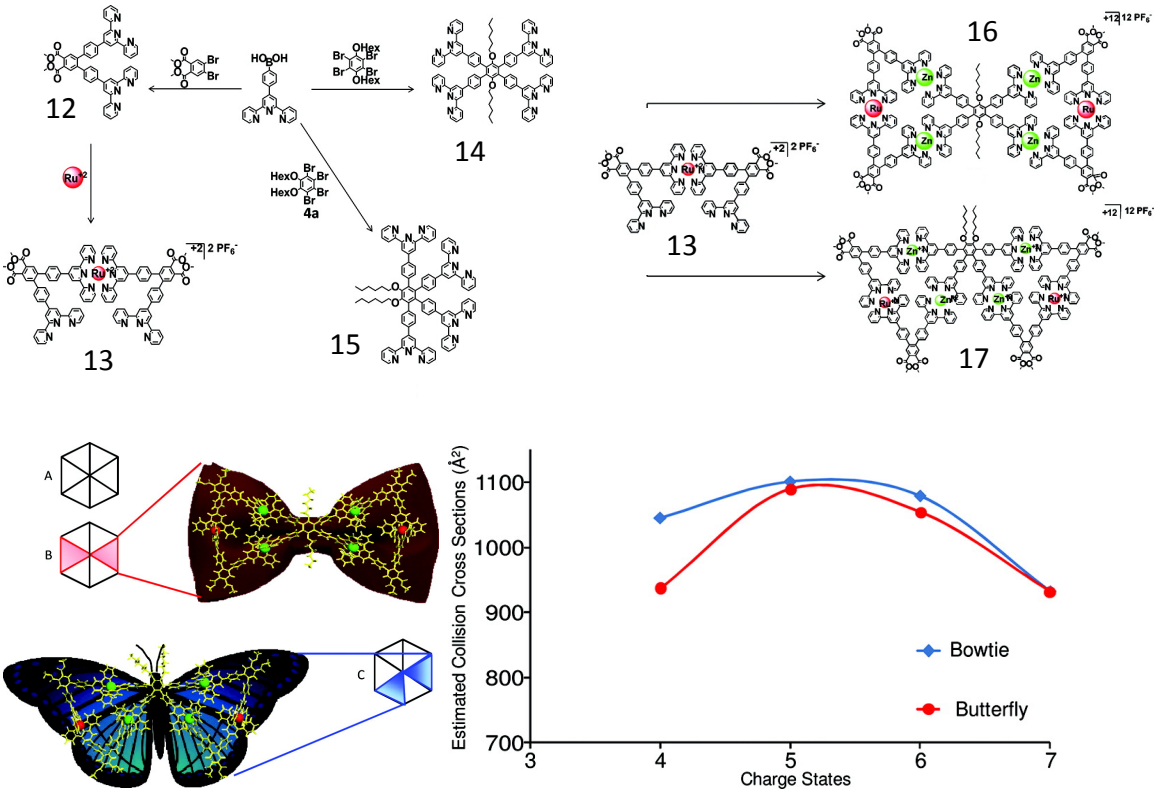


Figure 1.4 – Multicomponent synthesis using precoordinated $Ru^{II}$ with tetra*kis*ligands **14** or **15** to form bowtie **16** or butterfly **17** motifs. Experimental collisional cross sections of each as a function of charge state. [Modified with permission of the American Chemical Society: *J. Am. Chem. Soc.* **2012,** *134*, 7672-7675.]

Asymmetric 60°-based ligands have recently been studied as well. Three different ligands were synthesized with varying phenylene spacer lengths (**18** - **20**). Their self-assembly processes were found to be strongly dependent on the ligand geometry. Using labile <tpy-$Zn^{II}$-tpy>-connectivity, the authors found that one structure, 2,4''-di(4'-terpyridinyl)-1,1':4',1''-terphenyl (**19**) underwent self-selection to give a trinuclear metallomacrocycle with perfect heteroleptic connectivity (**21**); while **18** and **20** each afforded a mixture of constitutional isomers. Note that **19** has the most pronounced difference in arm length. These structures were characterized by NMR, ESI MS, and single-crystal X-ray diffraction. In particular, the identification of an isomeric architecture was accomplished using tandem mass spectrometry ($MS^2$) coupled with TWIM-MS.[94]

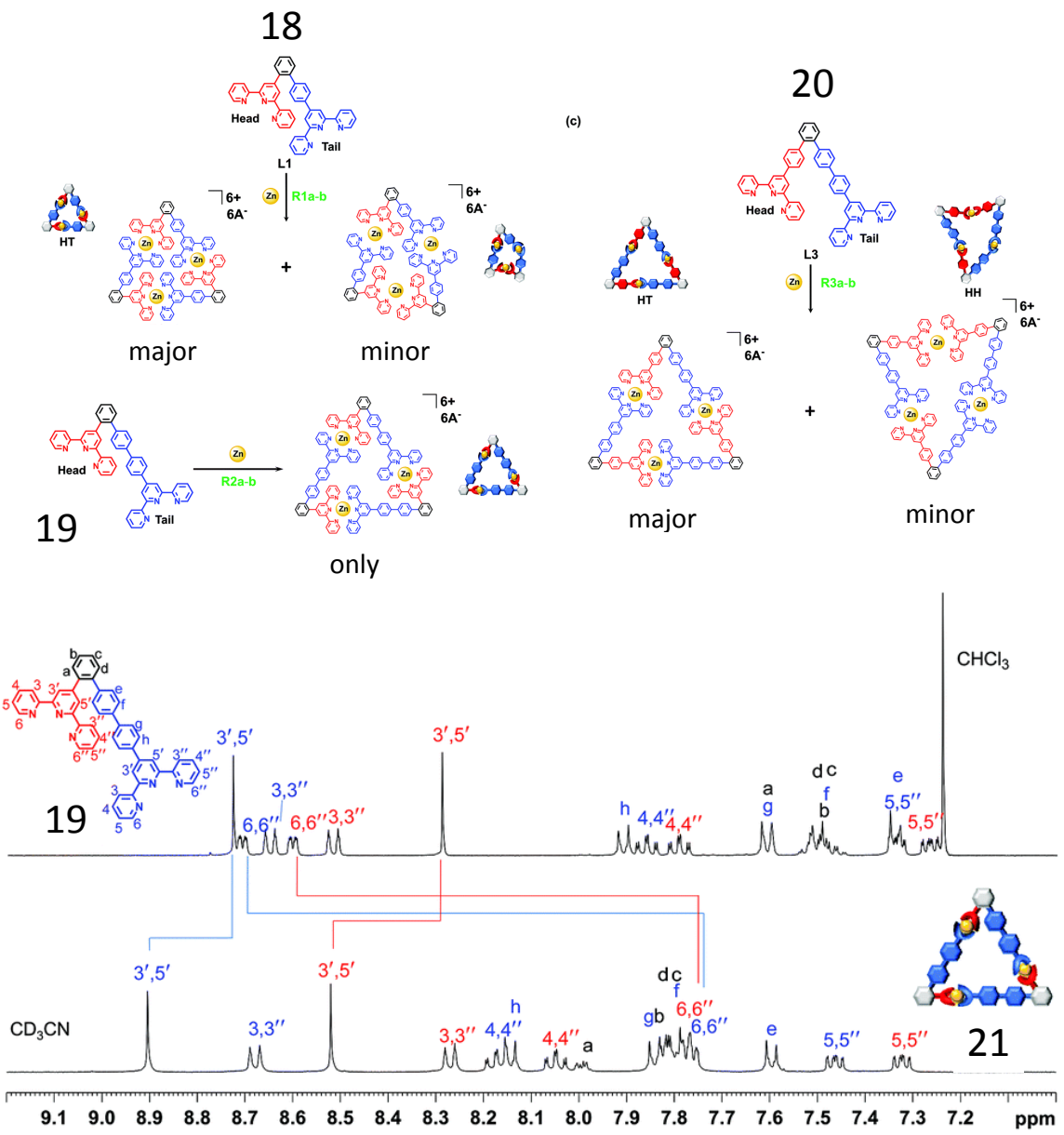


Figure 1.5 – Self-assembly of asymmetric 60° ligands **18**, **19**, and **20** using $Zn^{II}$. While **18** and **20** gave mixtures, **19** gave quantitative head to tail connectivity. $^{1}H$ NMR spectra of **19** before complexation and of triangle **21**. [Modified with permission from the Royal Society of Chemistry: *Dalton Trans.*, **2015**, *44*, 5139-5145.]

A unique, one-step approach to achieving an intricate structure without the use of 60°-based system was demonstrated by the Li group.[95] While self-assembly of 120°-based ligands with labile metals in a single step typically afforded mixtures of macrocycles of varying size (n = 5 through 9) instead of a single hexagon;[96] as shown in Figure 1.6, this was overcome through design and self-assembly from tritopic (**22**) and tetratopic (**23**) 120° tpy ligands with $Zn^{II}$. This increased the total number of coordination sites and instilled high geometric constraints to induce the formation of discrete structures. Using this approach, a strategy referred to as density-of-coordination (DOC), two supramolecular hexagonal wreaths or ring-in-ring structures **24** [$Zn_9$**22**$_6$] and **25** [$Zn_{12}$**23**$_6$] were generated. These structures exhibited fractal geometry and the shapes, sizes, and structures were fully characterized by NMR, ESI-MS, TWIM-MS, and TEM. With diameters around 5.5 nm for **24** and 5.8 nm for **25**, the remarkable rigidity of these fractal architectures was supported by TWIM-MS, contrasting with the high flexibility of macrocycles assembled by ditopic tpy ligands.[97] This successfully demonstrates discrete assembly, under thermodynamic control, of a ligand with 120° directionality. Notably, embedded non-labile hexamers have been reported before but *via* multistep assembly involving a template Grubbs' metathesis to form the outer cycles[98] in which the outer bonds are all covalent.

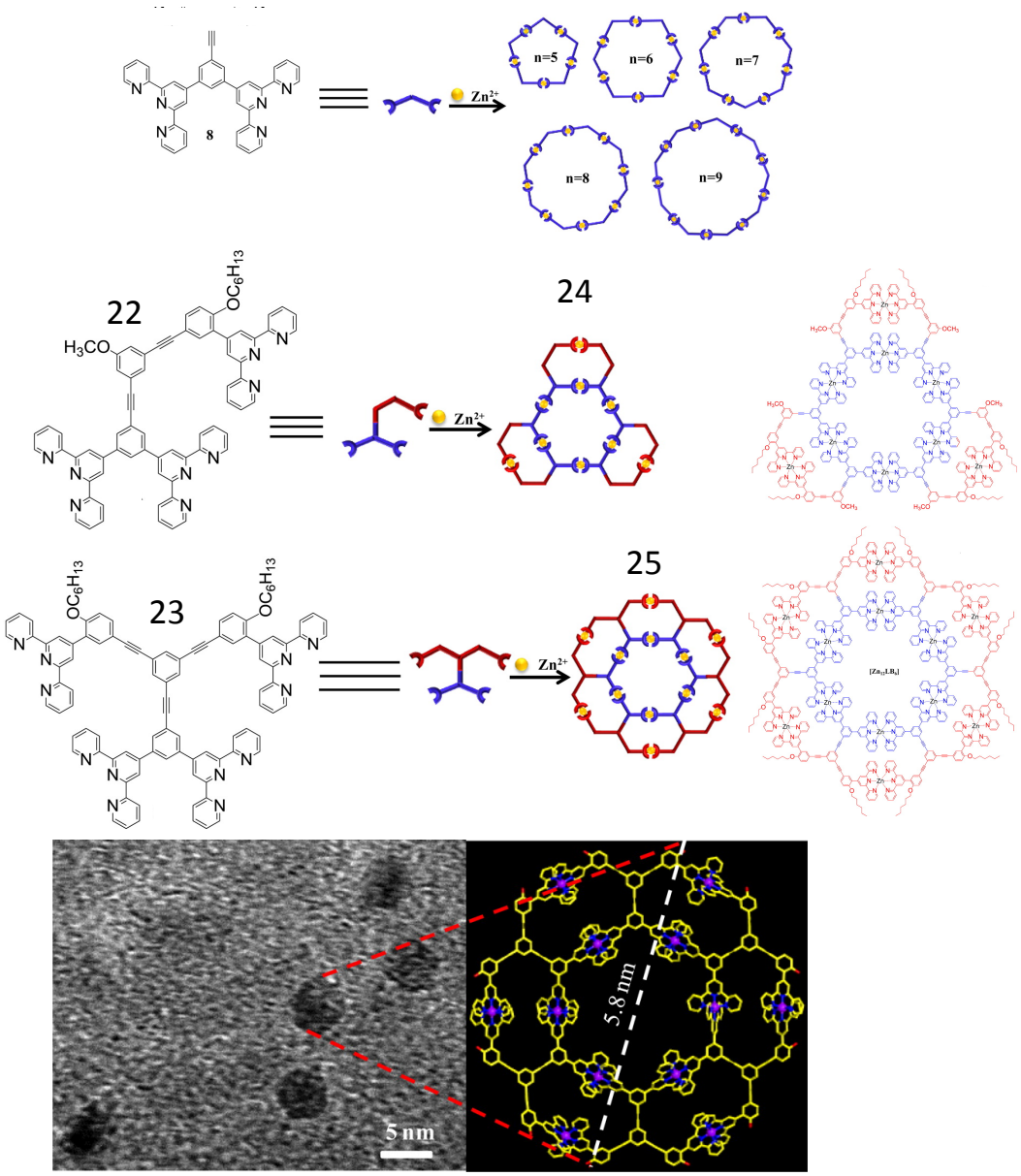


Figure 1.6 – Self-assembly of 120° ligand under thermodynamic control yields a mixture of macrocycles (top). A multi-step Sonogashira coupling was used to synthesize ligands **22** and **23**. Synthesis of wreath **24** using *tris*ligand **22** and synthesis of a wreath **25** using tetra*kis*ligand **23** both give single products and demonstrate the DOC strategy. TEM and molecular model dimensions of **25** (bottom) match well. [Modified with permission of the American Chemical Society: *J. Am. Chem. Soc.* **2014,** *136*, 6664-6671.]

Recently, enhanced formation of macrocycles was demonstrated by modified ligand solubility and incorporation of additional, non-covalent interactions, such as hydrogen bonding. Previously, carbazole-based *bis*terpyridine ligands with 105° bite angle have been complexed with non-labile $M^{II}$ and shown to form pentamers which could be isolated chromatographically.[99] Recently, metallacycles were constructed from such ligands using labile $Zn^{II}$ connectivity[100] to gauge the effects of solubility and hydrogen bonding on assembly. Two ligands, a parent carbazole (**26**) R = H, and an *N*-alkylated carbazole (**27**) R = $C_{12}$ were compared. Clean formation of pentagonal metallacycle **28** was observed for the N−H ligand; whereas, analogous attempts to assemble the dodecyl variant with $Zn^{II}$ ions resulted in a mixture of products. Although increased solubility is typically useful for self-assembly; in this case, the pentagonal metallacycle was rationalized as a kinetic product, and the lack of hydrogen bonding for the dodecyl-functionalized species enhanced solubilities and therefore assisted in the formation of equilibrium mixtures. The emission of the N−H metallacycle was centered at 401 nm, tailing out to 450 nm in THF. When MeCN was used, an excitation-dependent behavior was observed, with a growth of a shoulder peak at 459 nm, due to stabilization of an intraligand charge transfer state by the more polar solvent.

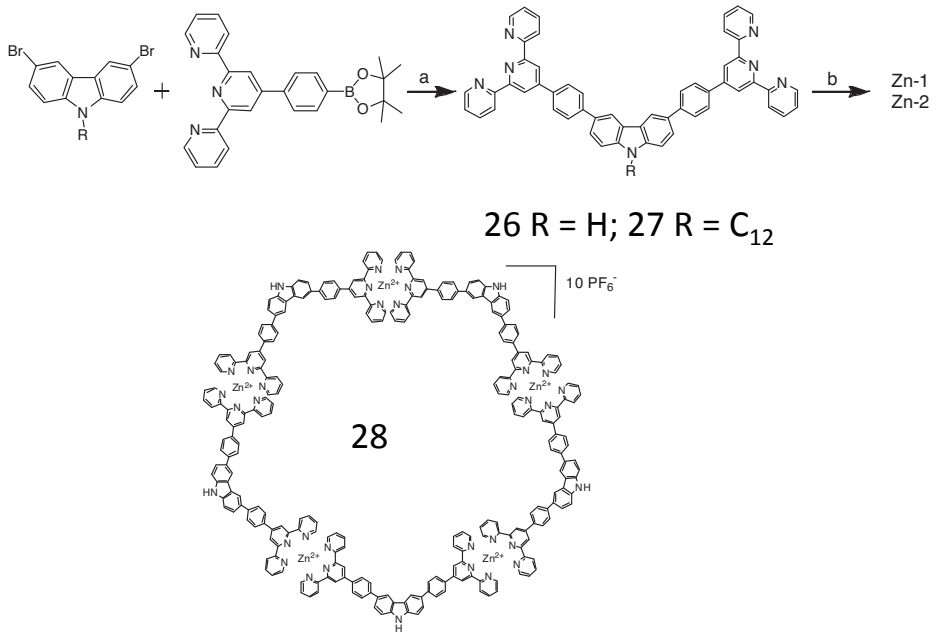


Figure 1.7 – Synthesis of **28** (R = H) from ligand **26** using $Zn^{II}$**.** Ligand **27** gave a mixture. **26** and **27** were synthesized using a) Suzuki coupling [$Pd(PPh_3)_4$]. Self-assembly conditions b) NMP, 100°C, 48 h. [Modified with permission of Wiley: *Macromol. Chem. Phys.*, **2014**, *215*, 753-762.]

A general distinction in design and synthesis of metallosupramolecular architectures has been corner *vs.* edge metal location.[42, 43, 101] In recent work[102, 103] combining these two approaches, a ligand containing a terpyridyl donor on one end and a 3-pyridyl donor on the other was used to form metalloligand **29** *via* precoordination of $Fe^{II}$ or $Ru^{II}$, as <tpy-$M^{II}$-tpy>. The resultant metalloligand **29** was subsequently self-assembled with $Pd^{II}$ using the terminal pyridines to form the hexanuclear triangle **30**. Photophysical and electrochemical properties of the multicomponent architecture were evaluated.

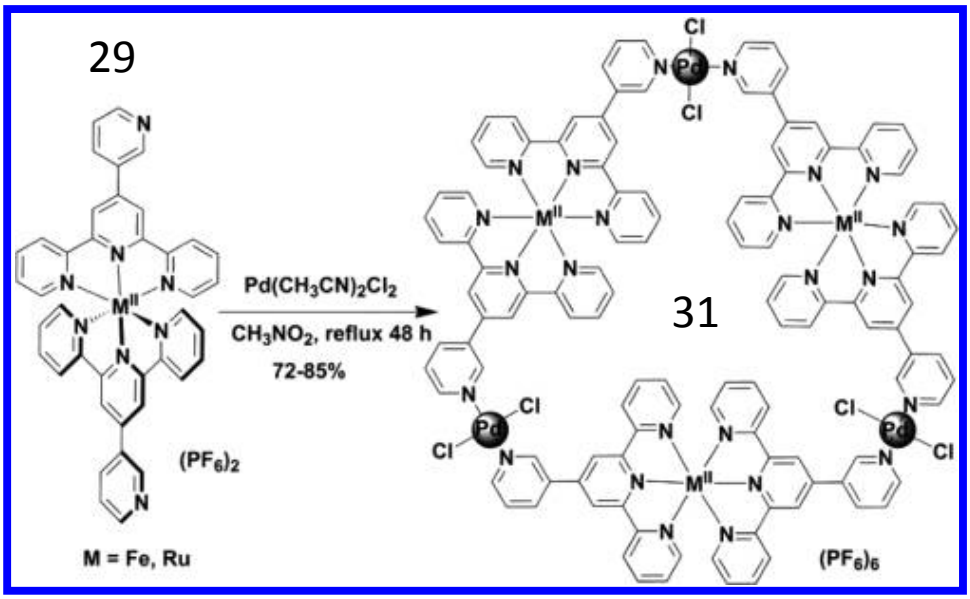


Figure 1.8 – Self-assembly of heterometallic Pd/Fe and Pd/Ru macrocycles *via* precoordination to form **29(M)** followed by self-assembly to the trimeric **30(M, Pd)**. [Modified with permission of the Royal Society of Chemistry: *RSC Adv.*, **2014**, *4*, 21262 - 21266.]

Similarly, as shown in Figure 1.9, self-assembly of metalloligands **31**(M), (M = Zn, Ni or Cu) with a terminal 4-pyridyl moiety, and half-sandwich organometallic units **32**(M), $[Cp^*_2M_2(\mu\text{-DHNA})Cl_2]$ (where M = Ir and Rh; Cp* = $\eta^5$-pentamethylcyclopentadienyl; DHNA = 6,11-dihydroxy-5,12-naphthacenedione) was used to form a series of [4+2] hexanuclear heterometallic macrocycles **33** containing box-like cavities. Structures were confirmed by single-crystal X-ray analysis. Interestingly, complexes with corner M = Ir encapsulated a triflate counterion in each cavity. In the other complexes, all counteranions were outside of the cavities.[104] Though not noted by the authors, $^1$H NMR spectra of the complexes indicate that the

5,5" tpy-*H*s shift to <7ppm, an effect which has been noted in structures with proximate or stacked <tpy-$M^{II}$-tpy> complexes. [62, 105]

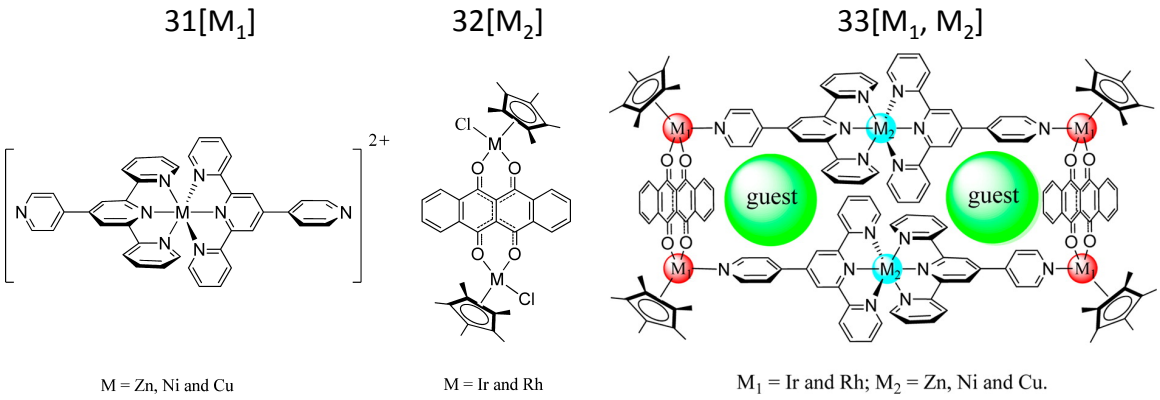


Figure 1.9 – Multicomponent assembly of pyridyl-terminated <tpy-$M^{II}$-tpy> complexes **31**[$M_1$] and organometallic **32**[$M_2$] to form heterometallic rectangles **33**[$M_1$, $M_2$]. [Modified with permission of the American Chemical Society: *Organometallics* **2014,** *33*, 1283-1290.]

In a strategy similar to directed flexibility,[62] a series of metallo-supramolecular ring-in-ring structures was generated by assembling $Cd^{II}$ ions and the multivalent terpyridine ligands (**34-36**) composed of one 60° bent and two 120° bent *bis*(terpyridine)s with varying alkyl linker lengths, n = 4, 6, and 8, respectively. Linker length had a profound effect on resultant structure with them forming dimeric **37** (2 ligands and 6 metals), trimeric **38** (3 ligands and 9 metals), and tetrameric **39** (4 ligands and 12 metals) bicyclic structures, respectively. A mechanistic study of the self-assembly process excluded an entropically templated pathway and showed that the intramolecularly complexed species is the key intermediate leading to ring-in-ring

formation. The next generation, tricyclic superstructure or spiderweb (**41**), comprised of three ligands and fifteen metals, was produced in quantitative yield using the elongated deca*kis*(terpyridine) ligand **40**.[106] The linker's length was a key factor in assembly and stability of the structures. The resultant structures were characterized by $^{1}$H NMR, ESI-MS, ESI-TWIM, DOSY, and TEM.

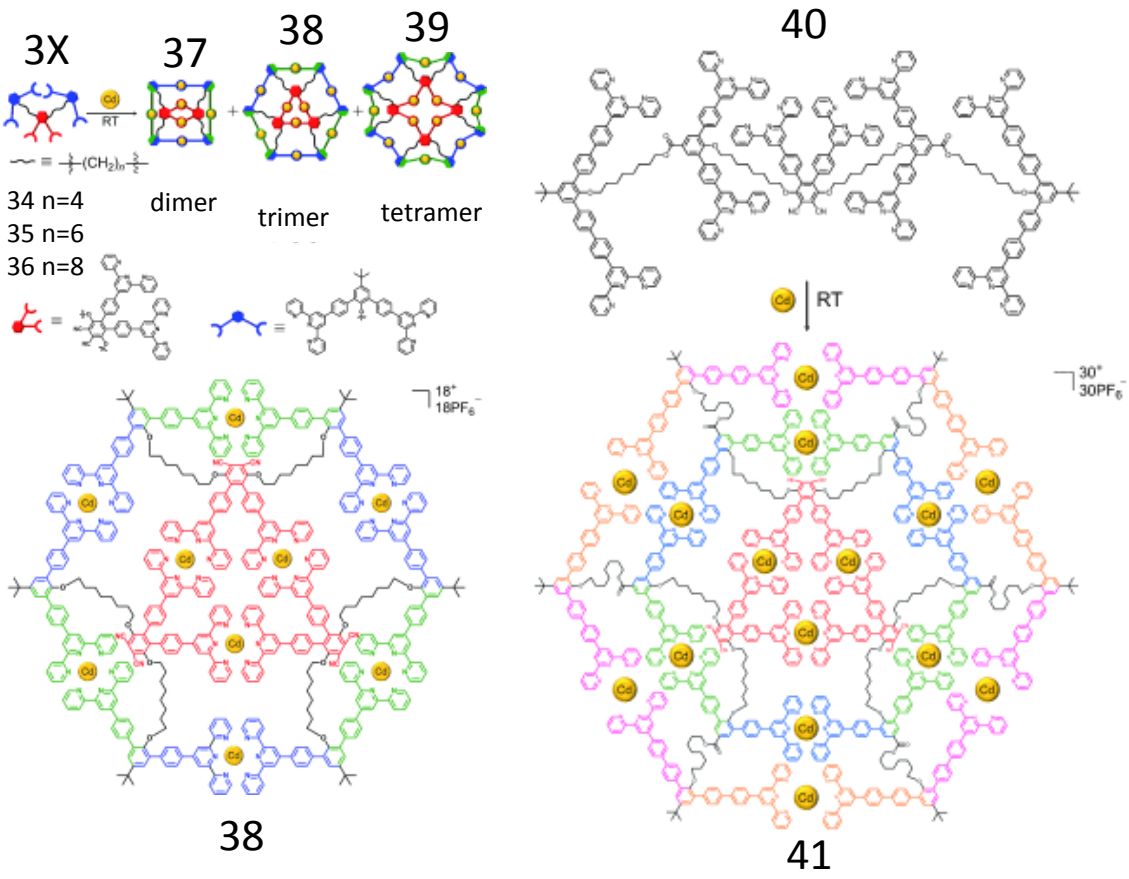


Figure 1.10 – Synthesis of ring-in-ring structures **38** and **41** using hexa*kis*- and deca*kis*-ligands and $Cd^{II}$. Linker lengths of n = 4, 6, and 8 were studied with the hexa*kis*-variant to also afford **37** and **39**. [Modified with permission of Wiley: *Angew. Chem. Int. Ed.*, **2015**, *54*, 6231-5.]

Recently, a balance of directionality and flexibility was used to create unique carborane functionalized macrocycles (**43**-**45**) including a dimer (**43**) with stacked <tpy-$M^{II}$-tpy> complexes. Molecular modeling, as shown in Figure 1.11, indicates the presence of both T-shaped and slipped parallel $\pi - \pi$ interactions. Modeling also indicates projection of the 4,4" and 5,5" protons into the adjacent complex resulting in dramatic upfield shift of their $^{1}H$ NMR signals relative to the trimeric species where such stacking is absent. The dimeric species was synthesized under both kinetic (using $Fe^{II}$) and thermodynamic (using $Zn^{II}$) control. Ligand arm length and flexibility enable favorable, intramolecular $\pi - \pi$ interactions within the unique dimeric macrocycle. Interconversion between the dimer (**43**) and trimer (**44**) under thermodynamic control was probed *via* variable temperature NMR and dilution studies and will be discussed in section 1.4.

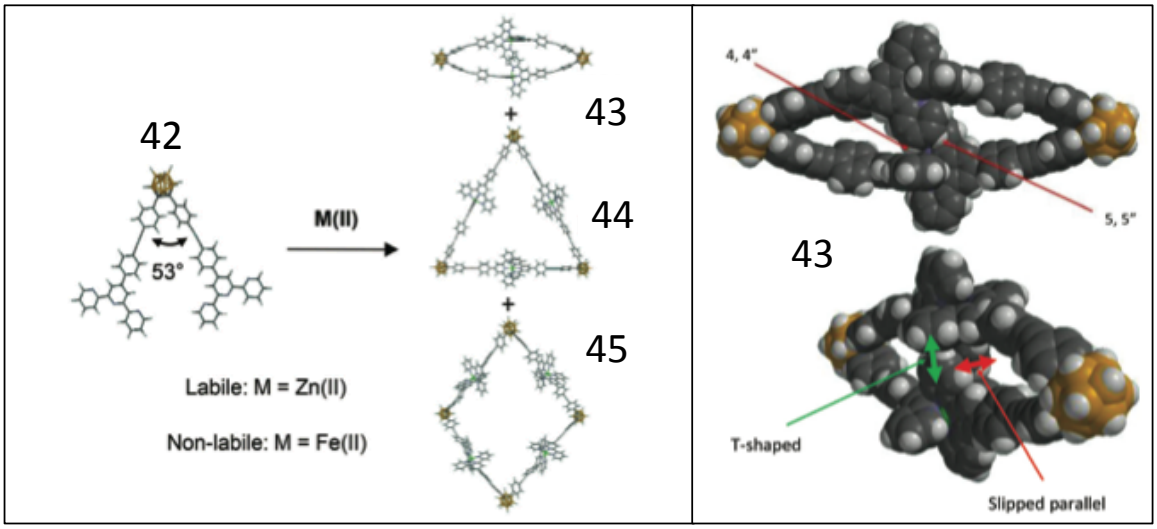


Figure 1.11 Complexation of **42** to form carborane-functionalized macrocycles **43** (dimer), **44** (trimer), and **45** (tetramer). Space-fill model of the dimeric structure showing interlocked <tpy-$M^{II}$-tpy> complexes. The 4,4"- and 5,5"-protons are indicated. Color scheme B: yellow; H: white; C: grey; C: grey; N: purple; Fe: green. [Modified with permission of the Royal Society of Chemistry: *Dalton Trans.*, **2014**, *43*, 9604 – 11]

## 1.3 3D/Cage

Cage-like supramolecular structures are found in biomolecular systems[107, 108] and their syntheses[101, 109-112] has been a focus in supramolecular chemistry. Various synthetic cages have been demonstrated using metal-ligand coordination.[24, 48] Different strategies have emerged to form 3D structures using <tpy-$M^{II}$-tpy> connectivity. These include *meta*-substitution on the phenylene spacer, introduction of multiple planes of directionality using appropriate vertices (*e.g.* - tryptycene and adamantane), combining directionality with a flexible vertices, and steric overlap.

*Tris* 120° ligands have been used as dendrimer cores[49, 50, 113] and to make prisms in heteroleptic systems.[32, 114] However, Xie *et al.* introduced a twist to enable the

synthesis of a three-dimensional, highly symmetric, terpyridine-based, spherical complex **47** synthesized *via* coordination of four novel, *tris*dentate ligands (**46**) with six $Ru^{II}$ ions. As shown in Figure 1.12, *meta*-substitution along the ligand's phenylene spacers allows the introduction of additional planes-of-directionality by simple bond rotation, enabling the formation of a discrete 3D structure. The structure, due to its <tpy-$Ru^{II}$-tpy> connectivity, exhibited excellent stability over a wide range of pH values (1-14). Structural confirmation was obtained by NMR and ESI-TWIM-MS.[115]

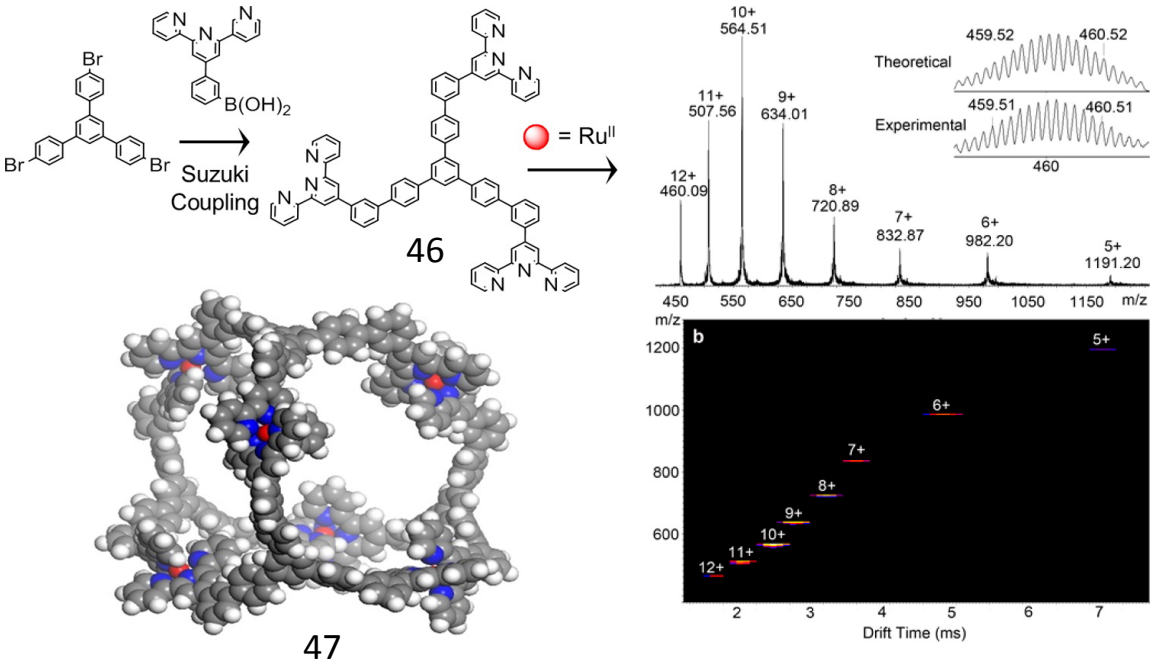


Figure 1.12. Synthesis of *tris*ligand **46** *via* a Suzuki coupling and its self-assembly to nanoball **47** under kinetic control with $Ru^{II}$ (left). ESI-MS (insert: isotope pattern of 10+ charge state) and TWIM spectra (m/z vs drift timer) showing charge states 12+ thru 5+ of **47**. [Modified with permission of the American Chemical Society: *J. Am. Chem. Soc.* **2014,** *136*, 8165-8168.]

Xie *et al.* also reported the design and construction of the 1st multicomponent step-wise assembly of a <tpy-$Ru^{II}$-tpy>-based, three-dimensional, propeller-shaped *tris*macrocycle (**51**). $Ru^{II}$ was precoordinated into the dimer **48**, which was then utilized in a two-step synthesis. The *bis* $RuCl_3$ adduct **49** was formed and subsequently coordinated under reducing conditions with a hexa*kis*terpyridinyl triptycene **50** prepared *via* a Suzuki coupling.[39] The novel hexa*kis*-ligand enforces three different planes-of-directionality from which the propeller-shape arises. Characterization includes ESI- and ESI-TWIM-MS and TEM, along with 1D and 2D $^1$H NMR spectroscopy.[44]

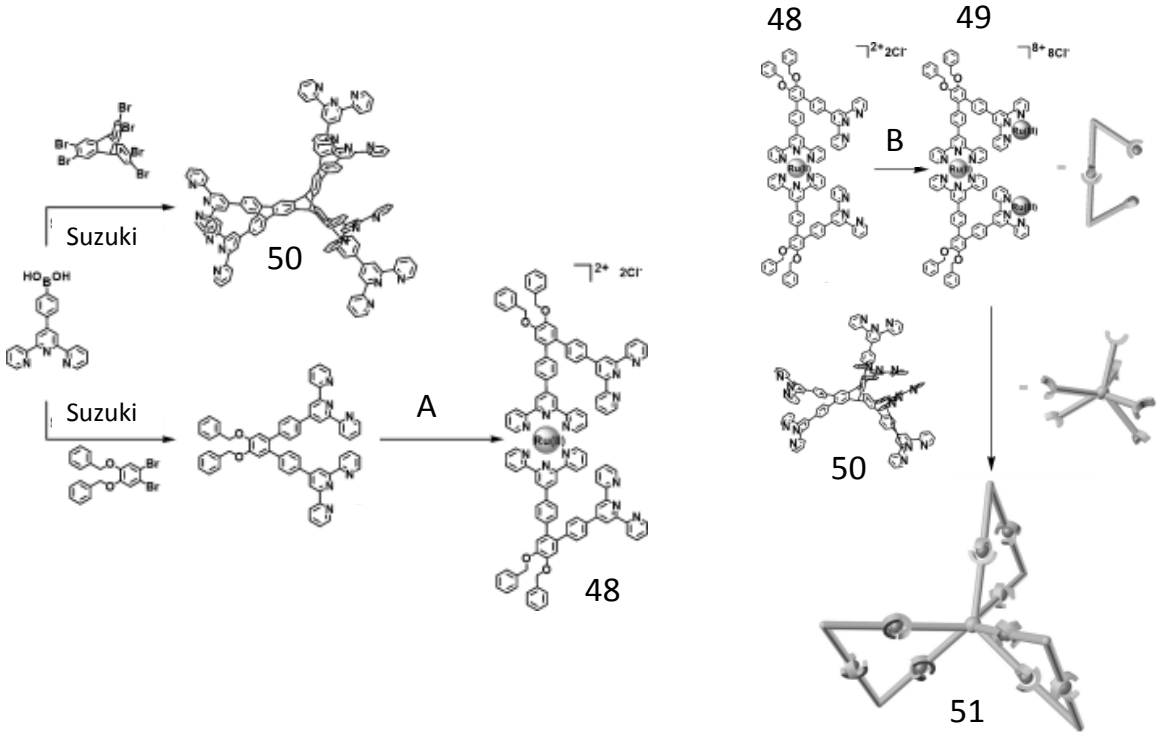


Figure 1.13. Synthesis of hexa*kis*ligand **50** from hexabromo triptycene. Formation of dimer **48** using 60° *bis*ligand, where A = $Ru(DMSO)_4Cl_2$ and its subsequent transfromation to adduct **49** where B = $RuCl_3$. Assembly of a propeller **51** combining **49** and **50** under reducing conditions. [Modified with permission of Wiley: *Chem. Eur. J*, **2014**, *20*, 11291-11294.]

Wang *et al.* demonstrated the self-assembly of 3-D giant metallo-supramolecular cubes using a variety of strategies. Three-armed terpyridine ligands were synthesized using an adamantane vertex to provide three planes possessing 109° directionality. Arm lengths and directionality were varied by using a *para* phenyl spacer, a thiophene spacer, and *meta* phenyl spacer to give ligands **52**, **53**, and **54**, respectively, which upon self-assembly under thermodynamic control to give the corresponding cube **55** (8 ligands and 12 metals), tetrameric cage **56** (4 ligands, 6 metals), and dimeric cage **57** (2 ligands, 3 metals). In each case, the giant cubes appear to be the sole product after self-assembly. The 3-D metallo-supramolecules were characterized and supported by NMR, DOSY, ESI-MS, TWIM-MS, and AFM.[42]

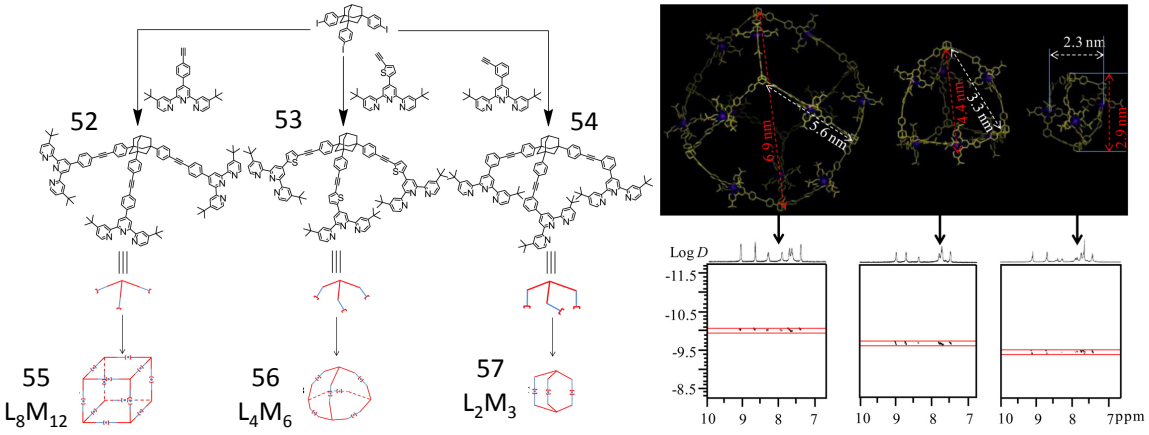


Figure 1.14. Synthesis of tritopic terpyridine ligands **52** - **54** using the Sonogashira coupling and their self-assembly into cage structures **55** – **57** under thermodynamic control with M = $Zn^{II}$. Energy minimized structures and dimensions and 2D DOSY NMR spectra of **55** (left), **56** (middle), and **57** (right). [Modified with permission of the American Chemical Society: *J. Am. Chem. Soc.* **2014**, *136*, 10499-10507.]

Terpyridine-based ligands used for self-assembly into macrocycles have generally been classified[68] as having flexible[116-119] or rigid[120-122] linkages. Highly dilute conditions are generally required to achieve macrocyclization with flexible linkers,[123] which also have been used for intramolecular cyclization with spirometallodendrimers.[124] A 3D structure was achieved using a strategy of 'directed flexibility' by connecting a trio of 60° *bis*-ligands with a flexible crown ether vertices **58**. The hexa*kis*ligand required a six-step synthesis culminating in Suzuki coupling utilizing the corresponding hexabromo-crown ether. Self-assembly of the tribenzo-27-crown-9 ether functionalized with six terpyridines **58** generated (85%) an expanded tetrahedral structure **59** comprised of four independent triangular surfaces interlinked by crown ether vertices.[62] The flexible vertices allow for introduction of additional planes-of-directionality and thus, formation of 3D structure, while the highly directional *bis*-ligands, in conjunction with intramolecular π-π interactions, allows for high yield formation of the tetrahedron.

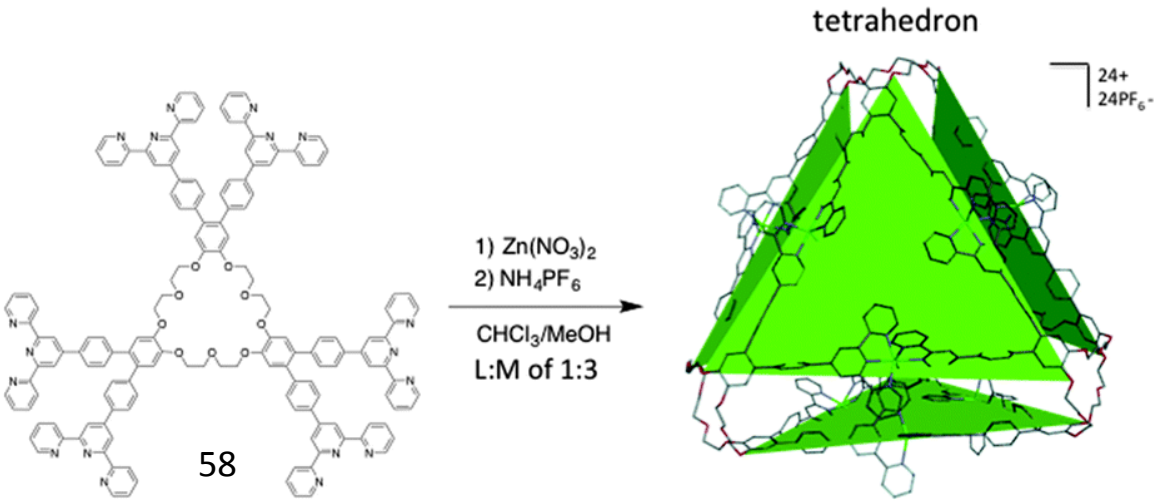


Figure 1.15. Synthesis of a supramolecular tetrahedron **59** from hexa*kis*ligand **58** to demonstrate directed flexibility. The structure's four individual triangles are highlighted in green to aid visualization. [Modified with permission from the Royal Society of Chemistry: *Chem. Commun.*, **2015**, *51*, 3820 – 3023.]

Recently, Xie *et al.* reported[43] the synthesis of an Archimedean polyhedron using the tetra*kis*terpyrdine ligand **60** synthesized from a tetrabromo-anthracene *via* Suzuki coupling. Ligand **60** contains both 60° and 90° directionality. A combination of 12 ligands and 24 $Zn^{II}$ ions forms a cuboctahedron structure **61**. Upon dilution, **61** converted to two entropically favored octahedral (**62** – Figure 1.22) structures, each comprised of 6 ligands and 12 $Zn^{II}$ ions. Such concentration dependent transformations have been previously demonstrated with <tpy-$M^{II}$-tpy>-based supramolecular structures.[105, 125] It was found that a larger counterion, $BPh_4^-$, preferentially stabilized the octahedron. The cuboctahedral structure was confirmed by X-ray crystallography.

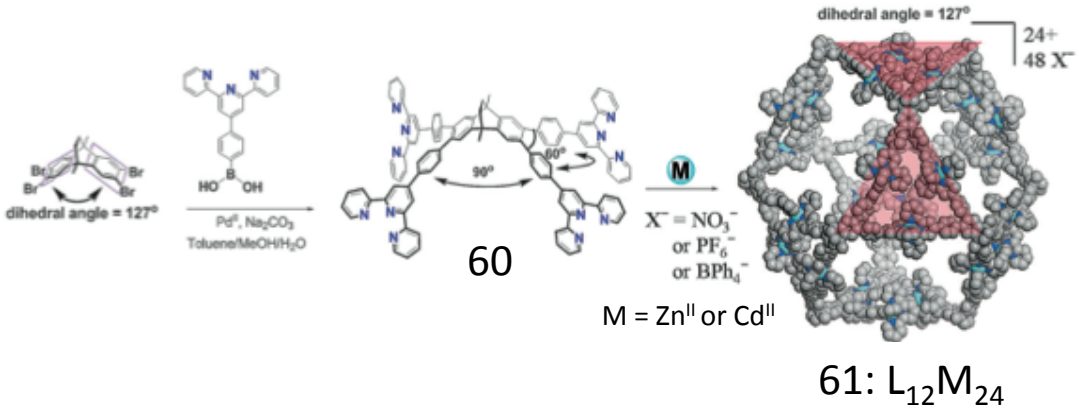


Figure 1.16. Synthesis of tetra*kis*ligand **60** *via* Suzuki coupling and its assembly into an Archimedean solid **61** (cuboctahedron) under thermodynamic control using $Zn^{II}$ or $Cd^{II}$. [Modified with permission of Wiley: *Angew. Chem. Int. Ed.*, **2015**, *54*, 9129-9129.]

A recent bicycle-like wheel demonstrates the use of steric overlap to generate a 3D structure (Figure 1.17). A pair of *tris*(terpyridine)s **63** provide the six spokes. And six units of *tris* ligand **64** provide the hexagonal rim. Under thermodynamic control with these ligands and twelve metals (1:3:6 ratio) combine to form a supramolecular bicycle wheel **65**. The two central 120° *tris*-tpy ligands are stacked with a common perpendicular axis to impart the 3D bicycle-wheel motif. Functionalization of **64** with β-glucose moieties increase the solubility of the predesigned complex.[126] The two tris ligands behave in concert to form a quasi hexa*kis*ligand. In contrast to the planar spoked wheel **8**, which uses the hexa*kis* rim ligand **7**, overlap of the two phenyl cores force projection into a 3-dimensional, bicycle wheel structure. A version of the planar spoked wheel **66**, using the same sugar functionalized *tris*ligand **64**, and 3D bicycle wheel were compared *via* ESI-TWIM-MS. Experimentally derived collision cross sections (CCS)s showed that the 3D wheel gave slightly higher values as predicted by molecular modeling.

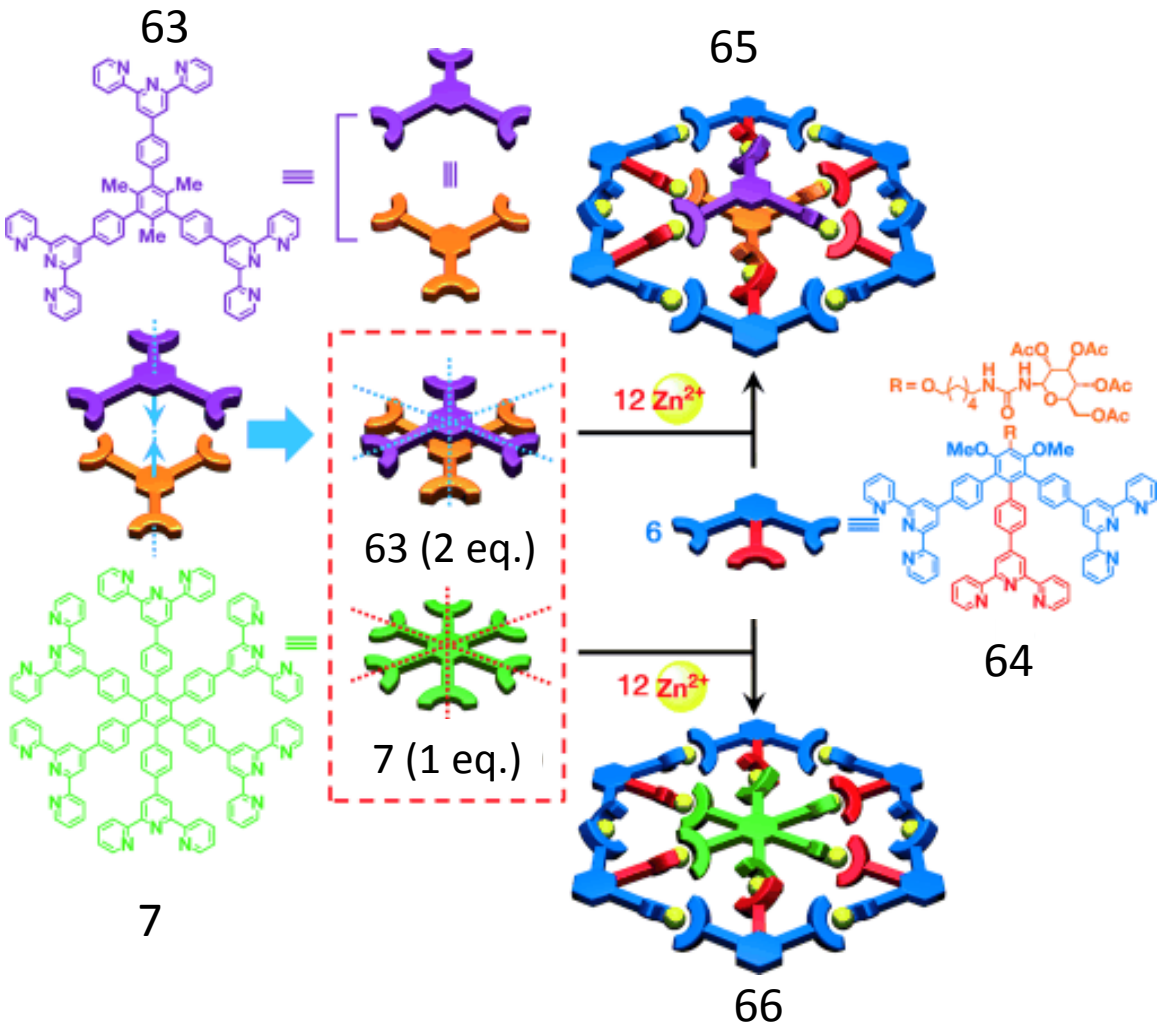


Figure 1.17. Synthesis of 3D bicycle wheel **65** using a pair of *tris*terpyridines in place of the hexa*kis*terpyridine used to make the spoke wheel **66.** Wheel **66** is a sugar functionalized version of **8**. [Modified with permission of Wiley: *Angew. Chem. Int. Ed.*, 2013, **52**, 7728 – 7731.]

Dondorff - metallomacrocyclic tetramers have been synthesized employing a 60° *bis*terpyridinyl ligand **67**. As previously reported, under thermodynamic control, **67** self-assembles to give triangles quantitatively.[127] Homometallic tetramers **68** could be trapped under kinetic control, as a minor product, with $Fe^{II}$ and then isolated *via*

chromatography. Heterometallic tetramers were prepared by precoordinating $Ru^{II}$ within the dimeric metalloligand **69**, which was subsequently self-assembled to form tetramers **70**. The strong <tpy-$Ru^{II}$-tpy> coordination bond within the dimer **69** circumvents formation of triangles during its self-assembly allowing only formation of tetramers. 3-D structure results from their folded conformation, which arises to relieve ring strain. Characterization by NMR, MS, UV/Vis, photoluminescence spectroscopy, and computer simulation confirm the structures and suggested that the tetramer is a stable motif.[128] This approach to 3D structure was also accomplished *via* synthesis of hexamers based on 60° ligands. [129]

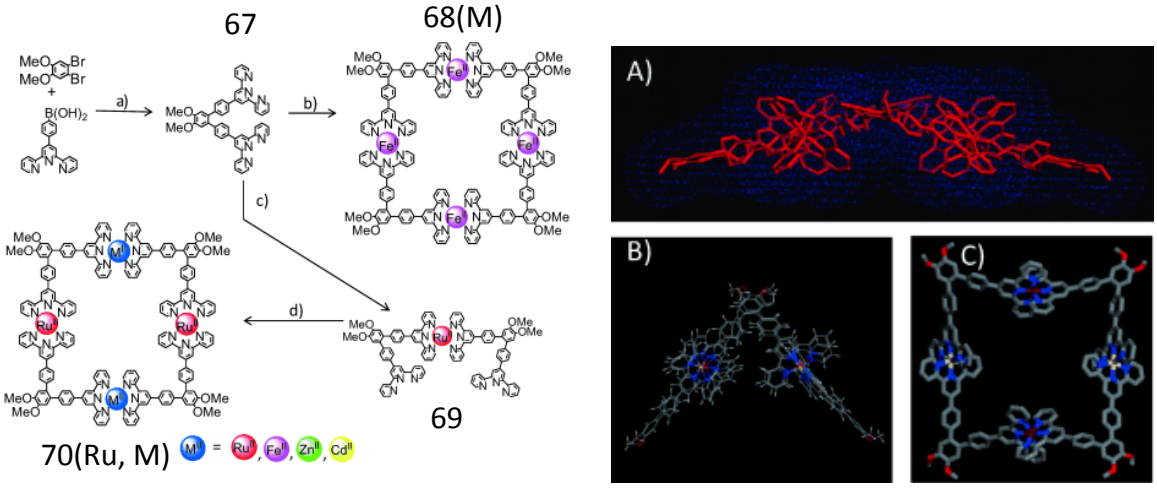


Figure 1.18. Reagents and conditions: a) $H_2O$/toluene/*t*BuOH (3:3:1 v/v/v), $Na_2CO_3$ (15 equiv), Δ, 48 h; b) 1.05 equiv $FeCl_2 \cdot 4\,H_2O$, MeOH, Δ, 12 h; c) 0.5 equiv $RuCl_2(DMSO)_4$, MeOH/$CHCl_3$ (1:1 v/v), Δ, 12 h; d) $M^{2+}$, $CHCl_3$/MeOH (1:1 v/v), Δ or 25 °C for 12–24 h. Computer simulation of tetramer **4**: A) side view with the solvent-accessible surface area as blue shell; B) lowest energy conformer of tetramer **4**; and C) stick model of the flattened, higher energy tetramer **4**. [Modified with permission of Wiley: *Chem. Eur. J.*, **2012**, *18*, 11569 – 11572.]

## 1.4 Metallomolecular Interconversions

Linear oligomers and the macrocyclic analogs of <tpy-$Ru^{II}$-tpy> complexes where tpy is a 120° *bis* ligand have been reported.[120] The resultant structures are highly stable due to the strong coordination bond formed with $Ru^{II}$. Recently, Wang *et al.* reported synthesis of a $Ru^{II}$ trimer **71** by combining a 60° ligand **72** with two 120° ligands **73** *via* a two-step synthesis using $RuCl_3$ adduct **74** (Figure 1.19); its subsequent reaction with $Fe^{II}$ gave polymer **75**, which is subsequently converted to macrocycle **76** through a thermodynamic disassembly process. Thus, the initial metallopolymer is a kinetic intermediate to the final stable hexanuclear metallomacrocycle, that was obtained through a thermodynamic dis-assembly/re-assembly route. The macrocycle **76** was characterized by NMR, UV, IR, CV, 2D-ROESY, DOSY, and ESI-MS.[130] Note that, as with the Dondorff structures,[128] angular constraints restrict formation of a planar conformation by the macrocycle, thereby impose a 3D chair-like conformation here.

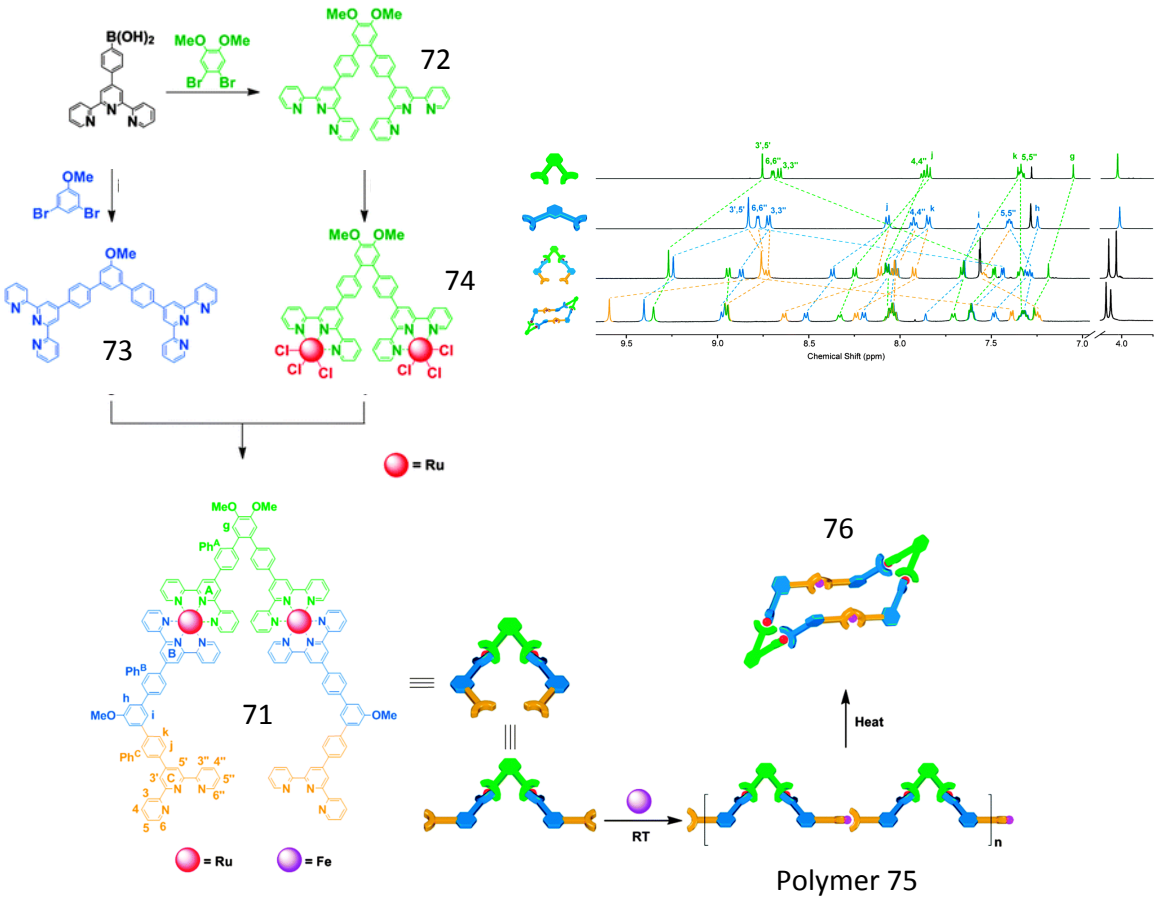


Figure 1.19. – Stepwise synthesis of metallo ligand **71** and its polymerization to form polymer **75**, which is then cyclized to form hexamer 7**6**. Top right - $^{1}$H NMR spectra of **72** ($CDCl_3$), **73** ($CDCl_3$), **71** ($CD_3OD$), and **76** ($CD_3OD$). [Modified with permission of the Royal Society of Chemistry: *Chem. Commun.*, **2015**, *51*, 5766-5769.]

As noted in Section 1.2, the self-assembly of the *o*-carborane-based, *bis*terpyridyl ligand **42**, utilizing either $Zn^{II}$ or $Fe^{II}$ in a precise metal : ligand ratio (1 : 1), generated metallomacrocycles that were studied *via* ESI-TWIM-MS, $^{1}$H NMR, and 2D NMR (COSY, NOESY). Under kinetic control, *via* formation of $Fe^{II}$ complexes, the main cyclic product was the triangular **44**. Under thermodynamic control, using more labile transition metal complexes, *e.g.* $Zn^{II}$, the ratio of cyclic species was found to be

concentration and temperature dependent, and under an adequate entropic driving force, the cyclic dimer **43** was formed exclusively. This system was probed *via* variable temperature NMR to reveal a dynamic equilibrium between the entropically favored dimer **43** and enthalpically favored trimer **44**.[105] A van't Hoff analysis was performed to measure the thermodynamics of interconversion between structures.

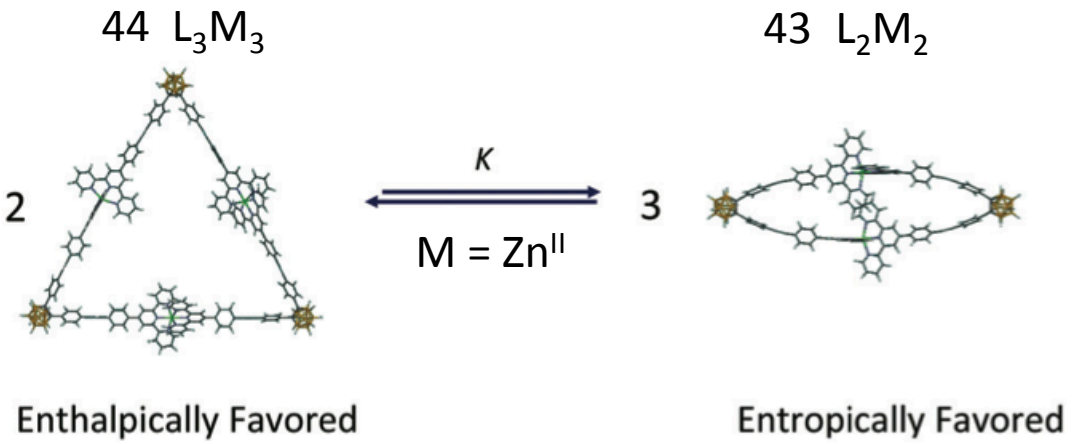


Figure 1.20 – Interconversion between **43** and **44** under thermodynamic control using <tpy-$Zn^{II}$-tpy> connectivity. [Modified with permission of the Royal Society of Chemistry: *Dalton Trans.*, **2014**, *43*, 9604 – 9611.]

A terpyridine-based, concentration-dependent, facile self-assembly process was reported, resulting in two three-dimensional metallosupramolecular architectures, a *bis*-rhombus **78** and a tetrahedron **79**, which are formed using a two-dimensional, *tris*-terpyridine ligand **77**. The equilibrium between the two structures was concentration-dependent: at a concentration higher than 12 mg/mL, only a *bis*-rhombus, composed of eight ligands and 12 $Cd^{II}$ ions, was formed; whereas a self-assembled tetrahedron, composed of four ligands and six $Cd^{II}$ ions, appeared upon sufficient dilution of the *tris*-

terpyridine-metal solution in MeCN. At concentrations less than 0.5 mg/mL, only the tetrahedron possessing an S4 symmetry axis was detected; upon attempted isolation, it quantitatively reverts to the *bis*-rhombus. [125]

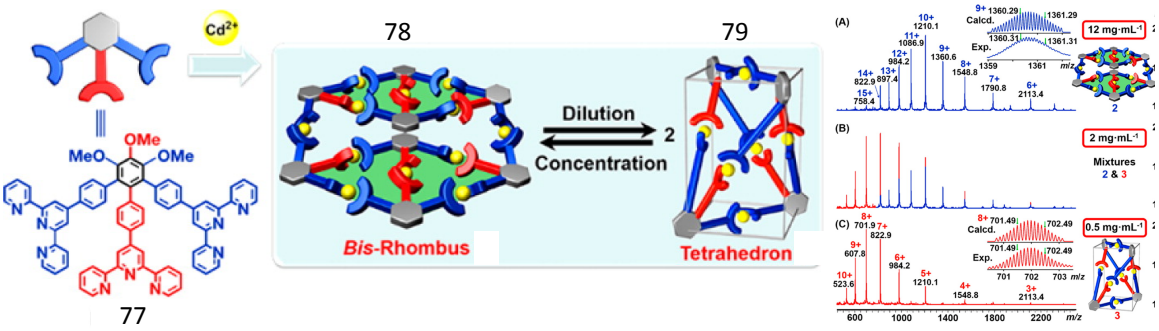


Figure 1.21. Self-assembly of *tris*-terpyridine building block **77** gives either a *bis*-rhombus **78** or a tetrahedron **79** depending on concentration. ESI-MS of (A) *bis*-rhombus **78** at high concentration (B) mixture of **78** and **79**, and (C) tetrahedron **79** at low concentration. [Modified with permission of the American Chemical Society: *J. Am. Chem. Soc.* **2014,** *136*, 18149-18155.]

In the aforementioned 3D system[43] utilizing a tetra*kis*terpyridine ligand **60** with an anthracene vertex, under thermodynamic control, using <tpy-$Cd^{II}$-tpy> connectivity and $PF_6^-$ counterions, a dynamic equilibrium exists between a cuboctahedron **61** and octahedron **62** depending upon concentration with the entropically favoured octahedron **62** being favored under dilute conditions. The equilibrium is shown in Figure 1.22. Notably, when $BPh_4^-$ counterion was used, the system gave only the octahedral structure.

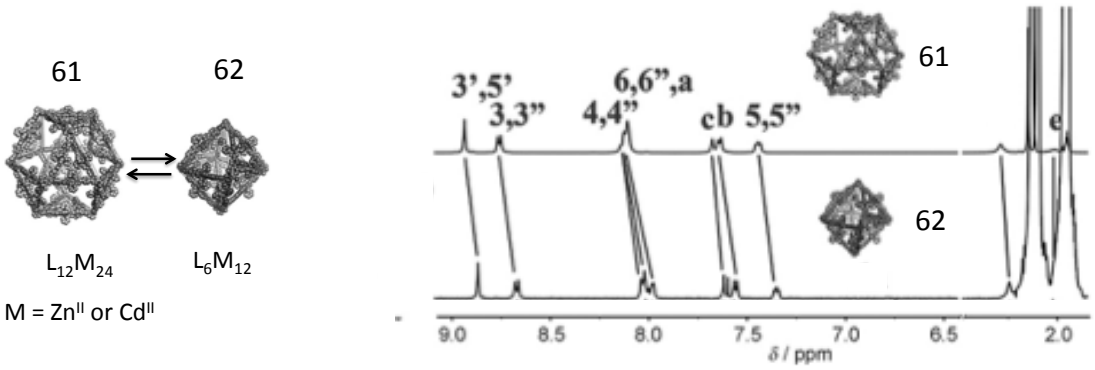


Figure 1.22 – Dynamic equilibrium between **61** and **62**. $^{1}$H NMR of each structure is shown. Signals from the octahedron **62** show a slight upfield shift relative to those of the cuboctahedron **61**. Both $^{1}$H NMR spectra are 500 MHz in $CD_3CN$/DMF-$d_7$ at 4:1. [Modified with permission of Wiley: *Angew. Chem. Int. Ed.*, **2015**, *54*, 9224 - 9229.]

## 1.5 Materials

As a result of the unique electrochemical, catalytic, photophysical, and magnetic properties of <tpy-$M^{II}$-tpy> complexes, they have been put into polymer backbones[41, 131] and side chains[132] to explore applications, such as organic solar cells. Recently, there has been an increasing emphasis on incorporating discrete metallosupramolecular architectures into materials. For <tpy-$M^{II}$-tpy> based structures, a variety of approaches have been explored including attachment to nanoparticles[133, 134], carbon nanotubes,[135, 136] and surfaces.[137] There is now increased focus on formation of supramolecular materials using hierarchical self-assembly of discrete metallomolecular architectures, based on non-covalent interactions.[138-140] Such materials, assembled by a bottom-up approach,[141-143] are projected to offer potential advantages including economic fabrication, self-healing, stimuli responsiveness, and recyclability.[144] Most recently, the metallocycles investigated have primarily been alkylated[138] or PEGylated[139, 145] and based on square

planar $Pt^{II}$ complexes. In the <tpy-$M^{II}$-tpy> arena, previous approaches have primarily focused on ion pairing. For example, the self-assembly of multi-ionic species through electrostatic interactions was demonstrated for these rigid polycationic macrocycles (12+) with a spherical polyanionic dendrimer (12-) (**81**). A C6-functionalized, $Ru^{II}$ coordinated hexamer **80** was studied (Figure 1.23). The hierarchical formation of the fiber and sphere-like cluster has demonstrated the potential to employ polyionic architectures, as aids in shape control, in contrast to that of traditional, monovalent counterions.[146] Molecular modeling, based on X-ray diffraction, indicated stacking of the complexes. The fibers had diameters on the order of greater than half a micron.

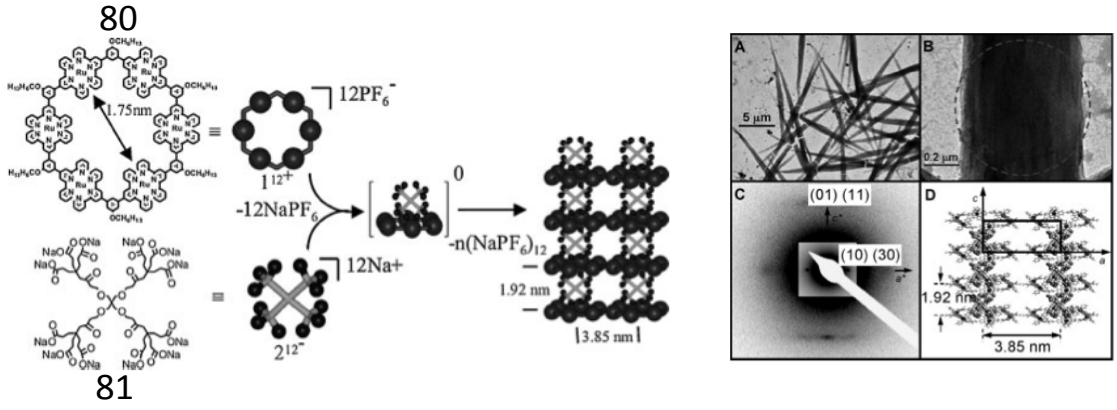


Figure 1.23. Illustration of hierarchical self-assembly of a C6 functionalized hexamer **80** and polyanionic dendrimer **81** into fibers using anion pairing approach. A, B) TEM image of the fibers; C) SAED pattern from fiber; D) molecular model of packing. [Modified with permission of Wiley: *Adv. Mat.*, **2008**, *20*, 1381-1385.]

More recently, a series of trimeric, $Zn^{II}$- and $Cd^{II}$-metallocycles (**82**) were synthesized using ligand **67** with $Zn^{II}$ and characterized by TWIM-MS and $gMS^2$. Their photophysical properties and hierarchical self-assembly to form fibers were described.[127]

Again, this used a ion pairing strategy, the triangles being 6+, paired with benzene hexacarboxylate (6-) counteranion. As shown in Figure 1.22, the isolated fibers were *ca.* half a micron in diameter. A proposed packing model, based on SAXD data, was reported as well.

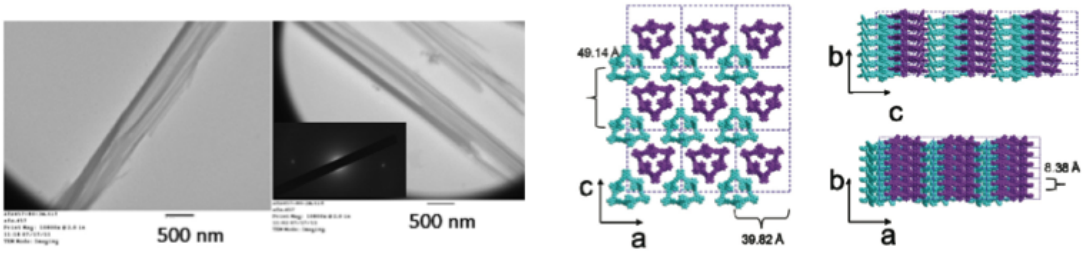


Figure 1.24. – (left) TEM images of fibers formed from **82** (inset: SAXD diffraction pattern) and (right) packing model based upon spacing values derived from powder and X-ray diffraction. Modified with permission of the Royal Society of Chemistry: *Dalton Trans.*, **2012**, *41*, 11573-11575.]

In both of these cases using an anion pairing strategy, the resultant fibers were prepared using a slow diffusion technique and were reported to be insoluble, potentially limiting some of the aforementioned advantages of supramolecular materials.

Conversely, using a sugar-functionalized 120° *bis*terpyridine ligand **83**, <tpy-$Fe^{II}$-tpy>-based pentameric **84** and -hexameric **85** metallomacrocycles were synthesized and characterized by NMR, UV/Vis spectroscopy, cyclic voltammetry, and MS. Self-assembled nanofibers of each macrocycle were generated by slow diffusion of hexane into a homogeneous solution of macrocycles.[147] These macrocycles had monovalent counterions ($NO_3^-$) and, based on TEMs in Figure 1.25, gave smaller diameter fibers than those reported *via* the ion pairing approach. Hydrogen bonding between urea linkers

and/or interactions between sugar moieties could play a role in the ordering process. However, non-functionalized controls were not included in the study.

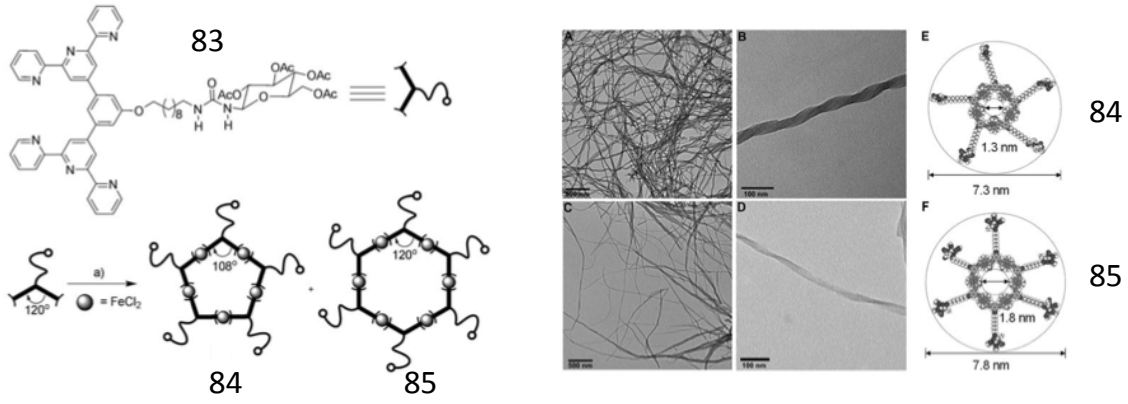


Figure 1.25. Self-assembly of **83** to form pentameric **84** and hexameric **85** macrocycles. a) $FeCl_2$-$4H_2O$, MeOH, 25C, 24h (left). TEM images of hierarchical self-assembled macrocycles **84** and **85** into fibers (center). Scale bars (A: 500nm; B: 100nm; C: 500nm; D: 100nm). Space-filling models of **84** and **85** (right). [Modified with permission of Wiley: *Chem. Eur. J.*, **2010**, *16*, 1768-1771.]

The Stang group recently reported[139] PEGylated, square planar $Pt^{II}$-based metallacyclic cores and their organization into nanostructures. The PEG moieties were complexed to the $Pt^{II}$ organometallic entity **88** using anionic, *bis*carboxylate ligands (**86** and **87**) with 120° directionality. They reported that rhomboids **89** and **90** (Figure 1.24) ordered into 0D micelles, 1D nanofibers or 2D nanoribbons depending on the PEG moieties decorating the parent rhomboid, concentration during self-assembly, and reaction duration. Their ordering into metallohydrogels was also studied. The intermolecular interactions driving the ordering were described as hydrophobic and π–π

stacking. While this system differs from the <tpy-$M^{II}$-tpy>-based systems in a number of ways including coordination geometry, use of anionic coordinating ligands, and absence of free anions, it provides a benchmark in terms of the degree-of-self-ordering of metallosupramacrocycles currently being reported.

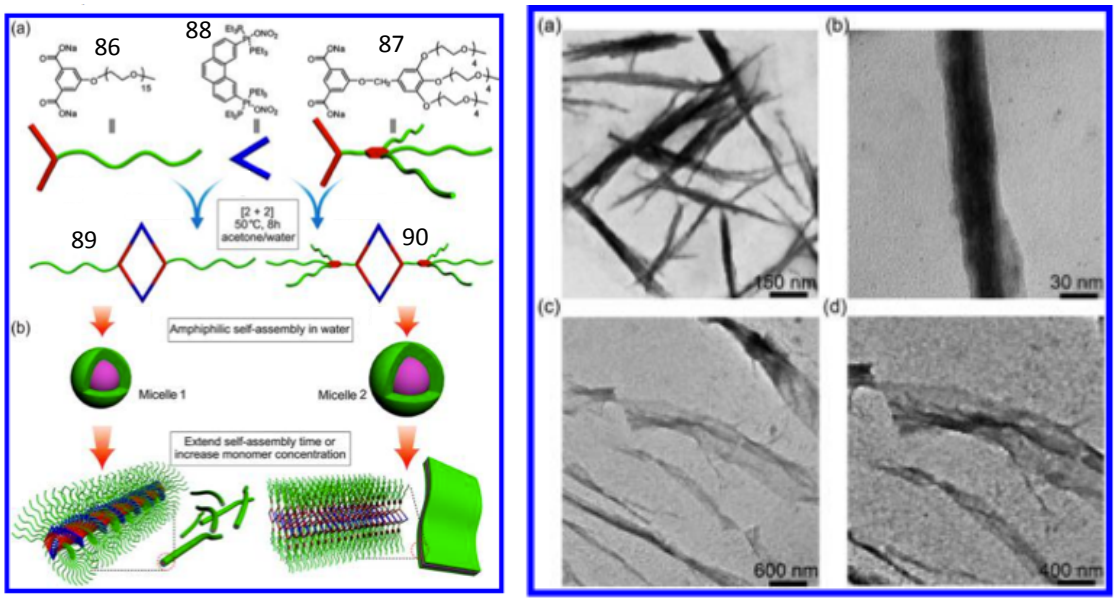


Figure 1.26. Self-assembly of **86-88** to form PEGylated rhomboids **89** and **90**. Illustration of hierarchical ordering of **89** and **90** into micelles, nanofibers, and nanoribbons. TEM images of (a,b) nanofibers of **89** and (c,d) nanoribbons of **90**. Solutions were cast at 5 X $10^{-5}$M. [Modified with permission of the American Chemical Society: *J. Am. Chem. Soc.*, **2013**, *135*, 14036-14039.]

The Yang group recently reported[138] coordination driven assembly of 120° *bis*pyridyl ligand **91** and the 120° bimetallic $Pt^{II}$ organometallic complex **92** to form hexagonal metallacycle **93** functionalized with multiple amide groups and long hydrophobic alkyl chains. Ordered nanofibers and stimuli-responsive supramolecular gels were formed *via* hierarchical self-assembly (Figure 1.27).

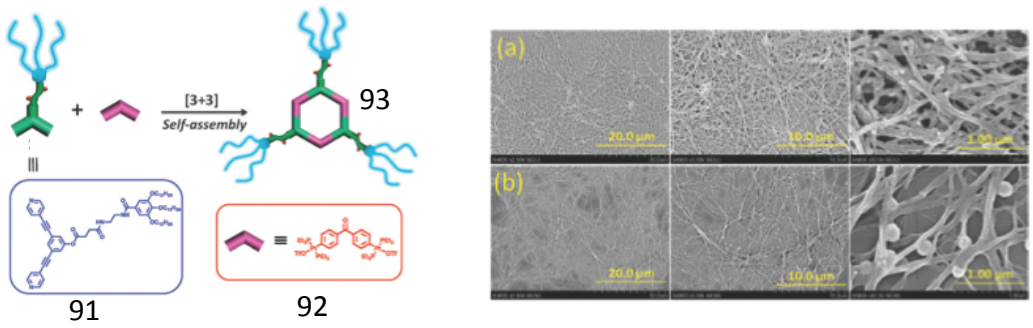


Figure 1.27. Self-assembly of alkylated metallocycle **93** from 120° donor, **91** and 120° acceptor, **92**. SEM images of **93** after its subsequent ordering *via* gelation technique in a) acetone/water (v/v 2/1) and b) $CH_2Cl_2$ (v/v 2/1) from an initial concentration of 5.0 X $10^{-2}$M. [Modified with permission of the Royal Society of Chemistry: *Chem. Commun.*, **2014**, *50*, 4231-4233].

An amphiphile-based strategy with <tpy-$M^{II}$-tpy>-based macrocycles was recently evaluated.[148] Conversion of metallotriangles into directional amphiphiles dramatically enhanced their self-ordering characteristics, enabling the formation of nanoscale structures. Long chain (C16) alkylated metallotriangles **95** were synthesized from ligand **94** and characterized *via* NMR and ESI-MS. Ordered aggregation of these amphiphiles was studied *via* TEM to gauge morphology and nanoscale structure as related to the effects of molecular topology, solvent, counterion, and metal center(s). Labile ($Zn^{II}$) and non-labile ($Fe^{II}$) systems were compared. SAXD suggests intramolecular π-π stacking. Nanotubes and evidence of their formation were observed. Lamellar or rod-like structures were observed depending upon solvent choice. In this study, the amphiphilicity provides a mechanism for promotion of molecular information sharing and thereby enhanced ordering relative to non-amphiphilic controls. Long chain

(C18) alkylated <tpy-$Ru^{II}$-tpy> hexamers have been reported;[149] however, their hierarchical ordering was not evaluated.

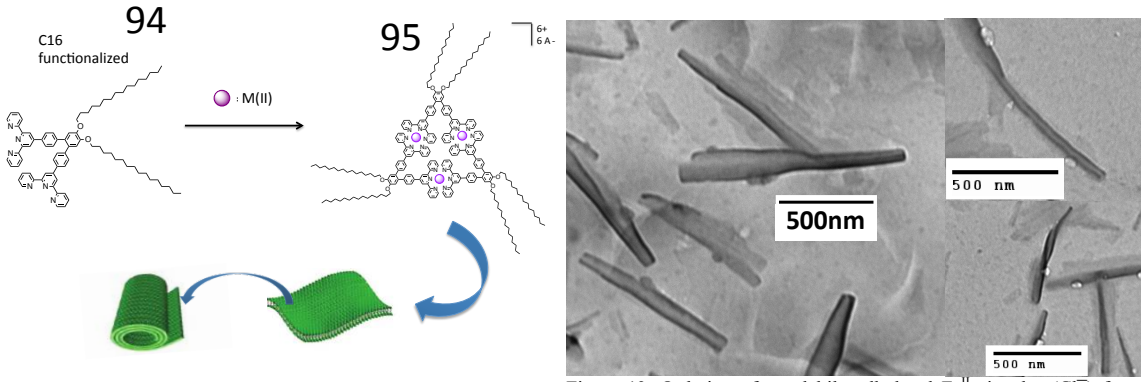


Figure 1.28. Self-assembly of bis-C16 functionalized bisterpyridine **94** with $M^{II}$ (Fe and Zn) to form amphiphilic metallotriangles **95** and an illustration of their subsequent hierarchical ordering into nanostructures (left). TEM images of 95 (M=Fe, with $Cl^-$ counterions) ordered into tube-like structures from $CHCl_3$/MeOH (v/v 2/1). [Illustration used with permission of *Acc. Chem. Res.*, **2011**, *44*, 72-82.]

Knowledge of binding strength of complexes in metallosupramolecular structures will become increasingly important aspect of supramolecular material design, as <tpy-$M^{II}$-tpy> based materials transition into the material sciences.[150] Given the growing interest in $Os^{II}$ based systems, the lack of suprametallomolecular architectures studied thus far is surprising. Recently, one-step synthesis of the first homoleptic <tpy–$Os^{II}$–tpy> metallomacrocycle **98** was synthesized. Characterization of the $Os^{II}$ complex, along with its $Fe^{II}$ and $Ru^{II}$ analogues (**96** and **97**), was accomplished by NMR, ESI-MS, TWIM-MS, gradient tandem-MS, and UV-VIS. Center-of-mass (COM) collision energies, derived from gradient tandem-mass spectrometry ($gMS^2$), reveal that the <tpy–

$Ru^{II}$–tpy>-based structures are more stable than those of <tpy–$Os^{II}$–tpy> and that the order of stability the complexes by metal is Ru > Os > Fe.

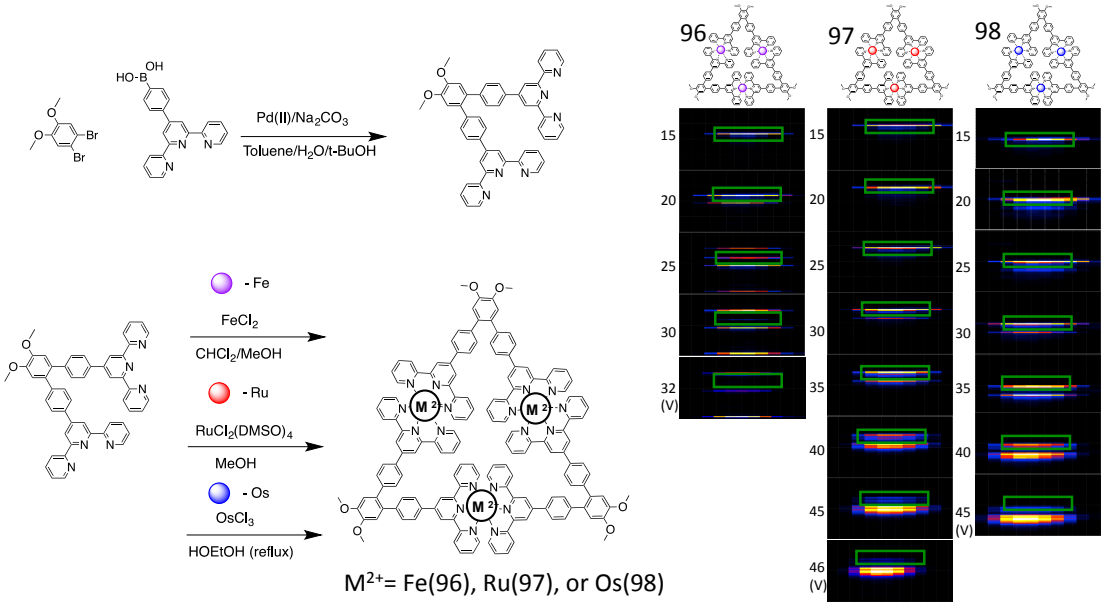


Figure 1.29. Synthesis of 60° *bis*terpyridine *via* Suzuki coupling and its self-assembly at 1:1 ratio with $Fe^{II}$, $Ru^{II}$, and $Os^{II}$ to form **96** – **98**, respectively (left). The $gMS^2$ spectra of the 5+ charge states of **96-98** to measure relative stability of the complexes/structures (right).

## 1.6 Monolayer Sheets

Monolayer sheets have gained attention due to their unique properties, derived from their two-dimensional structure. The <tpy-$M^{II}$-tpy>-based systems have recently been studied. Sheets **99** were formed under thermodynamic control ($Zn^{II}$) with hexa*kis*terpyridine ligand **7**, followed by site-to-site transmetalation ($Zn^{II}$ to $Fe^{II}$, $Co^{II}$, and $Pb^{II}$) to form sheets **100** with non-labile complexes. Transmetallation was done *via* immersion of **99** in $M^{II}$ solutions both randomly and at predetermined patterns defined by photolithography. Molecular structure of the sheets were modeled, based on density

functional theory calculations, and the models were used to hypothesize the mechanism of transmetallation. Applications such as surface coating, molecular electronics, device fabrication, imaging, and sensing are envisioned.[151] The tris analogue with 120° geometry was synthesized and studied as well.

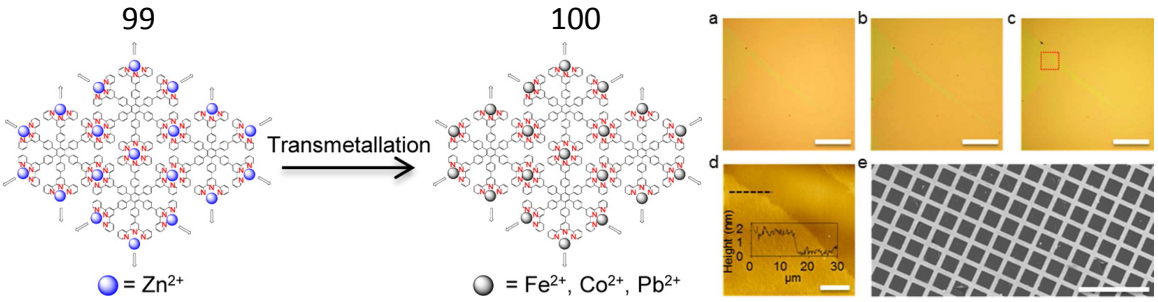


Figure 1.30. L - Model of $Zn^{II}$ based monolayer sheet and transmetallation to other $M^{II}$. R-Microscopic images of sheets prepared by transmetallation. Optical microscopy images of **99** ($Zn^{II}$) on 285 nm $SiO_2$ (a) before and (b) after 1 h immersion in 10 mmol/L $(NH_4)_2Fe(SO_4)_2$ and (c) of **100** after an additional 1 h immersion in 0.1 mol/L HCl sonication bath at ~20 W. (d) AFM topographic image of the red square inserted in (c) with a height profile. (e) TEM image of freely suspended **100** ($Fe^{II}$) sheet synthesized by transmetalation of **99** ($Zn^{II}$) over a copper grid. Scale bars: 200 µm (a–c); 20 µm (d); 100 µm (e). [Modified with permission of the American Chemical Society: *J. Am. Chem. Soc.* **2014,** *136*, 6103-6110.]

A hexathiobenzene functionalized with six terpyridine units **101** at the periphery was reported to combine aggregation induced phosphorescence of the hexathiobenzene core in the solid state, to the metal binding properties of the terpyridine units. Upon $Mg^{II}$ complexation to form **102** in a THF solution, phosphorescence of the hexathiobenzene core is activated. Metal ion coordination to form the resultant 2D supramolecular

polymer hinders intramolecular rotations and motions of core, thus favoring radiative deactivation of the luminescent excited state. Upon excitation of the <tpy-$M^{II}$-tpy> units of the polymeric structure, core phosphorescence is enhanced to >90% efficiency. The authors demonstrate that the 2D polymer can be disassembled upon the addition of fluoride ion, thereby switching off luminescence, providing a mechanism for fluoride (or other) ion sensing.[152]

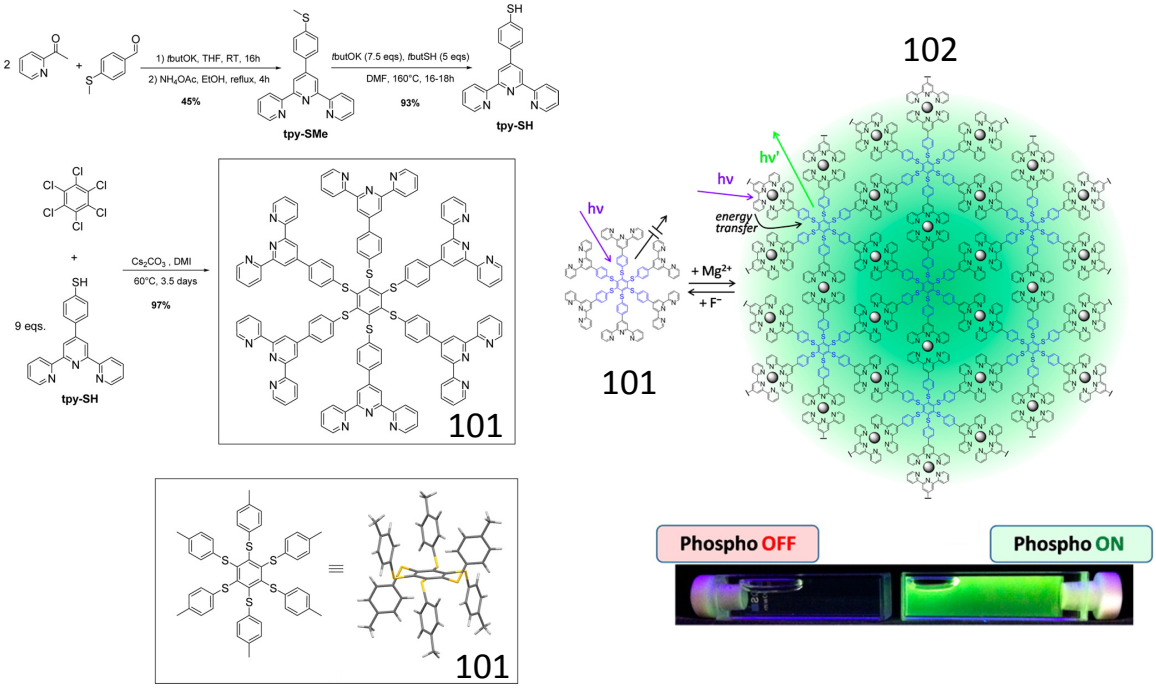


Figure 1.31. Synthesis of hexa*kis*terpyridine functionalized hexathiobenzene **101** *via* coupling reaction to hexachlorobenzene. Formation of 2D polymers **102** from **101**. [Modified with permission of the American Chemical Society: *J. Am. Chem. Soc.* **2014,** *136*, 6395-6400.]

## 1.7 Conclusions

A variety of themes emerge from recent progress in terpyridine-based metallosupramolecular architectures. These include increased use of triangle-based

frameworks, harnessing of additional noncovalent forces to enhance self-assembly, asymmetric ligands, and use of increased degree-of-coordination (DOC). Also, emerging strategies to attain three-dimensional structures including *meta*-substitution, multiplanar vertices, flexible vertices, and by restricting the availability of planar conformations *via* precoordination or predesigned steric hindrance. There is also increasing emphasis on interconversions between supramolecular structures in response to conditions such as concentration, temperature, and counterion type. On the supramolecular materials front, there is increasing emphasis on hierarchical self-assembly and 2D structures using geometrically appropriate, planar ligands.

Note: the term 'non-covalent' interactions is used in this document and in the field of supramolecular chemistry to classify bonding interactions other than a traditional covalent bond in which each atom is contributing electron/s to the bond. It is important to note that metal-ligand interactions do have covalent character, however, the difference is that the electrons come only from the donor (ligand). This is described in more detail in M. Gerloch and E.C. Constable's *Transition Metal Chemistry* (VCH, Weinheim, **1994**, pp.184-185).

# CHAPTER II

# SELF-ASSEMBLY OF METALLOSUPRAMACROCYCLES USING BIS-TERPYRIDINE FUNCTIONALIZED ORTHO-CARBORANE[†]

## 2.1 Introduction

Carborane-containing macromolecules exhibit several properties of interest including chemical and thermal stability,[153] aggregation induced emission (AIE),[154] radiation shielding coatings[155] that enable their use in medical applications, and boron neutron capture therapy (BNCT).[156, 157] Consequently, carboranes have been incorporated into a variety of macromolecular structures including polymers[154] and dendrimers[158-163] in order to instill water-solubility and enhance their properties and utility. These approaches primarily rely upon covalent bonding; however, biomolecular systems exploit a range of weaker, non-covalent inter- and intra-molecular forces, including van der Waals, hydrogen bonding, π-π stacking, electrostatic, and coordination to achieve macro-molecular structure.[48, 164] Notably, the incorporation of carborane into (metallo)supramolecular structures has received limited attention.[164-167]

Metal-ligand self-assembly has been utilized to form various metallosupramolecular structures including coordination polymers,[153] macrocycles,[90, 127]

[†] Parts of this chapter are reprinted with permission of the Royal Society of Chemistry: J. M. Ludlow III, M. Tominaga, Y. Chujo, A. Schultz, X. Lu, T. Xie, K. Guo, C. N. Moorefield, C. Wesdemiotis and G. R. Newkome, *Dalton Trans.*, **2014**, *43*, 9604 – 9611.

and 3D structures.[168] The incorporation of [2,2':6',2"]terpyridine (tpy) has received increasing attention due in part to its ability to coordinate with

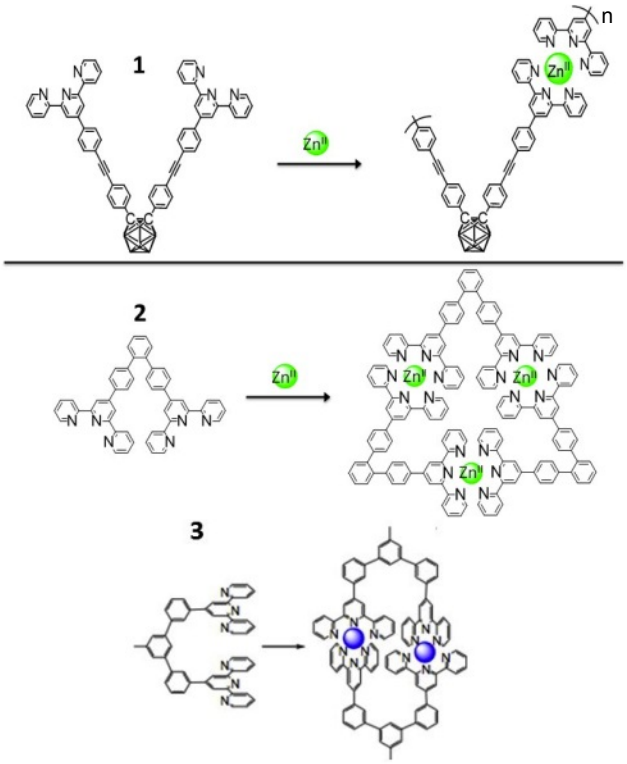


Figure 2.1. *Bis*terpyridyl *o*-carborane **1** and its reported assembly with $Zn^{II}$, reaction of a similar 60°-directed ligand **2** to give a triangle,[127] and assembly of parallel *bis*terpyridine **3** to generate a dimeric species.[169] [Redrawn with permission from the Royal Society of Chemistry: *Dalton Trans.* **2011**, *40*, 1919-1923; *Dalton Trans.* **2012**, *41*, 11573-11575; *Dalton Trans.* 2007, 626-628.]

diverse transition metals permitting control of bond strengths, properties, and desired molecular architectures.[47, 68] Terpyridine-based materials have found various applications including supramolecular chemistry,[48, 87, 170, 171] catalysis,[75] nanoparticles,[133] electroactive nanostructures,[137] and life science applications.[68] With metals that can form strong

coordinative bonds, such as $Os^{II}$, $Ru^{II}$, and $Fe^{II}$, the final product is kinetically determined by creation of irreversible <tpy-$M^{II}$-tpy> complexes; in contrast, metals capable of more labile coordinative bonds, *e.g.* $Zn^{II}$ and $Cd^{II}$, allow equilibration to the thermodynamic product.

Specific architectures are thus determined, in part, by building block geometry, *e.g.,* the angle between conjoined ligands. Exploitation of the angular orientation and stoichiometric control of precursors is generally known as the directional bonding approach to supramolecular synthesis.[48] *Ortho*-carboranes possess an angle of *ca*. 53° between substituents attached to the two adjacent carbon atoms[172] and are thus well-suited for macrocyclizations, as has been reported with 60°-oriented *bis*ligands.[127]

Chujo and Kokado recently reported[154] the synthesis and characterization of *bis*terpyridyl *o*-carborane **1**, which was subsequently complexed with $Zn^{II}$ (Figure 2.1) to give a coordination polymer that was investigated *via* $^{1}H$ NMR, UV-Vis, and fluorescence spectroscopies. The polymerization was also evaluated under various (metal-to-ligand) ratios. However, additional product characterization was not pursued with respect to possible discrete structure formation as is standard practice for polymeric reactions. With reports[127] detailing related 60°-based *bis*terpyridine ligands (*e.g.* **2**) that give almost exclusively cyclic structures, we investigated further.

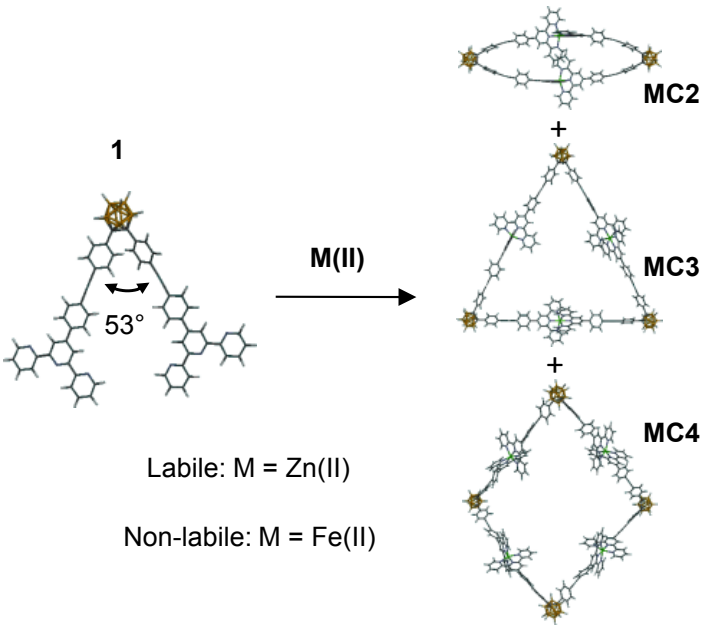


Scheme 2.1. Complexation of ligand **1**: Conditions for **ZnC2-4**: $Zn(OAc)_2 \cdot 2H_2O$, $CHCl_3$:MeOH (4:1 v/v); and for **FeC2-4**: $FeCl_2$, $CHCl_3$:MeOH (3:2 v/v). Representations of the cyclic dimer (MC2), trimer (MC3), and tetramer (MC4).

It was subsequently confirmed that, with a 1:1 metal to ligand ratio, *o*-carborane **1** forms predominately (85 %) macrocyclic structures, including the dimer, trimer, and tetramer along with traces of polymeric and oligomeric species. To assess the self-assembly of **1** in a non-labile system, $Fe^{II}$ was used to form stable <tpy-$Fe^{II}$-tpy>-based macrocycles (Scheme 1), which were easily separated by column chromatography. The ratio of trimer to dimer was *ca*. 8:1 with isolated yields of 30 and 4% after purifications steps. This indicates that the kinetic, cyclic product is a triangle, as is typical of a nominal 60° ligand, such as **1**. To assess self-assembly of **1** in a labile system, $Zn^{II}$ was used to form <tpy-$Zn^{II}$-tpy> complexes. Variable temperature $^1$H NMR and dilution studies indicated that the relative ratio of cyclic species was concentration and temperature dependent; whereas, with more dilute conditions and higher temperatures the dimer is

favored. As well, sufficient dilution drove the system exclusively to the cyclic dimer, a structure more characteristic of a *bis*-parallel ligand **3**. Furthermore, van't Hoff analysis indicated an equilibrium between the entropically favored dimer and the enthalpically favored trimer (Scheme 2.2). The resultant product distributions were characterized *via* ESI-TWIM-MS, $^{1}$H NMR, and 2D NMR (COSY, NOESY). Molecular modeling was undertaken on the dimer, trimer, and tetramer species in order to obtain additional structural insights.

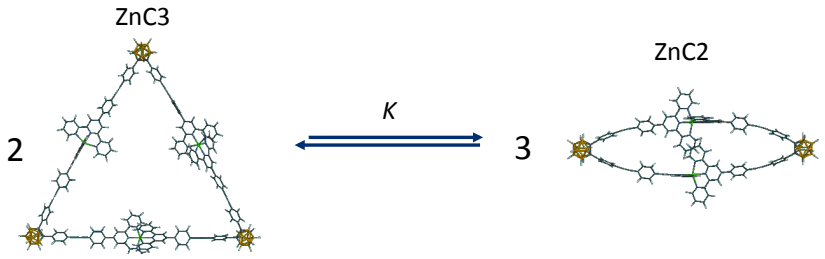


Scheme 2.2 Equilibrium between **ZnC3** (trimer) and **ZnC2** (dimer).

## 2.2 Results and Discussion

**$^{1}$H NMR of Zinc Complexes**. Following reaction of the *bis*ligand **1** with $Zn(OAc)_2$ to give $\mathbf{Zn_n(1)_n}$, the $^{1}$H NMR spectrum revealed two sets of terpyridine resonances with an integration ratio of *ca*. 0.8:1. suggesting that there are multiple species present. The $^{1}$H NMR spectrum was consistent with the presence of cyclic structures where the 6,6" tpy*H* signals shifted upfield from 8.75 ppm to 7.73 and 7.85 ppm (Figure 2.2), which is indicative of a *bis*terpyridine $Zn^{II}$ complex. COSY $^{1}$H NMR confirmed two discrete sets of terpyridine protons. For each set, cross peaks show coupling from the 3, 3" to 4, 4" to 5, 5" to 6, 6" protons as is shown in Figure 2.3.

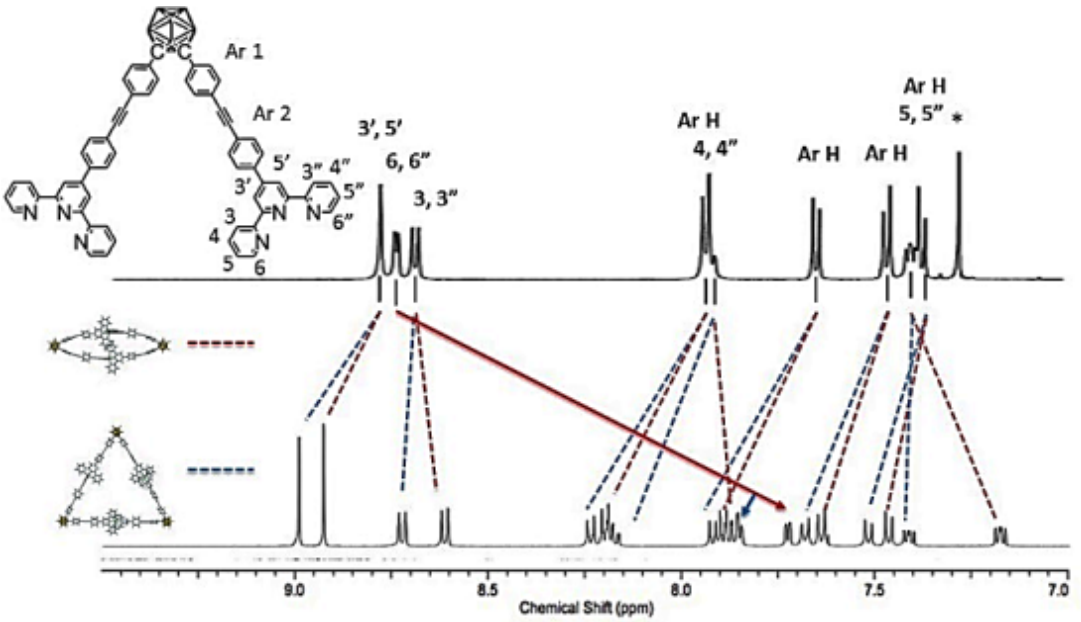


Figure 2.2 500 MHz $^{1}$H NMR spectra. Top – neat ligand **1** ($CDCl_3$) and bottom – **Zn$_n$(1)$_n$** in $CD_3CN$. (*- $CHCl_3$).

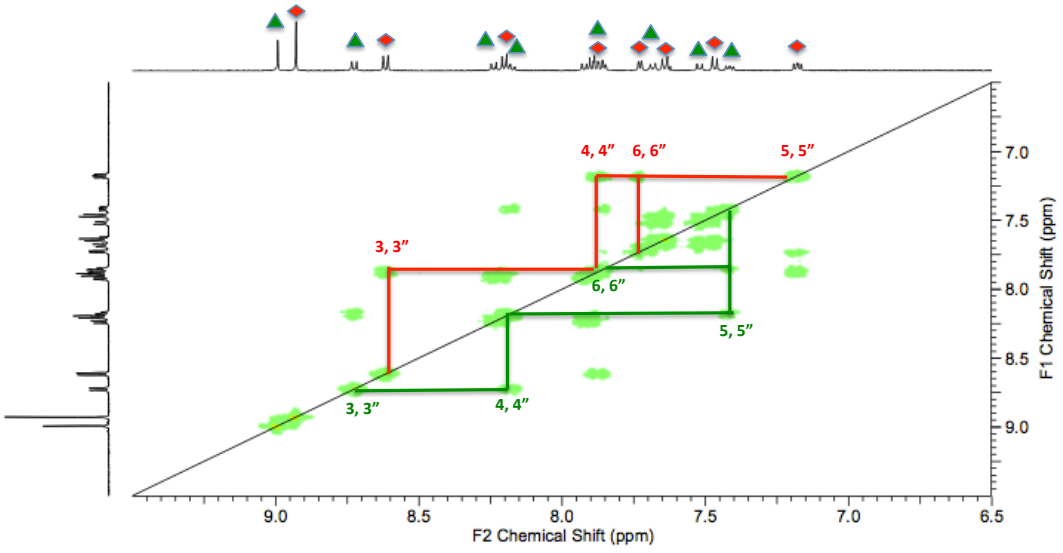


Figure 2.3 COSY spectra for **ZnC2 – C3** mixture, aromatic region, in $CD_3CN$. The red diamonds and lines are for **ZnC2** (dimer). The green triangles and lines are for **ZnC3** (trimer).

**Mass Spectrometry of the Zinc Complexes**. Multiple species were observed *via* ESI-MS including dimer (**ZnC2**), trimer (**ZnC3**), and tetramer (**ZnC4**) (Figure 2.4). The most prominent peaks correspond to the 4+, 3+, and 2+ states of the cyclic dimer, which was initially unexpected.

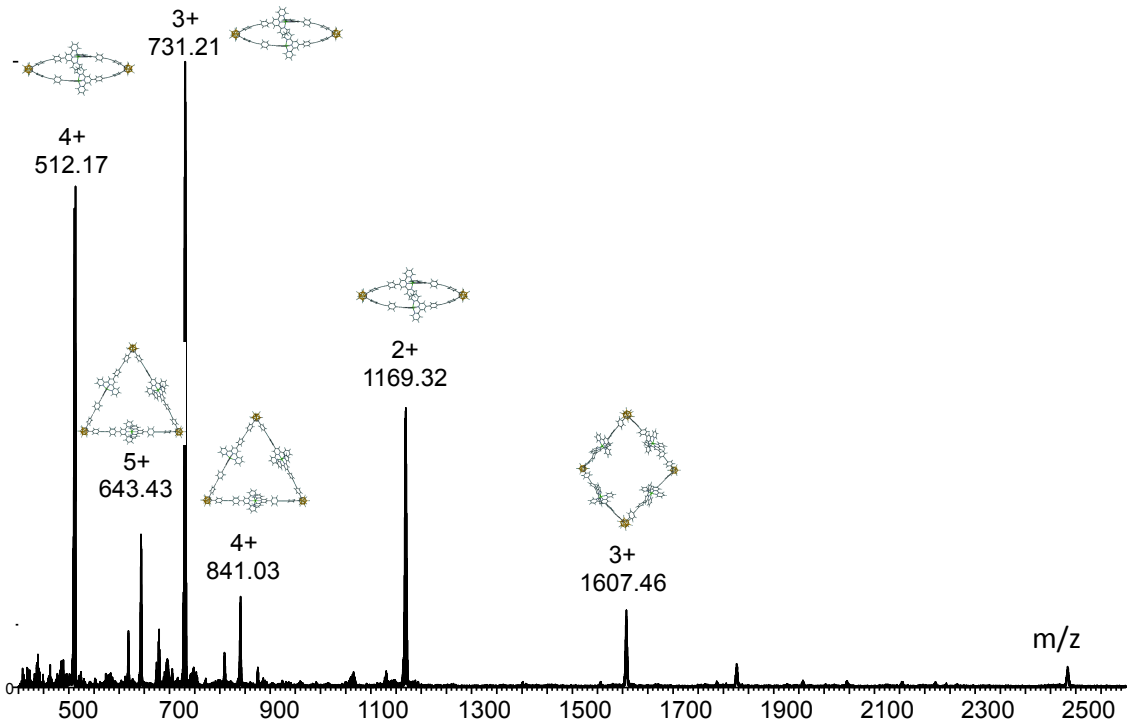


Figure 2.4 ESI – MS of zinc complexes (**ZnC2-ZnC4**) at 0.6 mg/ml.

**Effects of Concentration on the Zinc Complexes**. The $\mathbf{Zn}_n\mathbf{(1)}_n$ system showed a concentration dependence; thus, a dilution study was performed on the $\mathbf{Zn}_n\mathbf{(1)}_n$ system in $CD_3CN$. $^1H$ NMR spectra were taken at each concentration and the relative proportion of cyclic species was assessed *via* integration of the two 3',5' singlets (Figure 2.5). Upon dilution, the singlet at 8.99 ppm diminishes relative to the singlet at 8.93 ppm indicating an equilibrium shift toward the dimer relative to the trimer. And, the $^1H$ NMR and ESI-

MS data showed the dimer **ZnC2** as the major product (Figures 2.5 and 2.6). ESI–MS analysis of a dilute solution of $\mathbf{Zn}_n\mathbf{(1)}_n$ (20 μg/mL) supports the presence of the dimer **ZnC2** (Figure 2.6). The ESI-TWIM-MS plot (bottom of Figure 2.6) shows the expected step pattern and does not indicate the presence of superimposed isomers or conformers. Thus, the more shielded set of protons is exclusively from the dimer. This shift to an entropically favored species follows Le Chatelier's Principle. As concentration is decreased, the system responds by shifting the equilibrium toward the species assembled with fewer components. The sharp, distinct peaks from each set of tpy protons indicate a rapid equilibrium between molecular architectures relative to the NMR time scale.

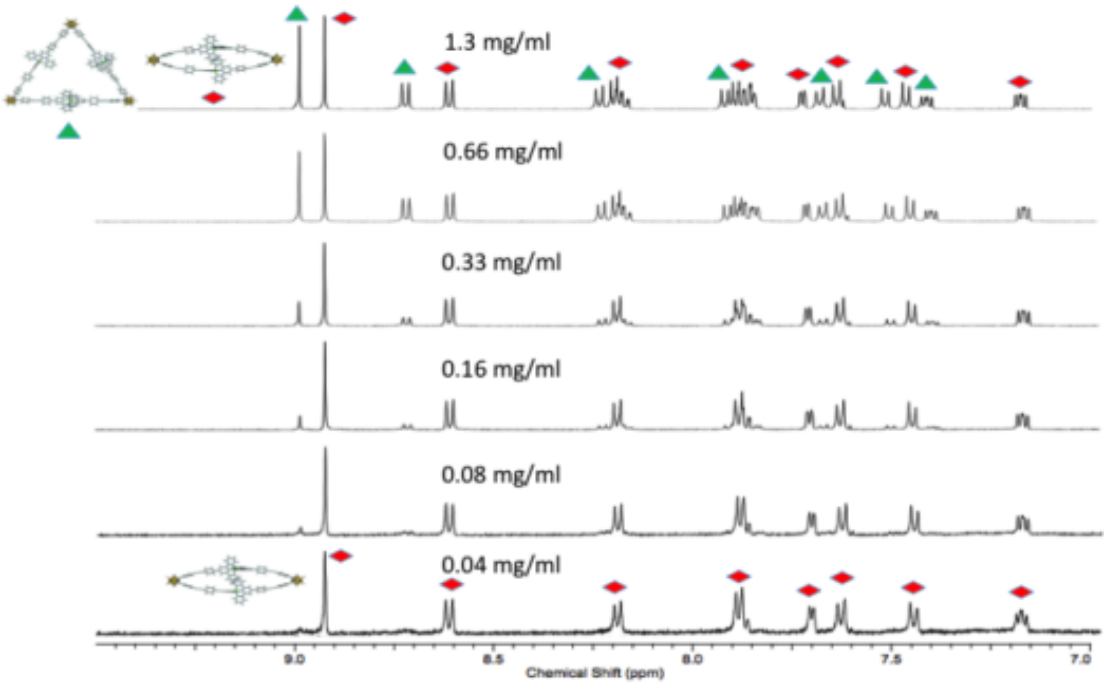


Figure 2.5 Dilution effect on ratio of **ZnC2** to **ZnC3**. Each subsequent spectrum was measured after 1:1 dilution with $CD_3CN$.

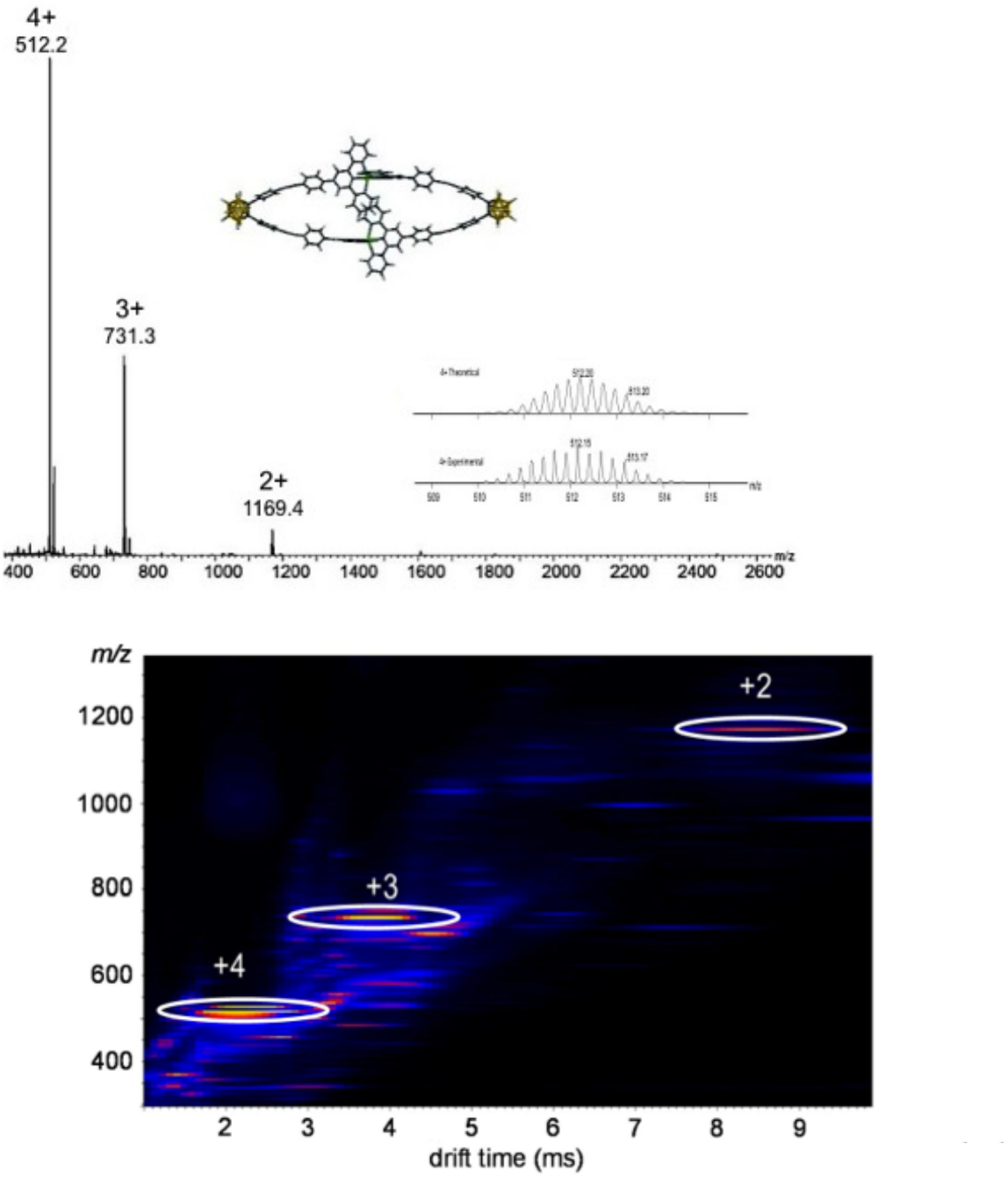


Figure 2.6 ESI-MS of **ZnC2** under dilute conditions ([$\mathbf{Zn}_n\mathbf{(1)}_n$] = 20 μg/mL) showing only the dimeric species, along with the theoretical and experimental isotope patterns of the 4+ charge state (top). 2D ESI-TWIM-MS plot (m/z *vs.* drift time) for **ZnC2** (bottom).

**Effect of Temperature on the Zinc Complexes**. As the temperature was lowered, the chemical shift of the trimer signals remains unchanged; however, the 4,4" and 5,5" peaks of **ZnC2** shifted upfield (Figure 2.7). This chemical shift was also observed in a previous report about interlocked <tpy-$M^{II}$-tpy> complexes.[169] This result implies that, as molecular motion is decreased, the shielding effect from the cyclic dimer's unique structure is enhanced. Conversely, the environment of the aromatic protons of **ZnC3** is much less sensitive to the degree-of-molecular motion. Previous reports indicate that the proton signals of cyclic <tpy-$M^{II}$-tpy> trimers assembled from 60° ligands show negligible change in chemical shift when the temperature is varied.[129]

Temperature also affected the relative proportions of cyclic species as measured *via* integration of the respective 3',5" peaks. The presence of the dimeric species (**ZnC2**) is proportional to temperature. At 70 °C, the ratio of the 3',5' *H*-signal of **ZnC2** to the 3',5' *H*-signal of **ZnC3** was 1:0.8; whereas, at -40 °C, the ratio was 1:1.3. The entropic driving force is proportional to temperature; thus, higher temperatures favor the dimeric construct. The shift toward dimer at higher temperatures also suggests that its formation is endothermic. At lower temperatures, peak broadening is indicative of the slowing equilibrium between molecular architectures relative to the NMR timescale.

The variable temperature NMR data were used to estimate the enthalpic and entropic components of the equilibrium.

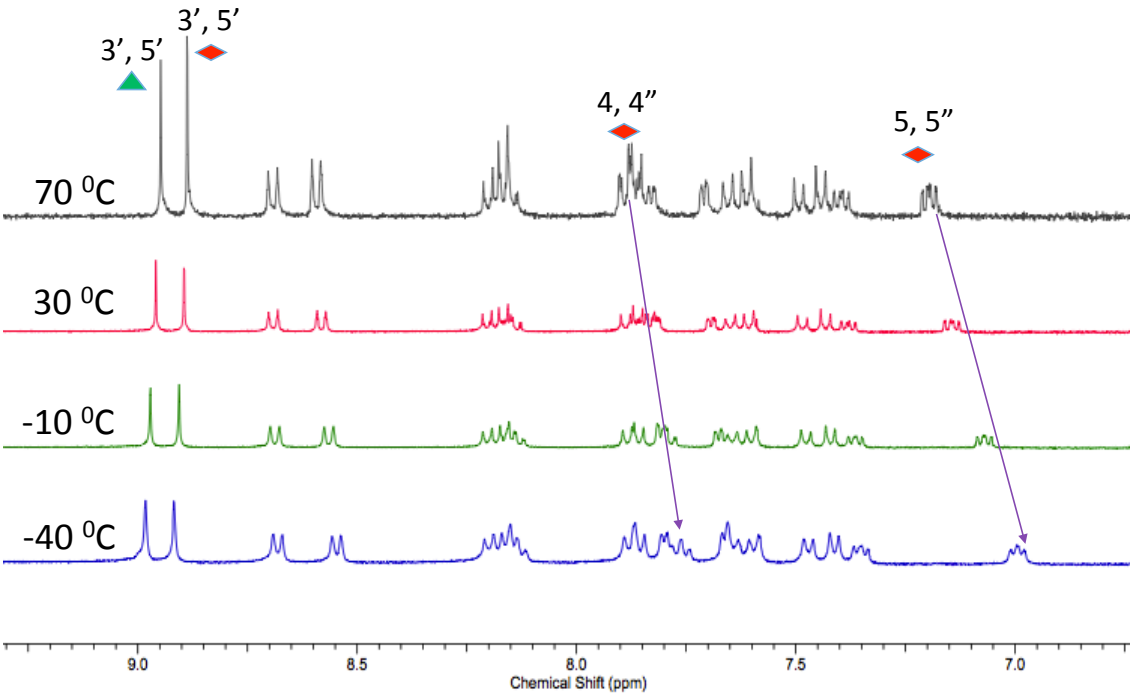


Figure 2.7 Variable temperature $^{1}$H NMR of $\mathbf{Zn_n(1)_n}$ study on a 400 MHz spectrometer in $CD_3CN$.

Mole fractions were derived from integration of each 3',5' peaks. The assumption was made that the upfield peak represents trimer, exclusively. This assumption is safest at the higher end of the temperature range studied so the data from 10 – 70 °C were used. Assuming ideal behavior, $K_{eq}$ for the equilibrium shown in Scheme 2 can be written:

$$K_{eq} = \frac{\{dimer\}^3}{\{triangle\}^2}$$

(1)

The van't Hoff equation is shown in (2).

$$ln\ K_{eq} = -\frac{\Delta H_{eq}}{RT} + \frac{\Delta S_{eq}}{R}$$

(2)

A van't Hoff plot was constructed and analyzed. Figure 2.8 shows a table of values and a plot of lnK vs. 1/T. $\Delta H_{eq}$ for conversion of two triangles into three dimers was found to be positive (*ca*. 12 kJ/mol) indicating that dimer formation is endothermic and suggesting that the cyclic dimer is the more strained structure. $\Delta S_{eq}$ was positive (*ca*. 40 J/mol K) reflecting the increase in macrocycles, as the equilibrium shifts to the dimeric species.

Table 2.1 van't Hoff data

| Set T(K) | T(K) | 3'5' dimer | 3'5' outer | Dimer mol frac | outer mol frac | K | 1/T | lnK |
|---|---|---|---|---|---|---|---|---|
| 343 | 345.521 | 1 | 0.83 | 0.64 | 0.36 | 2.1 | 0.0029 | 0.7 |
| 333 | 335.44 | 1 | 0.85 | 0.64 | 0.36 | 2.0 | 0.0030 | 0.7 |
| 323 | 325.359 | 1 | 0.92 | 0.62 | 0.38 | 1.6 | 0.0031 | 0.5 |
| 313 | 315.278 | 1 | 0.97 | 0.61 | 0.39 | 1.5 | 0.0032 | 0.4 |
| 303 | 305.197 | 1 | 1.06 | 0.59 | 0.41 | 1.2 | 0.0033 | 0.2 |
| 293 | 295.116 | 1 | 1.12 | 0.57 | 0.43 | 1.0 | 0.0034 | 0.0 |
| 283 | 285.035 | 1 | 1.17 | 0.56 | 0.44 | 0.9 | 0.0035 | -0.1 |

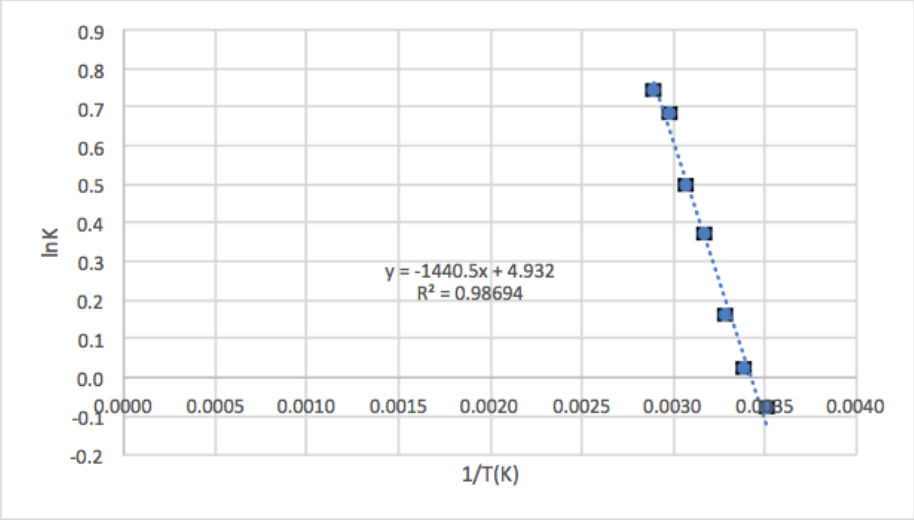


Figure 2.8 van't Hoff plot.

$\Delta H_{eq}$ was determined from the using the slope while $\Delta S_{eq}$ was determined from the y-intercept term. These results are similar to dynamic equilibration reported between triangles and squares in labile systems such as $Pd^{II}$ and $Pt^{II}$ with linear (180°) *bis*pyridyl

ligands.[173-178] Equilibrium pairs between dimeric and trimeric species are uncommon but have been reported.[179] This is, to best of our knowledge, the first reported cyclic dimer-trimer equilibrium driven *via* <tpy-$M^{II}$-tpy> complexation.

**Iron Complexes**

In order to isolate and study non-labile analogues of these cyclic species, **1** was reacted with $FeCl_2$ to generate <tpy-$Fe^{II}$-tpy> complexes, which are stable and separable *via* chromatography. ESI-MS of the crude reaction mixture revealed formation of a variety of cyclic species - primarily dimer, trimer, and tetramer (Figure 2.9). The most prominent species in the spectra is trimer, **FeC3**, showing charge states 3+ through 6+. Larger macrocycles, such as pentamer and hexamer, were detected at trace levels.

The dimer and trimer species were isolated chromatographically on alumina using $H_2O$/MeCN/sat'd $KNO_3$(aq) (1:30:1; v/v/v) and converted to $PF_6^-$ counterion. The trimer was the main cyclic product isolated as would be expected of a nominal 60° ligand. Both products were characterized by $^1$H NMR (Figure 2.10) and ESI-TWIM-MS. Figure 2.12 shows the spectrum and plot for **FeC2**.

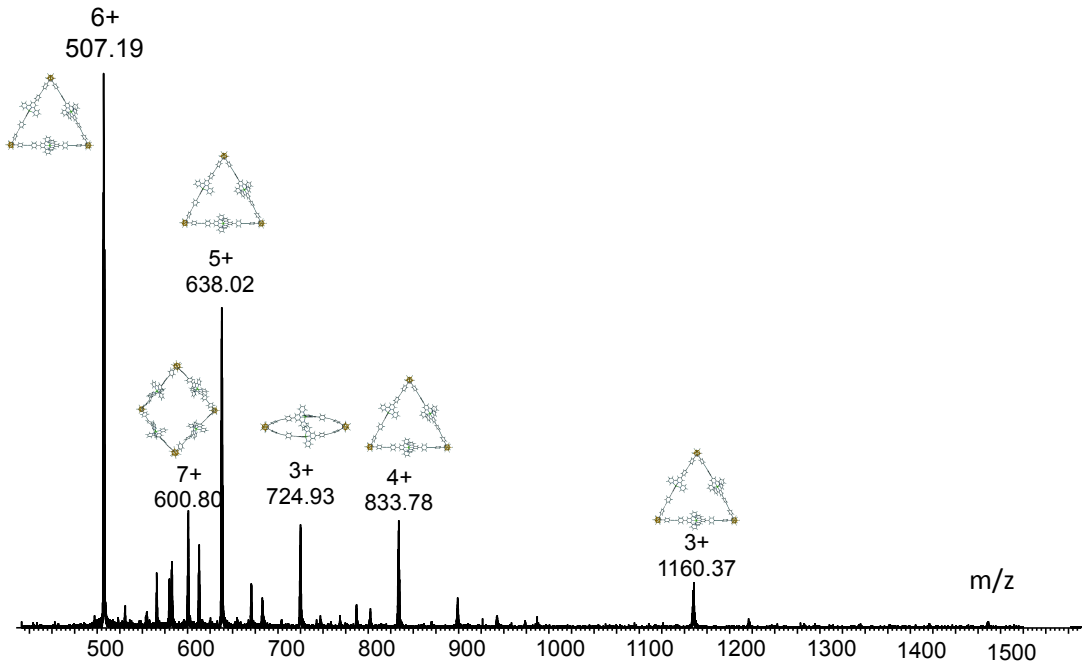


Figure 2.9 ESI-MS of the Fe(II) reaction mixture after precipitation with $NH_4PF_6$. Peaks for **FeC2** – **FeC4** are marked.

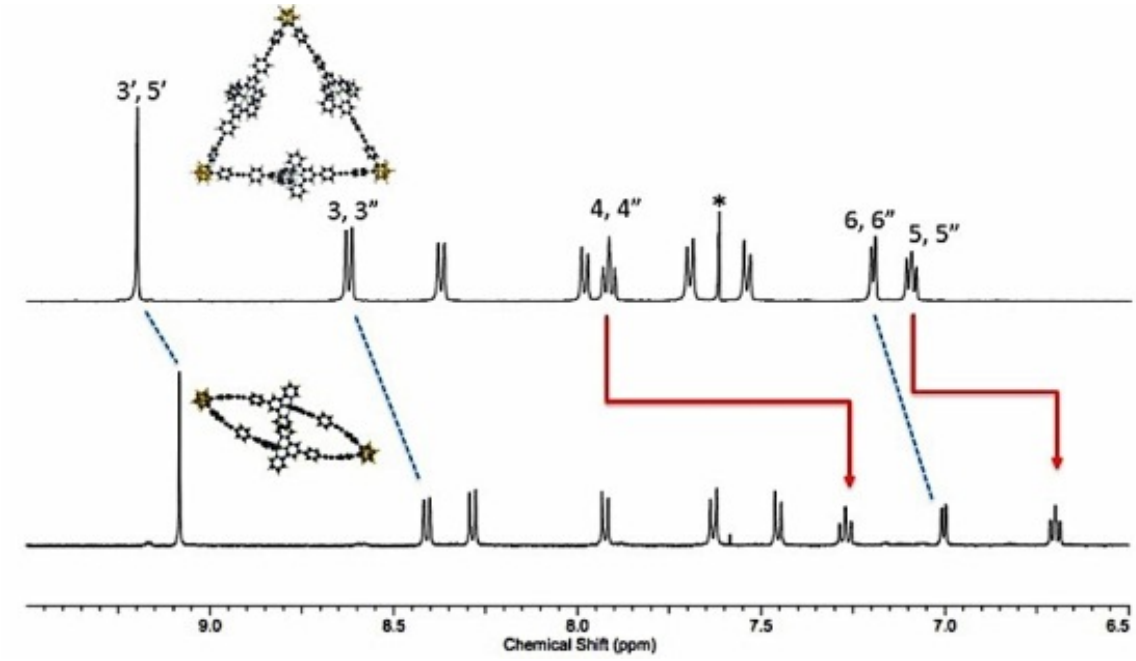


Figure 2.10 $^1$H NMR spectra of the cyclic dimer **FeC2** (bottom) and trimer **FeC3** (top) in $CD_3CN$. (*$CHCl_3$)

$^{1}$H NMR spectra of both species are consistent with a cyclic structure, as the 6,6" *H*-signals are shifted upfield indicative of *bis*terpyridine complex formation. The terpyridine protons of the complexed dimer show a dramatic upfield shift relative to those of the trimer, particularly the 4,4"- and 5,5"- protons. This observed difference can be attributed to the more highly shielded proton environment that results from proximity interactions of the dimer's complexes as seen in molecular models. The sharp tpy proton resonances observed in the dimer spectra also suggest correlated rotation of the close complexes at a rate greater than the NMR timescale. Note that superposition of these spectra would match the pattern seen with the initial zinc system *i.e.* two distinct sets of terpyridine protons and that the dimeric species is further upfield. Assignments were confirmed *via* COSY as shown in Figure 2.11. with cross peaks showing coupling from the 3, 3" to 4, 4" to 5, 5" to 6, 6" protons for each.

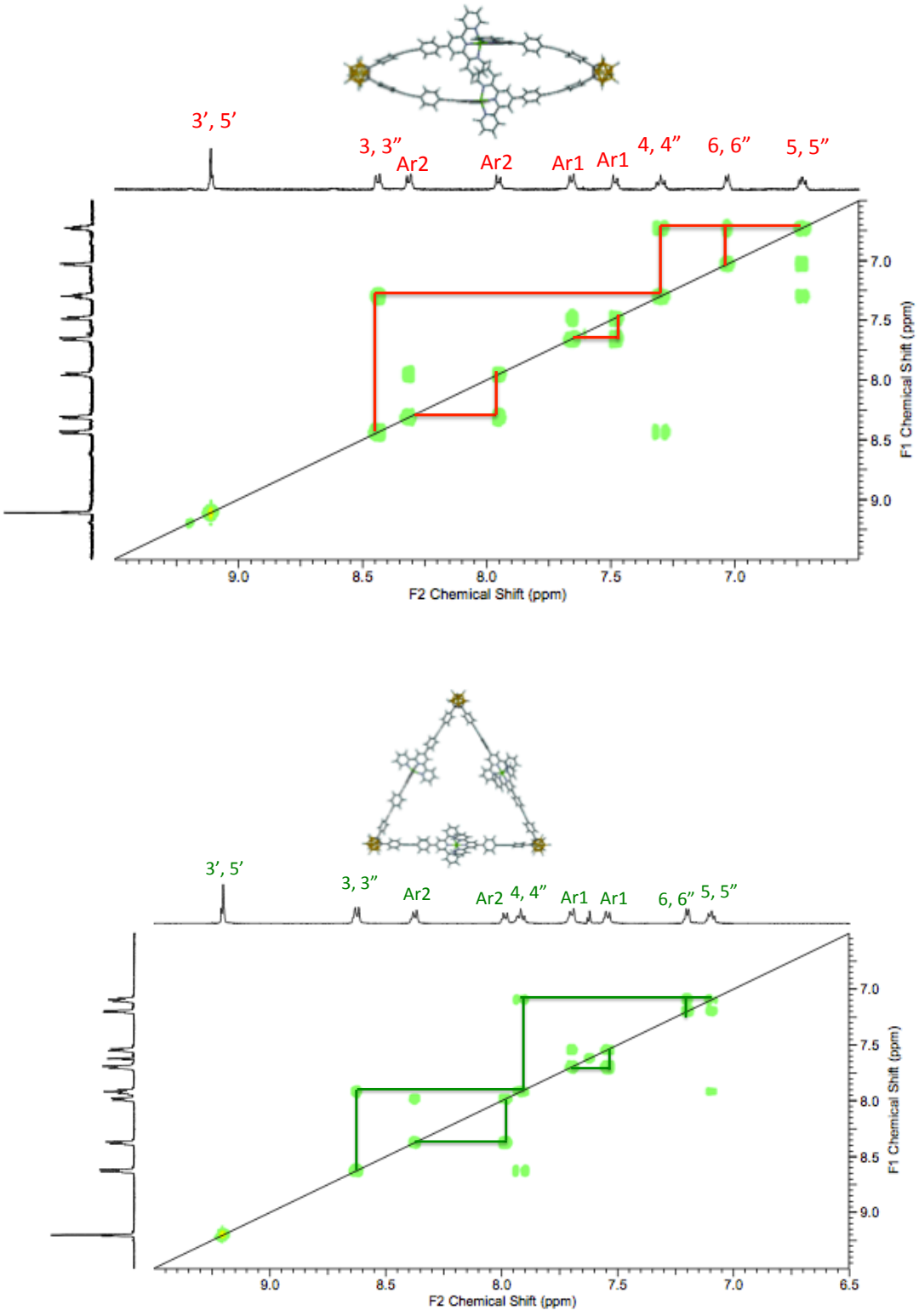


Figure 2.11 COSY NMR of **FeC2** (top) and **FeC3** (bottom) in $CD_3CN$.

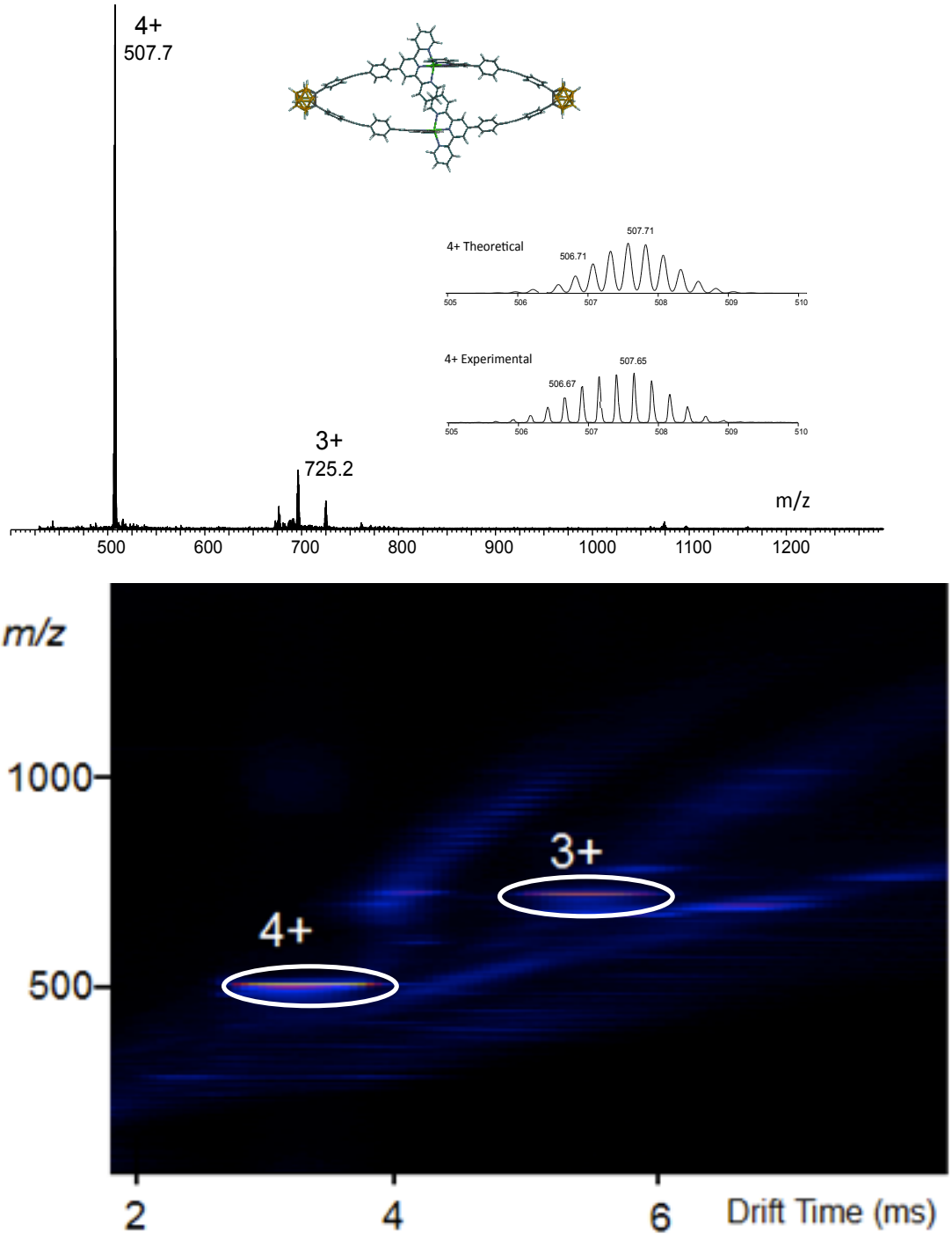


Figure 2.12 ESI-MS spectrum for **FeC2** (**1**) (top) and 2D ESI-TWIM-MS plot (m/z *vs.* drift time) for **FeC2** (bottom).

Figure 2.12 (top) shows the ESI-MS spectrum for the **FeC2** species, which includes the 4+ and 3+ charge states as well as theoretical and experimental isotope patterns for the 4+ charge state. The ESI-TWIM-MS plot (bottom) shows the expected step pattern and does not indicate the presence of superimposed isomers or conformers. Similar results were observed for the **FeC3** species.

Experimental Collisional Cross Sections (CCSs)[90, 180-184] were calculated, based on TWIM data, to further characterize the different architectures (Table 2.1). The CCS values are consistent from charge state to charge state, indicating shape persistence of these structures. Relative CCSs for these architectures show a linear trend with respect to mass. Energy minimized structures were generated for **FeC2**, **FeC3**, and **FeC4** *via* simulated annealing. Theoretical CCS values were calculated *via* the projection approximation (PA) method using MOBCAL and found to be 443+/-3, 720+/-2, and 925+/-11 $Å^2$ for **FeC2**, **FeC3**, and **FeC4**, respectively, corresponding well with experimental values. The population of model structures for both **FeC3** and **FeC4** each included a set of folded conformations (Figure 2.13) showing intramolecular π-π interactions. Their CCS values were calculated separately and found to be 580+/-3 and 668+/-40 $Å^2$, respectively; however, the experimental CCS values match closely with the circular, rather than folded structures.

Table 2.2 Experimental Collision Cross Sections (CCSs) of **FeC2**, **FeC3**, and **FeC4.**

| | CCS (Å$^2$) | | |
|---|---|---|---|
| **Z** | FeC2 | FeC3 | FeC4 |
| 3+ | 507 | 723 | - |
| 4+ | 496 | 770 | - |
| 5+ | - | 805 | - |
| 6+ | - | 756 | - |
| 7+ | - | - | 1068 |
| Average | 502 | 764 | 1068 |
| Std. Dev. | 8 | 34 | - |

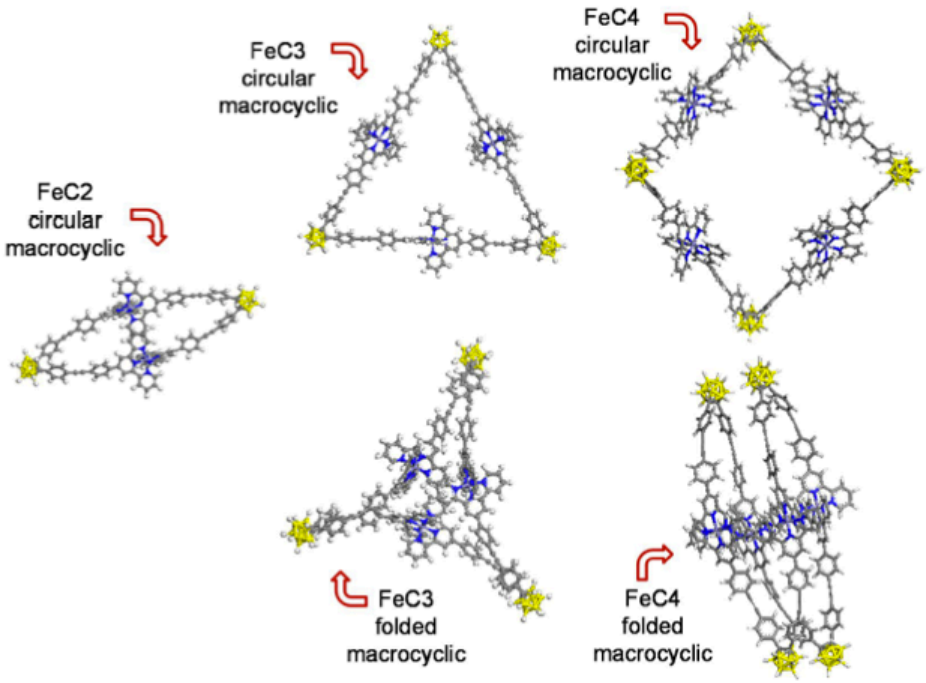


Figure 2.13 Energy-minimized structures of **FeC2**, **-C3**, and **-C4** obtained by molecular mechanics/dynamics simulations. [Used with permission of Wiley: *Macromol. Rapid Comm.*, **2015**, *36*, 1539 - 1552.]

**Molecular Modeling**

Molecular modeling provided insight into experimental findings including the proton shifts relative to the trimer and ligand's ability to behave similar to a *bis* parallel ligand. Figure 2.14 shows the cyclic, dimer species; the planar cyclic trimer; and the non-planar cyclic tetramer. The tetramer architecture is analogous to previously reported Dondorff rings.[128] The non-planar conformation of the tetramer reduces strain relative to a planar conformation and is typical for a nominal 60° bis-ligand. The angle between the ligand arms is essentially the same as for the trimer, thus there is little or no enthalpic penalty to its formation. A cyclic dimer species generally formed from *bis* parallel ligands such as **3**. A cyclic dimer such as this has not been previously reported with 60° oriented *bis*-terpyridyl ligands. Figure 2.15 shows a close up of the dimer model.

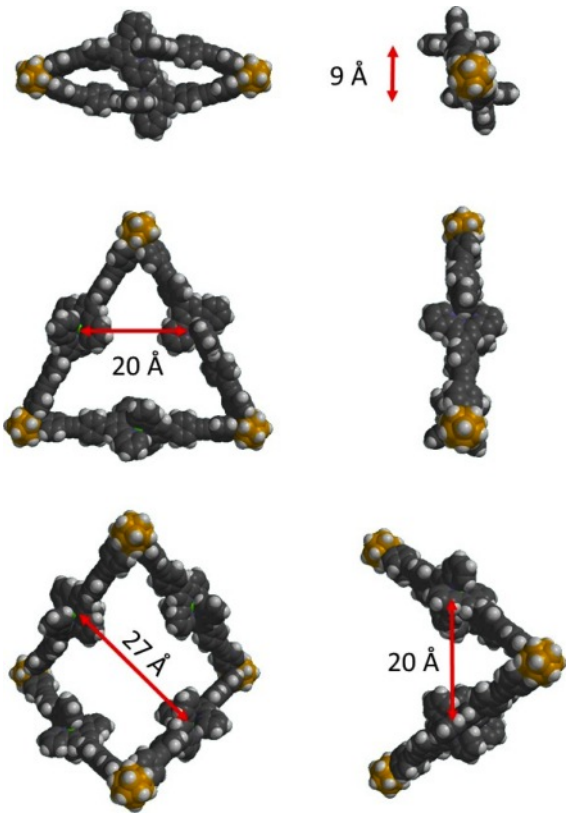


Figure 2.14 Space-filling models of **FeC2**, **FeC3**, and **FeC4**: top view (left) and side view (right). Color scheme: B: yellow; H: white; C: grey; N: purple; Fe: green; Fe-Fe distances are shown with red arrows.

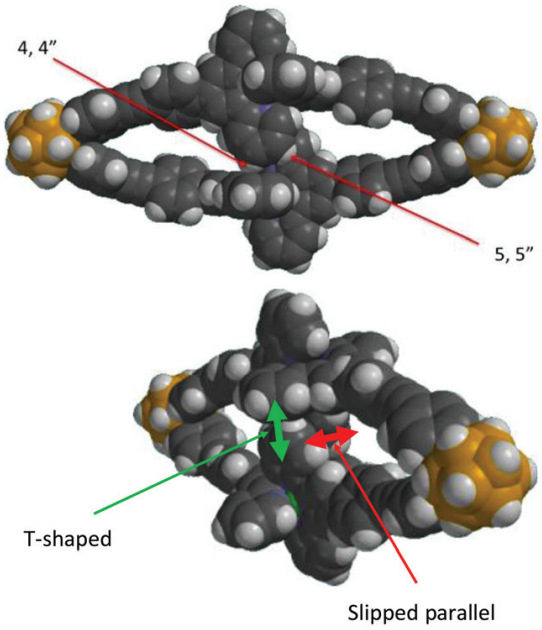


Figure 2.15 Space-filling models of **FeC2** showing interlocked <tpy-$M^{II}$-tpy> complexes. Color scheme: B: yellow; H: white; C: grey; N: purple; Fe: green. Shielded 4,4" and 5,5" protons are noted (top). Regions of T-shaped (CH-π) and slipped parallel (π-π) interactions are noted (bottom).

The model indicates that the ligand arms must adopt a tighter, more strained angle (*ca.* 30°) to form the cyclic dimer. The inner 4,4" and 5,5" protons are projected into the adjacent complex unit and should be more highly shielded than the cyclic trimer. In Figure 2.10, the $^{1}$H NMR of this cyclic dimer showed significant upfield shifting of the complexed 4,4" and 5,5" protons relative to the trimer as expected for a close-packed, metal-terpyridine moiety. $^{1}$H NMR also gave a very crisp, single set of tpy protons and yet the model shows that the 4,4" and 5,5" protons are also exposed to a non-shielded exterior of the molecule. This suggests gear-like correlated rotation of the intertwined complexes. These results match with observations seen in previous interlocked

species.[118, 169] Both slipped parallel (π-π) and T-shaped (CH-π) stacking interactions can be envisioned. Dimensions of the model also match closely those reported[169] for interacting tpy complexes formed from *bis*parallel ligands. For example, the metal to metal distance in **FeC2** is *ca.* 9Å *vs.* 8.8Å in the reported complex and π-π stacking distance in **FeC2** is *ca.* 4Å *vs.* reported 3.7-3.9Å for the reported complex.

Factors contributing to the ability of this ligand to form a cyclic dimer include: 1) inherent flexibility of the alkyne moieties, 2) favorable π-π and CH-π interactions between the interacting complexes, 3) length of the arm possessing two phenyls and an alkyne spacer, and 4) 53° angle and C-C bond length of *o*-carborane.

Though the alkyne group is generally linear, it is flexible as exhibited in cyclooctyne and larger cycloalkynes, where the alkyne group can adopt a *cisoid* bend due to covalent bonding constraints. In the case of cyclodecyne, the internal strain is reported to be *ca.* 20 kJ/mol.[185] So, while there would be an energetic penalty to adopting the more strained conformation of the dimer - it is not prohibited. Conversely, the π-π interactions upon dimer formation should be energetically favorable at a similar magnitude. Such π-π interactions are generally described as parallel, T-shaped, and slipped-parallel and their respective energies reported[186] to be -6.2, -10.3, and -10.4 kJ/mol, respectively. In the specific case of π stacking between *bis*terpyridine-metal complexes, evidence for its favorability is seen in Constable's examples, where the complexes interact, even when the spacers linking *bis*terpyridines are long and highly flexible.[118] Therefore, the enthalpic penalty of forming these more strained dimers is likely offset to some degree by favorable π-π and CH-π interactions. Also, adequate arm length *via* two phenyl spacers removes steric obstruction to dimer formation and, though the alkyne is the most flexible

part of the arm, it does provide additional structure for strain distribution. Molecular modeling also indicates slight bending of the phenyl rings in the dimer. Characteristics unique to carborane also likely play a role. Relative to the phenyl ring in a ligand, such as **1**, *o*-carborane has more narrow bite angle (53° *vs*. 60°) and longer C to C bond length. While the phenyl C to C bond length is *ca.* 1.4Å, in carborane the C to C bond is reported[187] to range from 1.65 to 1.75Å in the crystal state, indicating that it is not only longer but can adopt a variety of lengths depending upon conditions.

## 2.3 Conclusions

The self-assembly characteristics of the recently reported[2] *bis*terpyridyl *o*-carborane **1** were examined and it was found to undergo macrocyclizations when reacted with $Zn^{II}$ and $Fe^{II}$; characterization was achieved by NMR, ESI- and ESI-TWIM-MS, and molecular modeling. More specifically, using a 1:1 metal-to-ligand ratio, the cyclic dimer, trimer, and tetramer were confirmed as major products. Under kinetic control, *i.e*. for the $Fe^{II}$ complexes, the predominant cyclic product was trimeric; whereas, under thermodynamic control, *i.e*. for the $Zn^{II}$ complexes, ligand **1** formed the dimer exclusively, given adequate, entropic driving force. Molecular modeling suggests that the ligand's alkyne moieties, arm length, and favorable π-π interactions, upon complexation, play a role in enabling this unique behavior. Notably, the potential to obtain discrete products from polymeric-type reactions should be considered, as has been observed in other cases, where polydentate ligands were present.[44,48-50]

## 2.4 Experimental

Chemicals were commercially purchased and used without further purification. Thin layer chromatography (TLC) was conducted on flexible sheets (Baker-flex) precoated with $Al_2O_3$ (IB-F) or $SiO_2$ (IB2-F) and visualized by UV light. Column chromatography was conducted using basic $Al_2O_3$, Brockman Activity I (60-325 mesh) or $SiO_2$ (60-200 mesh) from Fisher Scientific. $^1H$ NMR spectra were recorded on a Varian 500 MHz spectrometer. Variable temperature NMR was conducted on a Varian 400 MHz NMR spectrometer; the temperature was varied from -40 to +70 °C in 10 °C increments. The temperature range was limited by the melting and boiling points of $CD_3CN$. Electrospray ionization (ESI) mass spectra (MS) were obtained on a Synapt HDMS quadrupole/time-of-flight (Q/ToF) mass spectrometer (Waters Corp., Milford, MA). The Synapt Q/ToF instrument contains a travelling wave ion mobility (TWIM) device, in which ions drift under influence of a traveling wave field against the flow of the carrier gas ($N_2$). This process disperses ions based on their mass, charge, and shape. The separated ions travel through a transfer cell from which they are conveyed to an orthogonal ToF analyzer for *m/z* measurement. The acquired data are typically displayed in 2-D plots of *m/z* ratio *vs*. the corresponding drift time through the IM cell. TWIM MS experiments were performed under the following conditions: ESI capillary voltage, 1 kV; sample cone voltage, 8 V; extraction cone voltage, 3.2 V; desolvation gas flow, 800 L/h ($N_2$); trap collision energy (CE), 3 eV; transfer CE, 1 eV; trap gas flow, 1.5 mL/min (Ar); TWIM cell gas flow, 22.7 mL/min ($N_2$); sample flow rate, 5 μL/min; source temperature, 30 °C; desolvation temperature, 40 °C; TWIM wave height, 7.5 V; and TWIM wave velocity, 350 m/s.

**Collision Cross-section (CCS) Calibration.** The drift time scale of the TWIM-MS experiments was converted to a collision cross-section scale by calibration with ions of known CCS, following the procedure established by Ruotolo and coworkers.[188] Briefly, the corrected collision cross sections of the molecular ions of insulin (bovine pancreas), ubiquitin (bovine red blood cells), and cytochrome C (horse heart), obtained from published work, were plotted against the corrected drift times (arrival times) of the corresponding molecular ions measured in TWIM-MS experiments at the same traveling-wave velocity, traveling-wave height and ion-mobility gas flow settings, *viz.* 350 $ms^{-1}$, 7.5 V and 22.7 mL $min^{-1}$. All charge states observed for the calibrants were used in the construction of the curve.

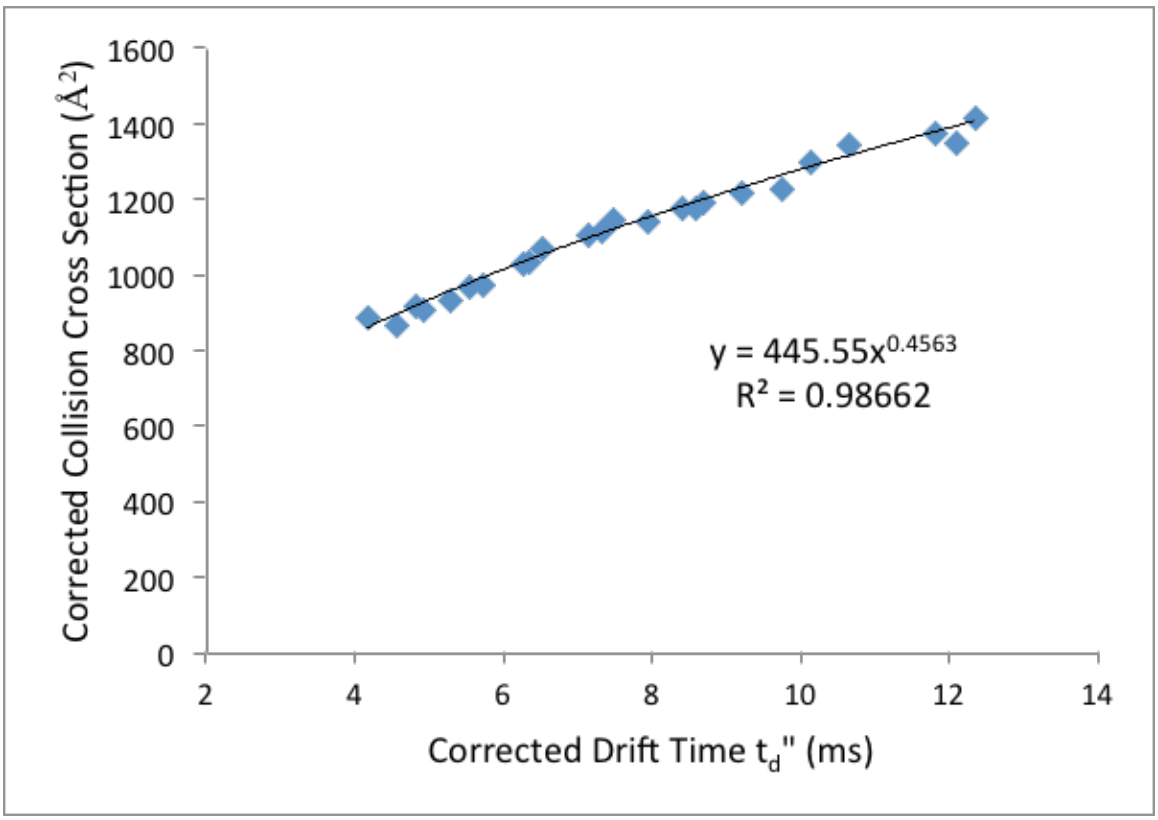


Figure 2.16 Calibration curve constructed from corrected drift times against corrected published cross sections for the multiply charged ions arising from insulin (bovine pancreas), ubiquitin (bovine red blood cells) and cytochrome C (horse heart). Drift times were measured at a traveling wave velocity of 350 m/s and a traveling wave height of 7.5 V.

TWIM data analyses were conducted using the MassLynx 4.1 and DriftScope 2.1 programs provided by Waters. Modeling and energy minimization of complexes were done with Spartan (Wavefunction, Inc.). Molecular dynamics for theoretical CCS of structures was conducted with the Materials Studio version 6.0 program using the Anneal and Geometry Optimization tasks in the Forcite module (Accelrys Software, Inc.). The counterions were omitted. An initially energy-minimized structure was subjected to 10 annealing cycles with initial and mid-cycle temperatures of 300 and 500 K, respectively,

five heating ramps per cycle, one hundred dynamics steps per ramp, and one dynamics step per femtosecond. Constant volume/constant energy (NVE) ensemble was used; the geometry was optimized after each cycle. All geometry optimizations used a universal force field with atom-based summation and cubic spline truncation for both the electrostatic and van der Waals parameters. 50 candidate structures were generated for the calculation of collision cross sections.

***Bis*terpyridyl *o*-carborane 1** was synthesized and characterized according to the literature.[154]

**Complex synthesis**.

**$Zn_n(1)_n$** ($n$ = 2 - 4) **(ZnC2 – ZnC4)**: To a stirred solution of ligand **1** (23 mg, 24 μmol) in $CHCl_3$ (10 mL), was added a MeOH (2.4 mL) solution of $Zn(OAc)_2 \cdot 2H_2O$ (2.4 mL, 24 μmol), and then the mixture was stirred at 25 °C for 1 h. Excess (10X) solid $NH_4PF_6$ was added and stirred. The resultant cream-colored precipitate was filtered and washed with MeOH to give (85 %) complex **$Zn_n(1)_n$**: 24 mg, m.p. >300 °C; $^1$H NMR ($CD_3CN$, 500 MHz): δ = 8.99 (s, 12H, 3',5'-tpy*H*), 8.93 (s), 8.73 (d, $J$ = 7.9 Hz), 8.62 (d, $J$ = 8.2 Hz), 8.24 (d, $J$ = 8.8 Hz), 8.18 (s), 7.81 - 7.97 (m), 7.73 (d, $J$ = 5.4 Hz), 7.68 (d, $J$ = 8.8 Hz), 7.64 (d, $J$ = 8.8 Hz), 7.52 (d, $J$ = 8.5 Hz), 7.47 (d, $J$ = 8.5 Hz), 7.41 (dd, $J$ = 8.8 Hz), 7.19 (dd, $J$ = 5.9 Hz), 2.30 – 3.00 (m); ESI-MS (*m/z*) **ZnC2**: 512.2 $[M\text{-}4PF_6]^{4+}$ (Calcd. *m/z* = 512.2), 731.2 $[M\text{-}3PF_6]^{3+}$ (Calcd. *m/z* = 731.3), 1169.3 $[M\text{-}2PF_6]^{2+}$ (Calcd. *m/z* = 1169.4); **ZnC3**: 643.4 $[M\text{-}5PF_6]^{5+}$ (Calcd. *m/z* = 643.4), 841.0 $[M\text{-}4PF_6]^{4+}$ (Calcd. *m/z* = 841.0); **ZnC4**: 1607.5 $[M\text{-}3PF_6]^{3+}$ (Calcd. *m/z* = 1607.4)

**$Fe_n(1)_n$** ($n$ = 2-4): To a stirred $CHCl_3$:MeOH (3:2 v/v, 300 mL) solution, **1** (28 mg, 29.2 μmol) was added, and a MeOH solution of $FeCl_2 \cdot 4 \cdot H_2O$ (2.92 mL, 29.2 μmol)

was added dropwise. After stirring at 25 °C for 16 h, the reaction mixture was concentrated *in vacuo* to give a purple solid, which was column chromatographed ($SiO_2$) using $H_2O$/MeCN/satd. $KNO_{3(aq)}$ (1:30:1; v/v/v) to give the cyclic dimer ($R_f$ = 0.15) and trimer ($R_f$ = 0.07). Counterion exchange to $PF_6^-$ was achieved by dissolving the complex in $CHCl_3$:MeOH (1:1 v/v) and precipitating with excess (*ca.* 10X) $NH_4PF_6$. ESI-MS and $^1$H NMR were performed with a $PF_6^-$ counterion.

**Dimer [$Fe_2$(1)$_2$]** (**FeC2**): 1.5 mg (4%); $^1$H NMR ($CD_3CN$, 500 MHz): δ = 9.08 (s, 3',5'-tpy*H*, 8H), 8.41 (d, *J* = 8.1 Hz, 3,3"-tpy*H*, 8H), 8.29 (d, *J* = 8.3 Hz, Ar*H*, 8H), 7.92 (d, *J* = 8.3 Hz, Ar*H*, 8H), 7.63 (d, *J* = 8.6 Hz, Ar*H*, 8H), 7.45 (d, *J* = 8.3 Hz, Ar*H*, 8H), 7.27 (dd, $J_1 = J_2$ = 8.4 Hz, 4,4"-tpy*H*, 8H), 7.00 (d, *J* = 5.6 Hz, 6,6"-tpy*H*, 8H), 6.70 (dd, *J* = 6.5 Hz, 5,5"-tpy*H*, 8H), 2.32 - 2.95 ppm (m); ESI-MS (*m/z*): 725.2 $[M\text{-}3PF_6]^{3+}$ (Calcd *m/z* = 725.2), 507.7 $[M\text{-}4PF_6]^{4+}$ (Calcd *m/z* = 507.7)

**Trimer [$Fe_3$(1)$_3$]** (**FeC3**): 11.4 mg (30%); $^1$H NMR ($CD_3CN$, 500 MHz): δ = 9.17 (s, 3',5'-tpy*H*, 12 H), 8.60 (d, *J* = 8.0 Hz, 3,3"-tpy*H,* 12H), 8.35 (d, *J* = 8.3 Hz, Ar*H*, 12H), 7.95 (d, *J* = 8.7 Hz, Ar*H*, 12H), 7.89 (t, *J* = 7.8 Hz, 4,4"-tpy*H*, 12H), 7.66 (d, *J* = 8.7 Hz, Ar*H*, 12H), 7.51 (d, *J* = 8.7 Hz, Ar*H*, 12H), 7.17 (d, *J* = 5.4 Hz, 6,6"-tpy*H*, 12H), 7.03-7.11 (m, 5,5"-tpy*H*, 12H), 2.24 - 3.00 (m); $^{13}$C NMR (125 MHz, $CD_3CN$, ppm): δ = 85.47, 89.98, 91.31, 121.69, 124.09, 124.9, 125.37, 127.55, 128.38, 130.70, 131.5, 131.76, 133.00, 137.24, 138.97, 149.51, 153.25, 158.13, 160.59; ESI-MS (*m/z*): 507.6 $[M\text{-}6PF_6]^{6+}$ (Calcd *m/z* = 507.5), 638.0 $[M\text{-}5PF_6]^{5+}$ (Calcd *m/z* = 638.0), 833.9 $[M\text{-}4PF_6]^{4+}$ (Calcd *m/z* = 833.8), 1160.1 $[M\text{-}3PF_6]^{3+}$ (Calcd *m/z* = 1160.0)

**Tetramer [$Fe_4$(1)$_4$]** (**FeC4**): Not isolated but detected *via* ESI-MS (*m/z*): 600.7 $[M\text{-}7PF_6]^{7+}$ (Calcd *m/z* = 600.7).

# CHAPTER III

## DIRECTED FLEXIBILITY: DESIGN AND SYNTHESIS OF A SUPRAMOLECULAR TETRAHEDRON[†]

### 3.1 Introduction

Metal–ligand self-assembly has been utilized to form various metallosupramolecular structures including coordination polymers,[68] macrocycles,[48, 90, 127, 164-166] and 3D structures.[48, 168] The *N*-heteroaromatic ligand [2,2':6',2"]terpyridine (tpy) has received increasing attention due in part to its ability to coordinate diverse transition metals permitting control of bond strengths, properties, and desired molecular architectures.[47, 68] With metals that can form strong coordinative bonds, *e.g.* $Os^{2+}$, $Ru^{2+}$, and $Fe^{2+}$, the final product is kinetically determined by creating irreversible <tpy-$M^{2+}$-tpy> linkages; in contrast, metals capable of more labile coordinative bonds, *e.g.* $Zn^{2+}$ and $Cd^{2+}$, give access to the thermodynamic products.

Specific architectures are determined, in part, by the geometry of the building blocks, *i.e.* angle(s) of the conjoined ligands with respect to one another. Exploiting the angular orientation and stoichiometric control of precursors is generally known as a directional bonding approach to supramolecular synthesis.[48] As shown in Scheme 3.1, ligands with 60° angles have been used to form triangular structures.[36, 127] The structural

[†] Parts of this chapter are reprinted with permission from the Royal Society of Chemistry: J. M. Ludlow III, T. Xie, Z. Guo, K. Guo, M. J. Saunders, C. N. Moorefield, C. Wesdemiotis and G. R. Newkome, *Chem. Commun.*, **2015**, *51*, 3820 – 3023.

and kinetic favorability of triangular-based systems has been harnessed, through use of multitopic 60°-based ligands to create large and intricate architectures, such as a spoked wheel[90] and the Sierpiński triangle.[91] A synthetic improvement *via* replacement of a 120° angle with two 60° angles has also been demonstrated.[89] These triangle-based architectures are planar and utilize 60° ligands, *e.g*. *ortho*-aryls, and can introduce a rigid framework into the resultant end product. Likewise, in biomolecular systems, directionality and positioning of non-covalent interactions are critical to molecular recognition and supramolecular structure formation, for example hydrogen bonding in protein structures and base pairing in DNA. Also, flexibility plays a key role in such systems to allow the folding and winding necessary to achieve the required structure and function. Using a similar strategy of balanced directionality and flexibility, Scheme 1 depicts the quantitative construction of a rigid triangular component[127] that can be used to align other highly flexible components, such as the tribenzo-27-crown-9 ethereal vertices (Schemes 3.2 and 3.3). Flexible linkages such as crown ethers have been used in conjunction with multitopic terpyridine ligands;[118] however, these examples did not incorporate angular directionality and isolation of cyclic species required use of non-labile metals and purification *via* chromatography. Flexibility can also be incorporated into cage forming *N*-donor ligands *via* methylene bridges[189, 190] and polyester moieties.[191] Herein, we describe the design and synthesis (Scheme 3.2) of a novel hexa*kis*terpyridine ligand containing three 60° juxtaposed *bis*ligands connected by a flexible crown ether vertex (**5**) and demonstrate its self-assembly with $Zn^{2+}$ to generate an expanded tetrahedral structure under thermodynamic control (Scheme 3). The flexible vertex allows its extension into a 3D structure, which was studied *via* ESI-TWIM-MS, TEM, 1D and

2D NMR, as well as molecular modeling. The NMR studies and molecular modeling indicate the presence of parallel ($\pi$-$\pi$) and T-shaped (CH-$\pi$) interactions of stacked tpy complexes, which would be forbidden by more traditional, rigid architectures. A model 'free triangle' (**2**) is synthesized for comparison (Scheme 1) to demonstrate the influence of the tetrahedral structure.

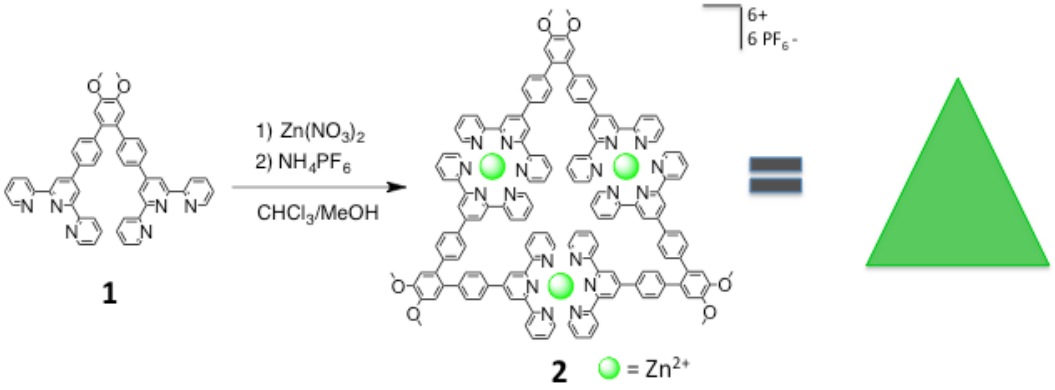


Scheme 3.1 Synthesis of the simplest 'free triangle' **2**.

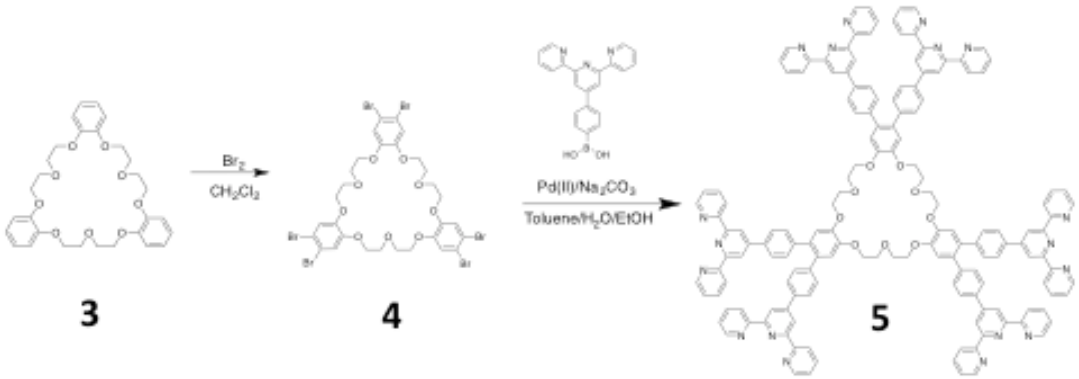


Scheme 3.2 Synthesis of the vertex reagent **5.**

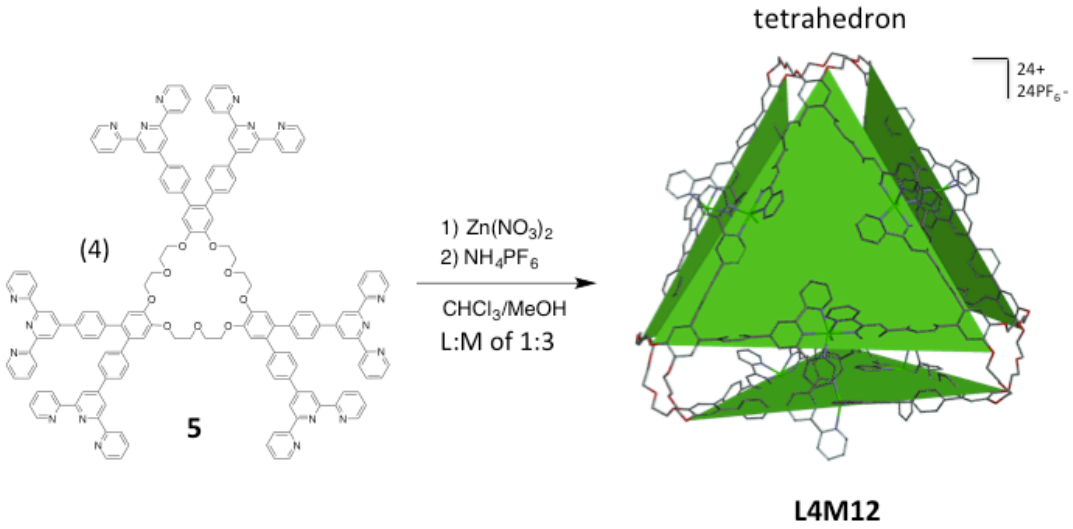


Scheme 3.3 Complexation of **5** to form **L4M12**. The structure's four independent triangles, each analogous to **2**, are highlighted in green to aid in visualization of the structure. **L4M12** is a combination of 4 ligands and 12 metals ($Zn^{II}$). (4) = 4 equiv.

## 3.2 Results and Discussion

Tribenzo-27-crown-9 (**3**), synthesized using literature methods,[192] was brominated and then subjected to a Suzuki coupling[39] with 4-([2,2':6',2"]terpyridin-4'-yl)phenylboronic acid to give the desired ligand **5**, which was subsequently self-assembled with $Zn^{2+}$ (Scheme 3.3) to give the desired tetrahedron **L4M12**.

The $^{1}$H NMR of **L4M12** reveals a single set of terpyridine resonances indicative of a highly symmetrical structure. The spectrum is consistent with fully complexed cyclic structures that exhibit the expected upfield shifted 6,6"-tpy*H* signals (8.65 to 7.59 ppm, Figure 3.1) thereby supporting the *bis*terpyridine $Zn^{II}$ complexation; no uncomplexed terpyridine was observed. Both COSY and NOESY $^{1}$H NMR confirmed proton assignments.

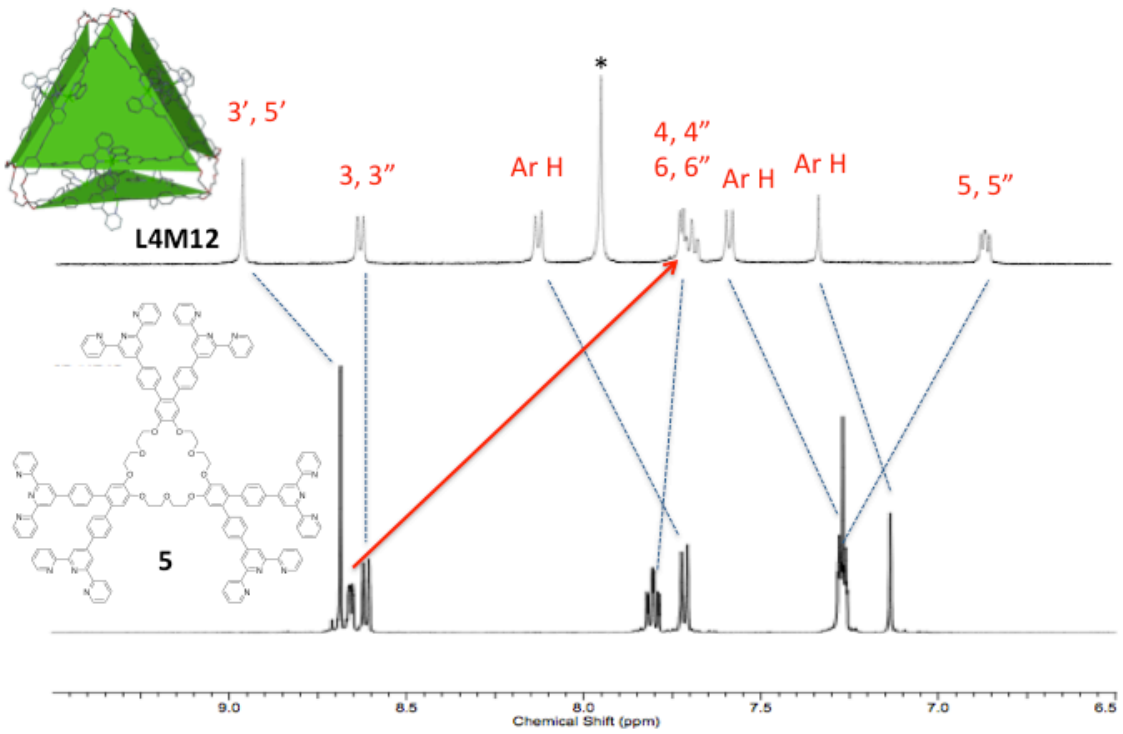


Figure 3.1 500 MHz $^{1}$H NMR spectra – aromatic region at 20 °C. Bottom: neat ligand **5** ($CDCl_3$) at 10 mg/mL and top: **L4M12** in $CD_3CN$/DMF-$d_7$.(5:1) at 0.6 mg/mL *-DMF.

Figure 3.2 compares the aromatic regions of **2** and **L4M12**. Since the 'free triangle' **2** is, essentially, chemically identical to the interlinked triangles of **L4M12**, any differences observed in chemical shift must arise from the **L4M12**'s supramolecular structure. A single set of terpyridines is observed for each, with the sole exception of the aryl singlets, all of the resonances of **L4M12** are shifted upfield, most notably the 4,4"-, 5,5"-, and 6,6"-tpy protons, suggesting that the tetrahedral structure has a significant shielding effect. Molecular modeling shows that the complexes of adjacent triangles are stacked; thus, the observed shielding effect is consistent with previously reported structures involving stacked <tpy-$M^{2+}$-tpy> complexes.[105, 169]

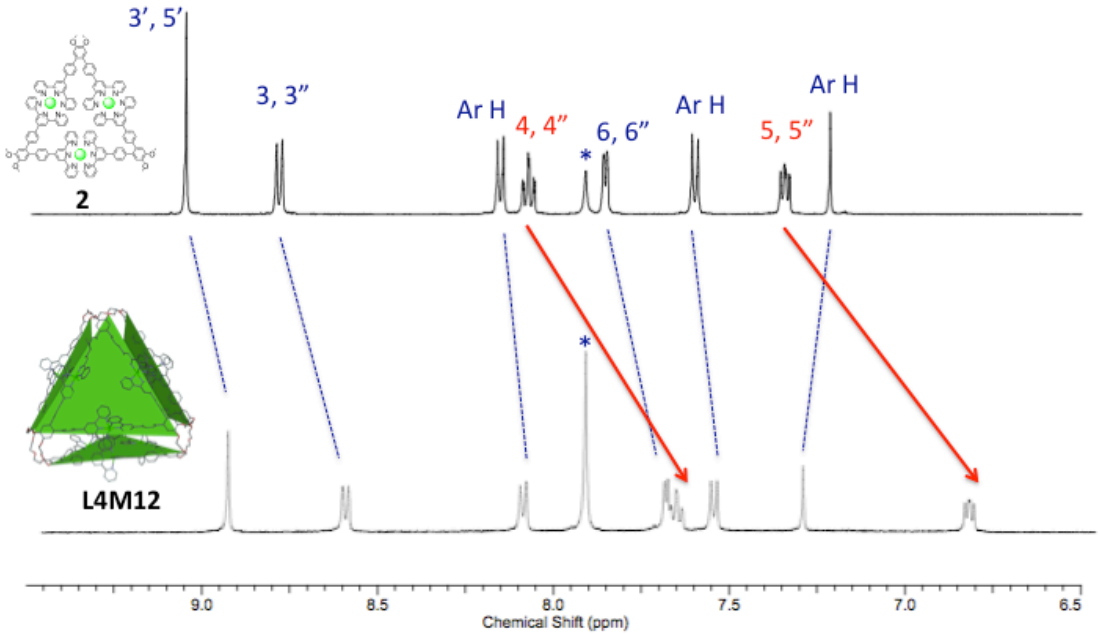


Figure 3.2 500 MHz $^{1}$H NMR of **2** (top, 3.0 mg/mL) and **L4M12** (bottom, 0.6 mg/mL) both in $CD_3CN$/ DMF-$d_7$ (5:1) at 20 °C. *-DMF.

Both COSY and NOESY $^{1}$H NMR confirmed proton assignments (Figures 3.3 – 3.5).

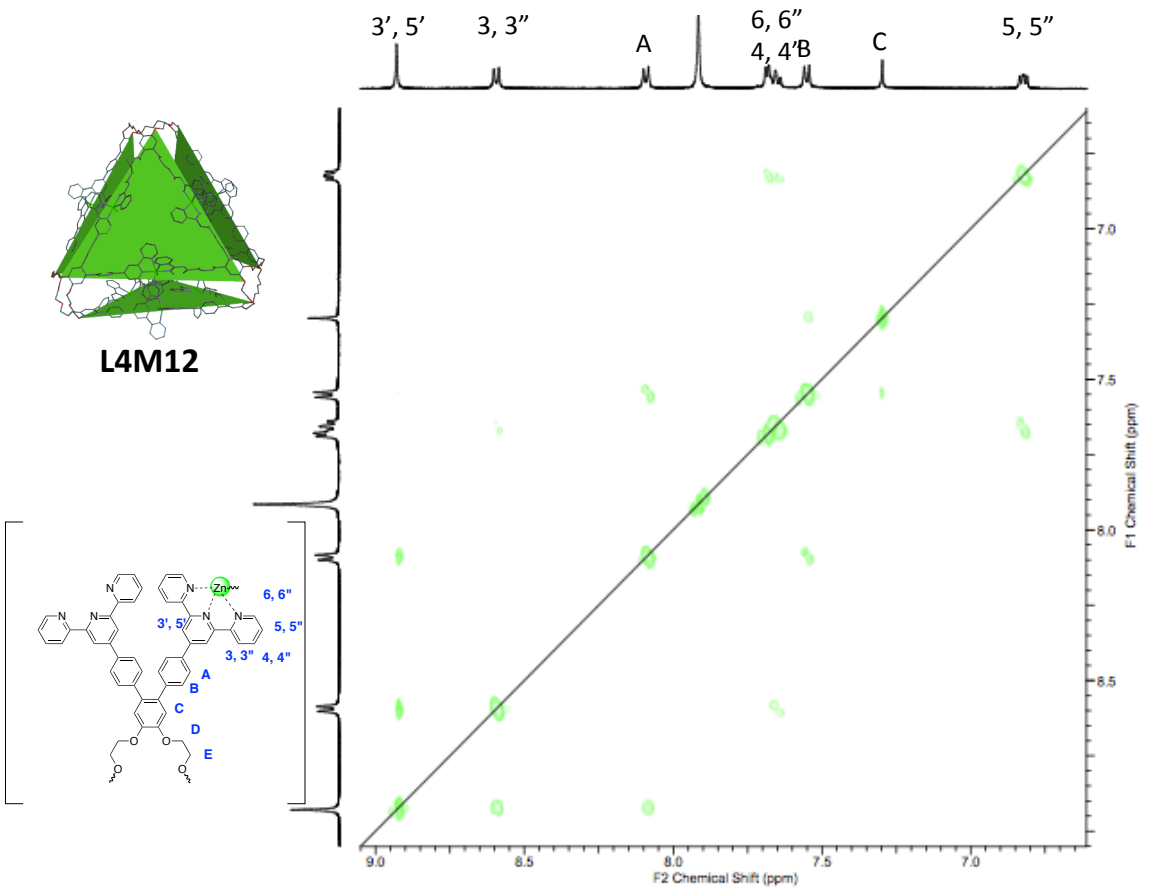


Figure 3.3 NOESY spectra of **L4M12**, aromatic region in $CD_3CN$/DMF- $d_7$ at 5:1 (0.6 mg / mL).

Cross peaks in the NOESY spectra (Figure 3.3) shows that the 3',5' *H*-singlet has cross peaks with the 3,3"-*H* and the doublet for aryl proton A. The through-space interaction with the 3,3"-*H* confirms that the terpyridine is complexed. Proton A shows through space interactions with proton B, which shows a cross peak with the singlet for proton C. Looking at the expanded spectra in Figure 3.4, we see that proton C shows through space interactions with the alkoxy protons at position D.

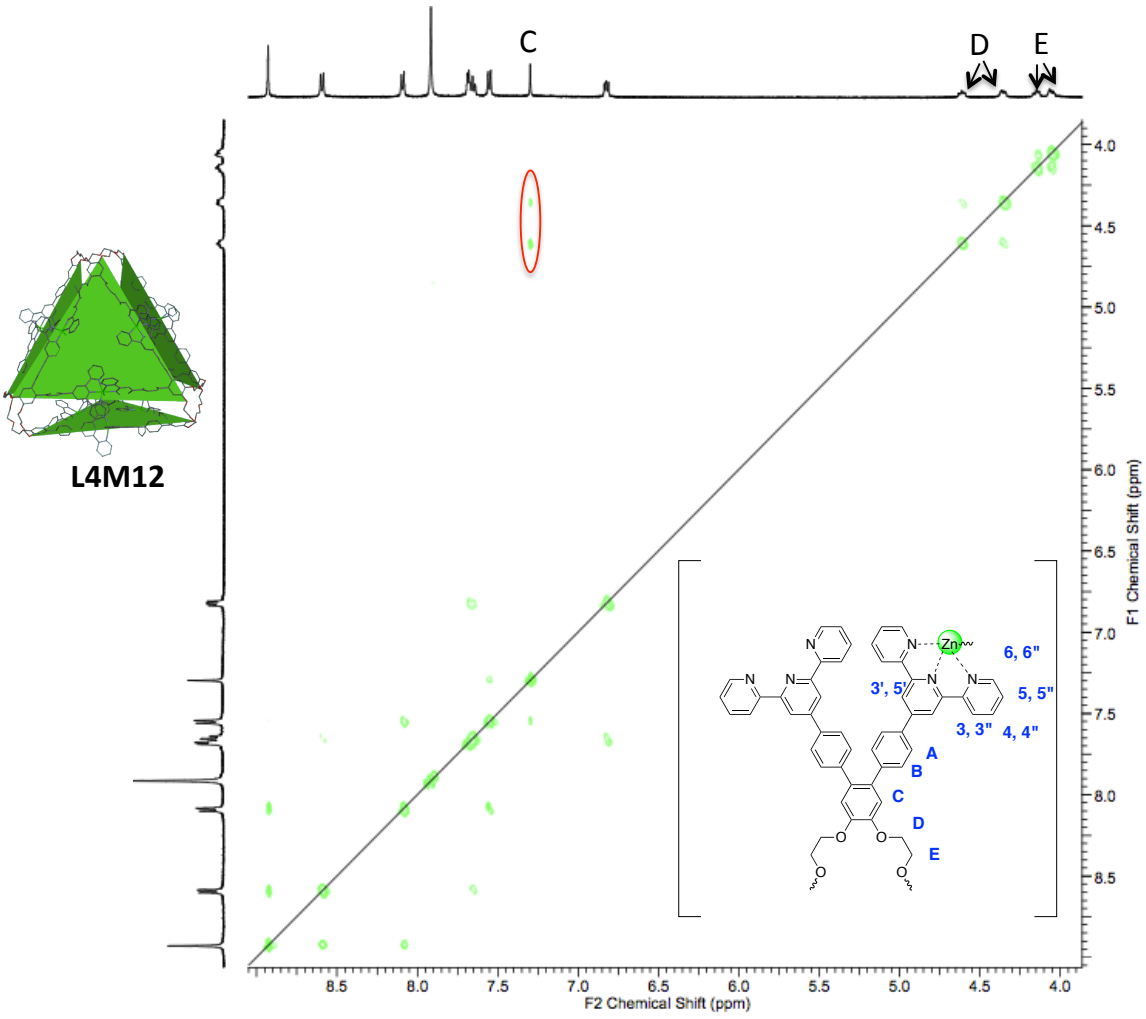


Figure 3.4 NOESY spectra of **L4M12** in $CD_3CN$/DMF- $d_7$ at 5:1 (0.6 mg / mL). Cross peaks between protons C and D are circled.

COSY spectra (Figure 3.5) supported the structure as well, showing coupling from the 3,3"-*H* to 4,4"-*H* to 5,5"-*H* to 6,6"-*H* and coupling between aryl protons A and B.

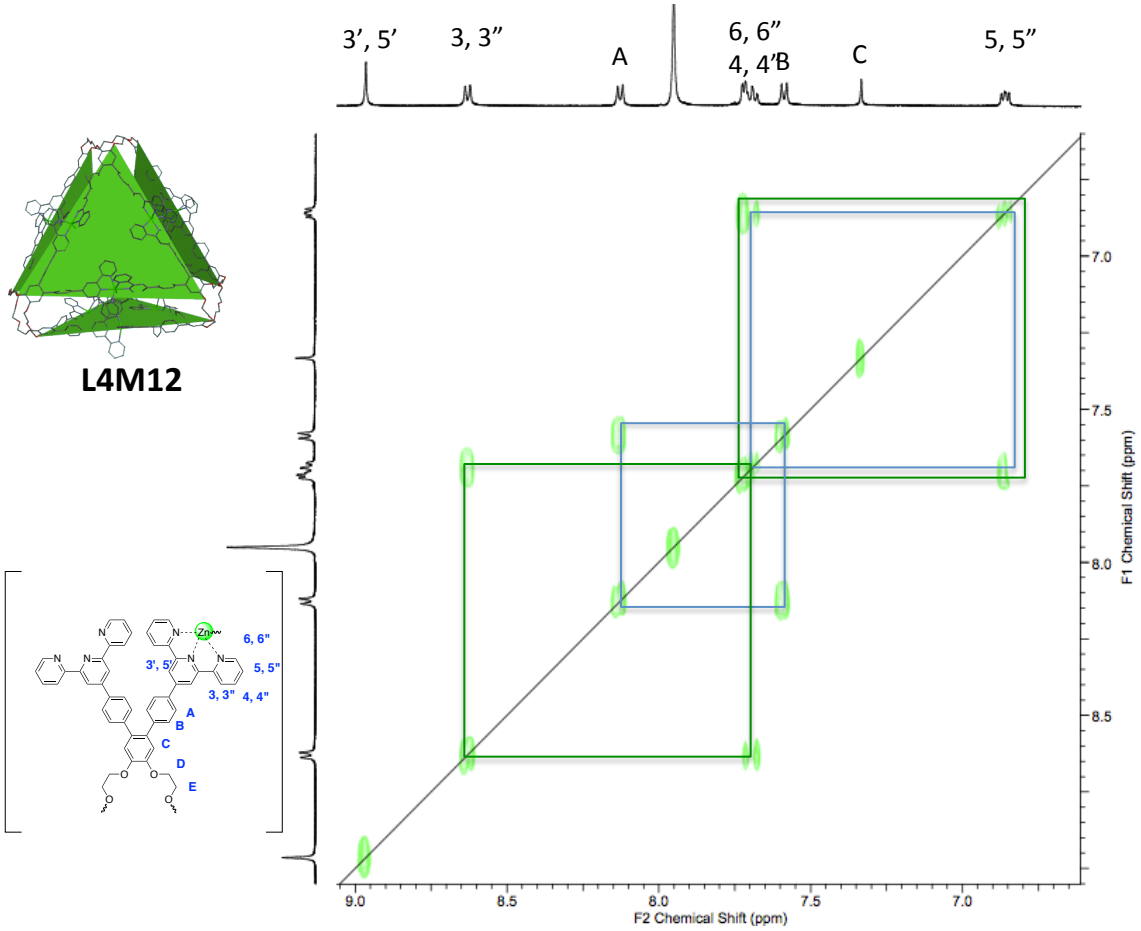


Figure 3.5 COSY spectra of **L4M12** in $CD_3CN$/DMF- $d_7$ at 5/1 (0.6 mg / mL).

Variable temperature (VT) $^1$H NMR experiments were conducted on both **L4M12** and **2**. As the temperature was lowered, the chemical shift attributed to the **L4M12** shows that the 5,5" peaks are shifted upfield. Conversely, the chemical shifts of the protons in **2** were insensitive to temperature variations (Figure 3.6).

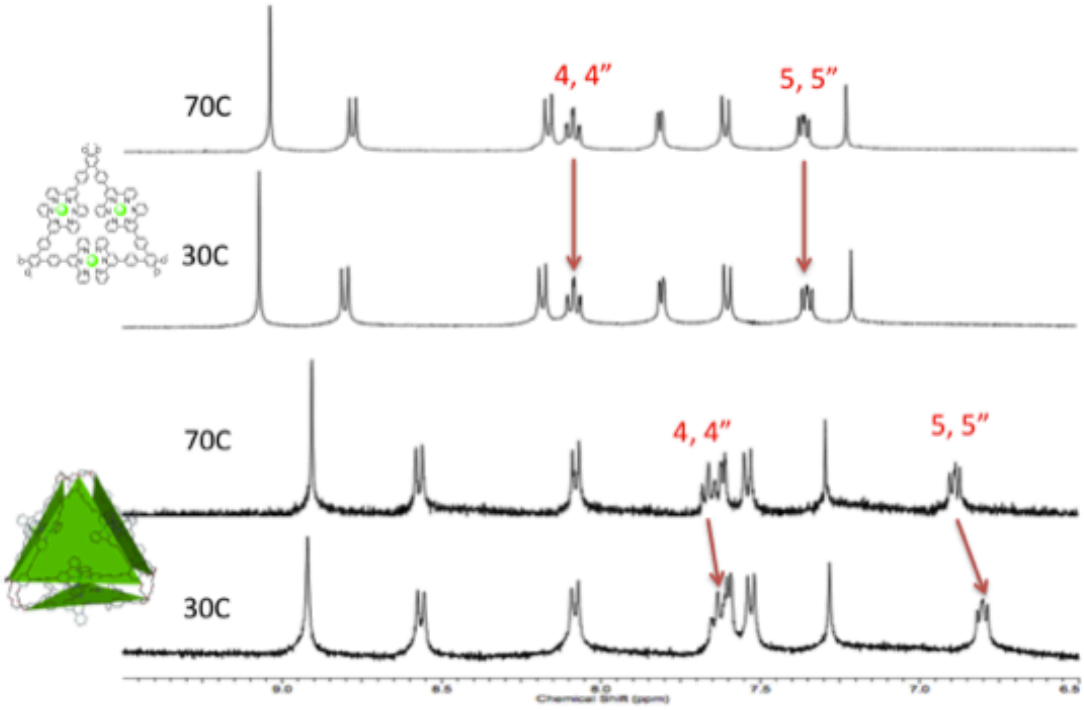


Figure 3.6 Variable temperature $^{1}$H NMR of 'free triangle' **3** (3.0 mg/mL) and **L4M12** (0.6 mg/ mL) in $CD_3CN$/DMSO-$d_6$ (10:1).

Similar chemical shift changes with temperature were also observed with stacked <tpy-$M^{II}$-tpy> complexes.[105, 169] This result implies that, as molecular motion is decreased, the shielding effect from the tetrahedral structure is enhanced. Conversely, the environment of the aromatic protons of **2**, where intramolecular stacking cannot occur, has been shown to be insensitive to the degree-of-molecular motion. Previous reports[129] indicate that the proton signals of cyclic <tpy-$M^{II}$-tpy> trimers, such as **2,** show negligible chemical shift changes when the temperature is varied.

**L4M12** was characterized by ESI–MS (Figure 3.7). The series of peaks match with charge states 5+ through 10+ for the combination of 4 ligands, 12 metals ($Zn^{2+}$), and the corresponding number of $PF_6^-$ anions. ESI-MS coupled with travelling wave ion

mobility[97] (TWIM) was used to further support the tetrahedral structure (Figure 3.8). **L4M12** shows the expected step pattern of charge states. Each charge state has a narrow drift time distribution, indicative of an absence of superimposed isomers or conformers.

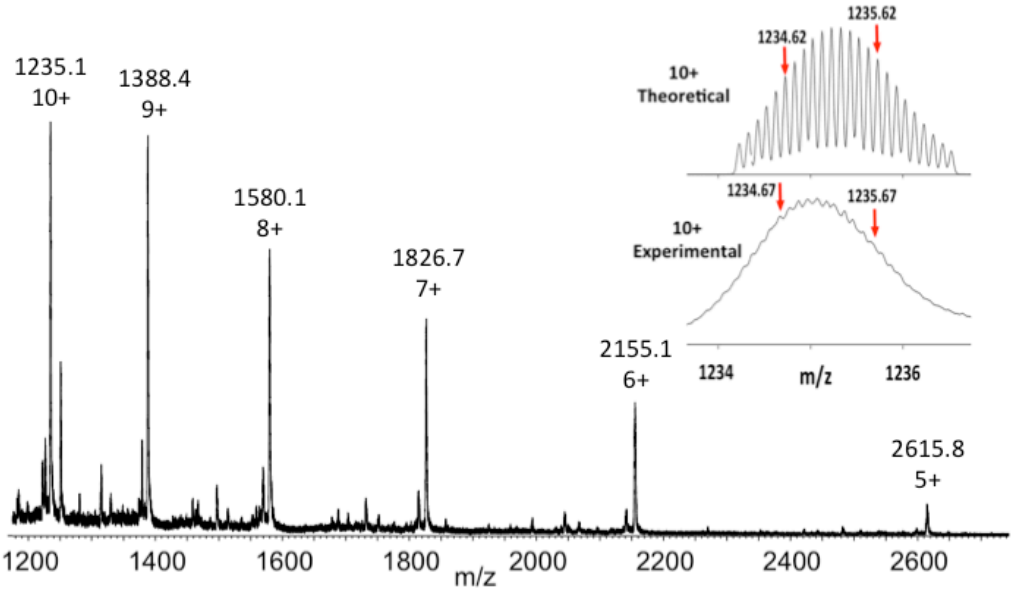


Figure 3.7 ESI-MS of **L4M12** showing a series of peaks corresponding to charge states 5+ thru 10+ and (inset) theoretical and experimental isotope patterns for the 10+ charge state; 0.6 mg/mL in MeCN/ DMF (5:1).

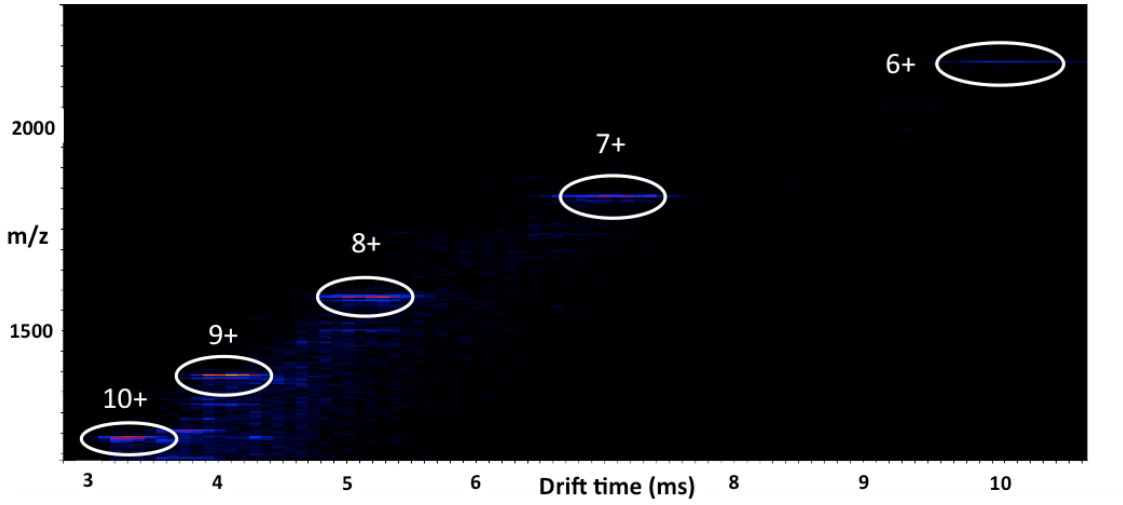


Figure 3.8 ESI-TWIM-MS plot of **L4M12** (*m/z vs*. drift time). 0.6 mg/mL in MeCN/DMF (5:1).

Experimental collision cross-sections were calculated using the TWIM data and are shown in Table 3.1[90, 180-184]; the Collision Cross-Section (CCS) of an ion can be viewed as its apparent forward-moving surface area. The experimental CCS values are consistent (within 10%) across charge states 6+ through 10+, indicating the shape persistence of the tetrahedral architecture. Energy minimized structures were used to calculate a theoretical CCS for the counterion-free assembly using the Projection Approximation (PA), Trajectory Method (TM), and Exact Hard Sphere Scattering (EHSS) methods available in the MOBCAL program. The correlation between the theoretical and experimental values provides further support for the proposed architecture.

Table 3.1 Experimental and theoretical CCS values for **L4M12**. Standard deviations are in parenthesis.

| **Z** | **$CCS_{exp}(Å^2)$** | **$CCS_{exp}(Å^2)$** | **$CCS_{theo}(Å^2)$** |
|---|---|---|---|
| 6+ | 1351.6 | Average | 1409(8)-EHSS |
| 7+ | 1306.6 | 1284.4(40.8) | 1385(19)-TM |
| 8+ | 1278.9 | | 1136(6)-PA |
| 9+ | 1265.0 | | |
| 10+ | 1219.7 | | |

Gradient tandem mass spectrometry[97] ($gMS^2$) was used to probe the stability of **L4M12** by subjecting the 10+, 8+, and 6+ charge states to collisionally activated dissociation (with Ar gas) prior to ion mobility separation (Figure 3.9). Collision energies of 45, 60, and 80 eV, respectively, were required to fully dissociate the complex. These translate into center-of-mass collision energies ($E_{cm}$) of 1.0184, 1.0614, and 1.0376 eV.

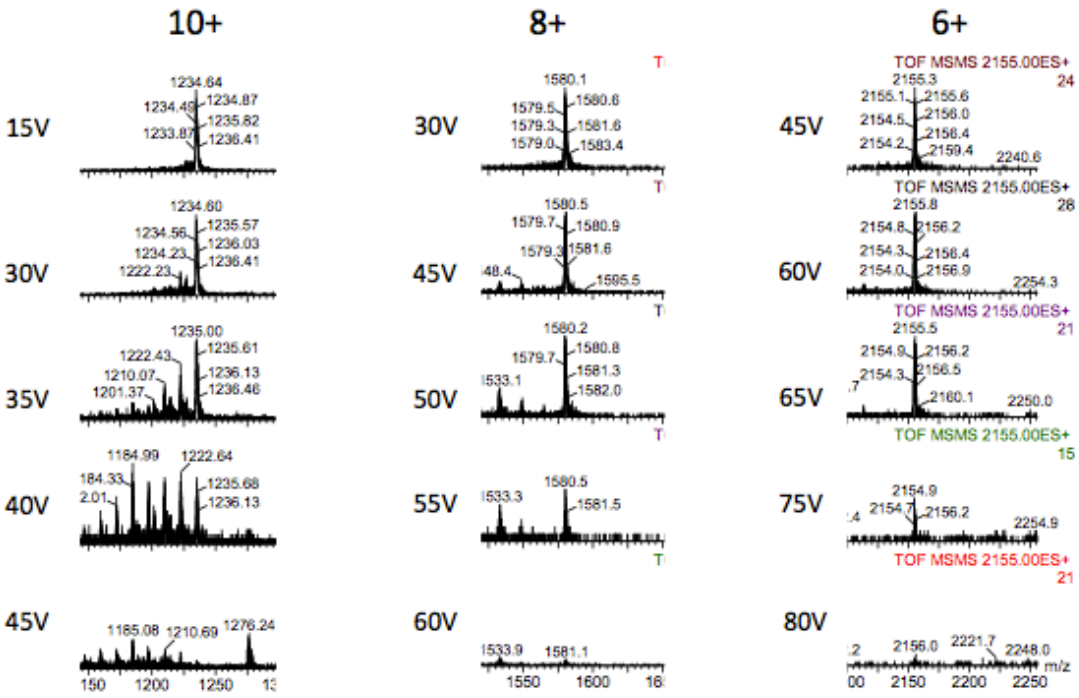


Figure 3.9 Gradient tandem mass spectrometry results for **L4M12.** 10+, 8+, and 6+ charge states have m/z values of 1235, 1580, and 2155, respectively.

A dilute solution of **L4M12** (*ca*. $10^{-5}$ M, MeCN/DMF, 5/1) was cast onto Cu grids and observed *via* transmission electron microscopy (TEM). Dimensions of the observed, discrete nanostructures (Figure 3.10) correspond well with measured molecular model dimensions. The calculated edge length for the tetrahedron is *ca*. 3.5 nm, which closely matches the *ca*. 4 nm. observed in the TEM. Molecular modeling of **L4M12** (Figure 3.10) also indicates close proximity of adjacent complexes. The <tpy-$M^{II}$-tpy> protons are projected into the adjacent complex unit and should, therefore, be more highly shielded than in a non-stacked complex, such as the free triangle, as demonstrated in Figure 3.2. These results match with observations seen in previously reported stacked <tpy-$M^{II}$-tpy> species.[118, 169] The presence of the slipped parallel ($\pi$-$\pi$) and T-shaped

(CH-$\pi$) stacking interactions are shown; these $\pi$-$\pi$ interactions are generally regarded as energetically favorable, and are reported[186] to be -6.2 and -10.3 kJ-mol$^{-1}$, respectively, in model systems. Such cooperative interactions could stabilize the tetrahedral structure and/or promote its formation relative to other structures in which such intramolecular interactions do not occur. Metal-to-metal distances in the model closely match those reported[169] for stacked tpy complexes formed from parallel *bis*-ligands. For example, the metal-to-metal distances in **L4M12** ranged from *ca.* 9.2 to 9.5 Å *vs*. 8.8 Å in the reported complex.[169] Stacked tpy complexes have been confirmed in a variety of solid-state structures.[170]

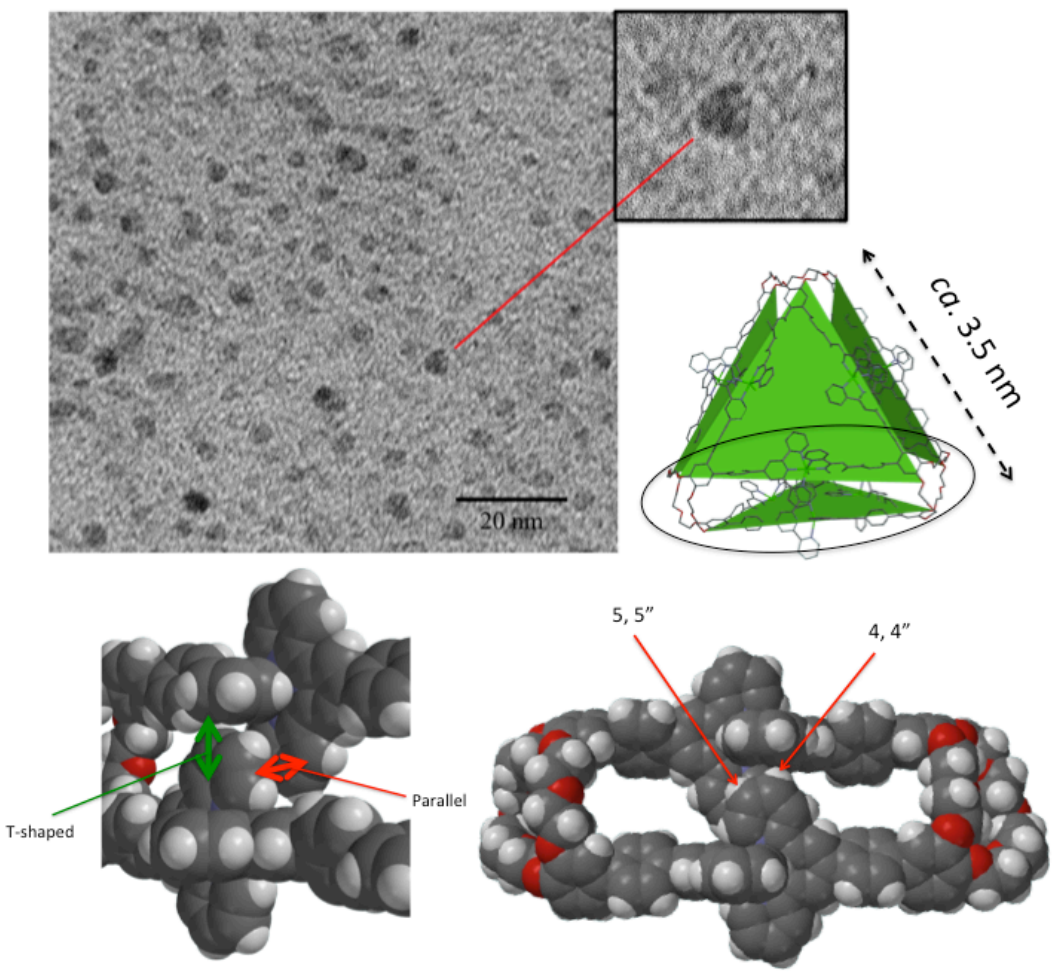


Figure 3.10 TEM with magnified inset and space filling model cutaways of **L4M12** showing stacked <tpy-$M^{2+}$-tpy> complexes. Color scheme: H: white; C: grey; N: purple; O: red; Zn: green. The 4,4" and 5,5" protons are noted (right). Regions of T-shaped (CH-π) and parallel (π-π) interactions are noted (left).

Internal volume of **L4M12** was estimated at *ca.* 2400 Å$^3$, making it an excellent candidate for guest-host chemistry.[193] $^{19}$F NMR was used to probe anion encapsulation properties of **L4M12** in solution state. $^{19}$F spectra of **L4M12** with $PF_6^-$ counterions (volume 62Å$^3$) only showed one peak. Previous studies[189] of cage-like structures using

$PF_6^-$ have reported that this occurs with rapid endo-exo anion exchange relative to the NMR timescale.[189, 194] To reduce the exchange rate, the larger and tetrahedral anion, tetrakis(perfluorophenyl)borate (BARF) (volume 446 $Å^3$), was used to precipitate **L4M12**. The $^{19}F$ NMR of **L4M12** with BARF counterions showed the presence of additional, smaller peaks at -151.6, -182.7, and -183.8 ppm (Figure 3.11) suggesting the presence of a dynamic equilibrium of one or more BARF counterions within the cavity. As expected, these endo peaks were not detected with **2** using BARF counterions.

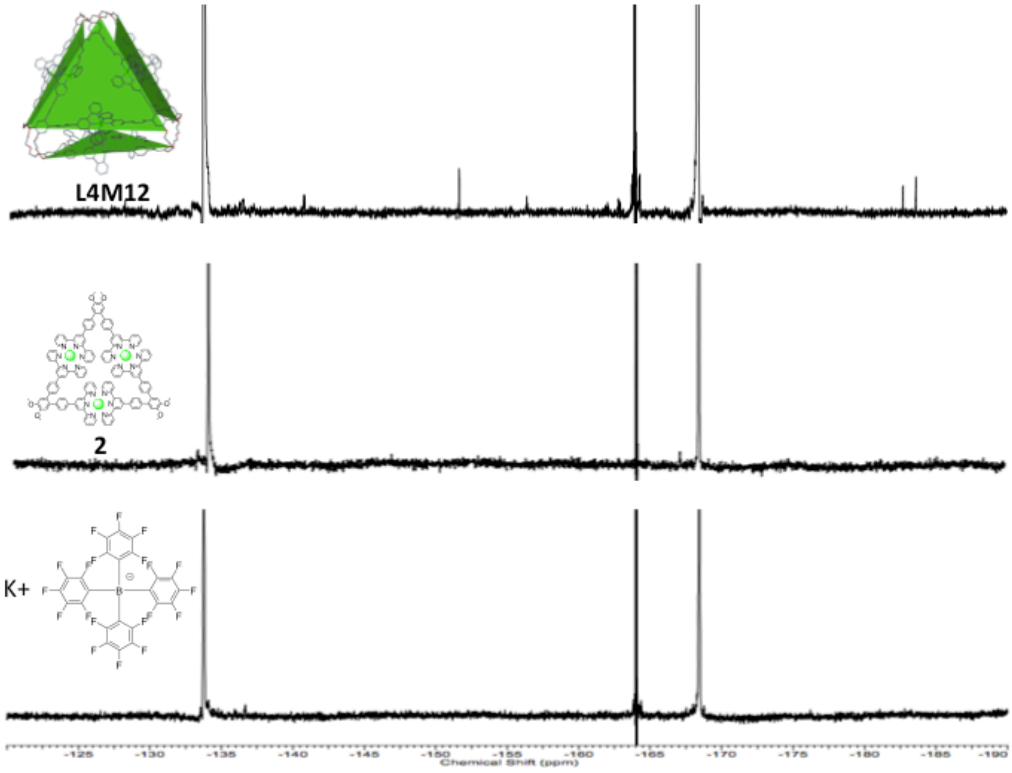


Figure 3.11 470 MHz $^{19}F$ NMR of **L4M12** (top) and **2** (middle) both in $CD_3CN$/ DMF-$d_7$ (5:1) at 20 °C, 1 mg/mL with BARF counterions. Bottom spectra shows neat K-tetra*kis*(perfluorophenyl)borate.

Diffusion-ordered NMR spectroscopy (DOSY) in Figure 3.12 shows that all of the proton signals are in a narrow band indicating that all the signals are coming from the same, discreet supramolecular structure.

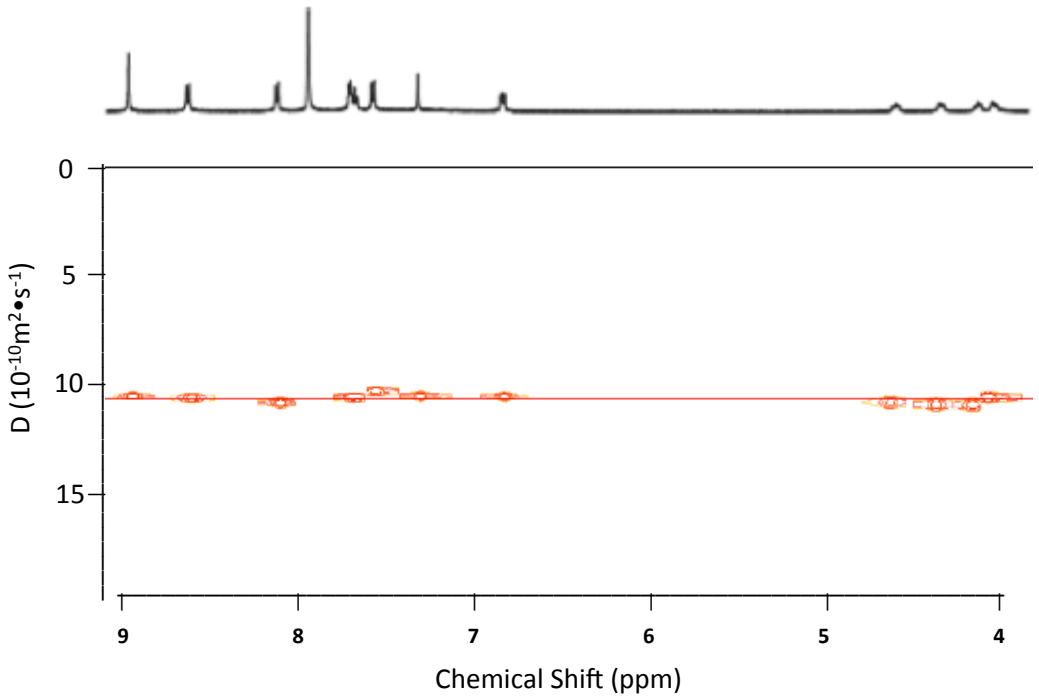


Figure 3.12 DOSY spectra ($CD_3CN$/DMF-$d_7$ (5/1), 500 MHz) of **L4M12**.

## 3.3 Conclusions

Finally, using a strategy of balanced directionality and flexibility, we describe the design and synthesis of a novel hexa*kis*terpyridine ligand containing a trio of 60°-directed *bis*ligands connected by crown ether vertices and its self-assembly into a tetrahedral structure under thermodynamic control. The flexible vertex allows a controlled extension into new 3D structures facilitated by intramolecular interactions ($\pi$-$\pi$). Molecular modeling supports the NMR data suggesting the presence of parallel ($\pi$-$\pi$) and T-shaped (CH-$\pi$) interactions in the close-packed tpy complexes. Variable temperature NMR

experiments support this model in which $^{19}F$ NMR experiments are indicative of the presence of BARF within the cavity. DOSY spectra is consistent with **L4M12** being a discreet supramolecular structure.

## 3.4 Experimental

See Section 2.4 for general experimental procedures.

**Synthetic Procedures**

**Tribenzo-27-crown-9** (**3**) was synthesized and characterized according to the literature.[192]

**2,3,13,14,24,25–Hexabromo-6,7,9,10,17,18,20,21,28,29,31,32-dodecahydrotribenzo[*b*,*k*,*t*][1,4,7,10,13,16,19,22,25]nonaoxacycloheptacosine** (**4**)**:** To a stirred solution of **1** (480 mg, 880 μmol) and $I_2$ (9 mg, 36 μmol) in $CH_2Cl_2$ (50 mL), a solution of $Br_2$ (1.06 g, 6.66 mmol) in $CH_2Cl_2$ (15 mL) was added dropwise over one hour. This solution was maintained at 25 °C for an additional 7 h. The mixture was dried *in vacuo* to give a solid, which was recrystallized from EtOH to give (82%) of **4**, as a colorless solid: 740 mg, mp 152-153°C; $^1H$ NMR ($CDCl_3$, 500 MHz, ppm): 7.11 (s, 6H), 4.10 (m, 12H, ArOC$H_2$), 3.90 (m, 12H, ArOCH$_2$C$H_2$); $^{13}C$ NMR (125 MHz, $CDCl_3$, ppm): 148.76, 118.98, 115.45, 69.92, 69.61; MALDI-MS (*m/z*): 1036.9 [M+Na] (Calcd. = 1036.7).

**2,3,13,14,24,25–Hexa*kis*(4-[2,2':6',2'']terpyridin-4'-ylphenyl)-6,7,9,10,17,18,20,-21,28,29,31,32-dodecahydrotribenzo[*b*,*k*,*t*][1,4,7,10,13,16,19,22,25]nonaoxacycloheptacosine** (**5**): A mixture of **4** (322 mg, 318 μmol), (4-[2,2':6',2'']-terpyridin-4'-ylphenyl)boronic acid (1.009 g, 2.86 mmol), $Pd(PPh_3)_2Cl_2$ (135 mg, 190 μmol), and $Na_2CO_3$ (504 mg, 4.74

μmol) was added to a dry round bottom flask, which was then evacuated and backfilled with argon (5X). A mixture of toluene (150 mL), MeOH (60 mL), and $H_2O$ (90 mL) was degassed with argon for 15 min and added to the flask, under argon. The resultant mixture was refluxed for 60 h, and cooled. The aqueous layer was extracted with $CHCl_3$ and then combined with the organic layer. The solution was dried ($MgSO_4$), filtered, and concentrated to dryness. The resultant solid was column chromatographed ($Al_2O_3$) using $CHCl_3$/EtOAc/hexanes (1:1:1), followed by pure $CHCl_3$ to give (43%) **5**, as a colorless solid: 325 mg, mp 218-220 °C; $^1$H NMR ($CDCl_3$, 500 MHz, ppm): 8.70 (s, 12H, 3',5'-tpy*H*), 8.65 (d, *J* = 5 Hz, 6,6"-tpy*H*, 12H), 8.60 (d, *J* = 8 Hz, 3,3"-tpy*H*, 12H), 7.77 (dd, $J_1 = J_2 = 8$ Hz, 4,4"-tpy*H*, 12H), 7.73 (d, *J* = 8 Hz, 12H), 7.23 - 7.31 (m, 32H), 7.14 (s, 6H), 4.34 (t, *J* = 5 Hz, 12H), 4.09 (t, *J* = 5 Hz, 12H); $^{13}$C NMR (125 MHz, $CDCl_3$, ppm): 69.65, 70.29, 117.24, 118.75, 121.24, 123.62, 126.95, 130.41, 133.28, 136.24, 136.69, 142.00, 148.62, 149.05, 149.72, 155.78, 156.29; MALDI-MS (*m/z*): 2382.9 (Calcd. *m/z* = 2382.9).

**Self-assembly to tetrahedral structure L4M12**: To a stirred solution of **5** (21.3 mg, 8.91 μmol) in $CHCl_3$/MeOH (3:2, 20 mL) at 25 °C, a 250 mM solution of $Zn(NO_3)_2 \cdot 6H_2O$ in MeOH (1.062 mL) was added. After 30 min, $NH_4PF_6$ (90 mg) was added. The resultant yellow precipitate was filtered, washed with MeOH and $H_2O$, then dried *in vacuo* to give (84%) **L4M12**, as a yellow solid: 25.9 mg, mp >300°C; $^1$H NMR ($CD_3CN$/DMF-$d_7$, 500 MHz, ppm): 8.97 (s, 48H, 3',5'-tpy*H*), 8.64 (d, *J* = 8 Hz, 48H, 3,3"-tpy*H*), 8.13 (d, *J* = 8 Hz, 4H, Ar*H*), 7.64 - 7.77 (m, 96H, 6,6"-tpy*H*, 4,4" -tpy*H*), 7.58 (d, *J* = 8 Hz, 48H, Ar*H*), 7.33 (s, 24H, Ar*H*), 6.86 (m, 48H, 5,5"-tpy*H*), 4.59 - 4.71 (m), 4.34 - 4.44 (m), 4.13 - 4.24 ppm (m), 4.04 - 4.13 ppm (m);$^1$H NMR

($CD_3CN$/DMSO-$d_6$, 500 MHz, ppm): 8.92 (s, 48H, 3',5'-tpy*H*), 8.56 (d, *J* = 8 Hz, 48H, 3,3"-tpy*H*), 8.08 (d, *J* = 8 Hz, 4H, Ar*H*), 7.56 - 7.67 (m, 96H, 4, 4"-tpy*H*, 6,6" -tpy*H*), 7.53 (d, *J* = 8 Hz, 48H, Ar*H*), 7.28 (s, 24H, Ar*H*), 6.73 - 6.83 (m, 48H, 5,5" -tpy*H*), 4.50 - 4.66 (m), 4.24 - 4.38 (m), 3.96 - 4.17 ppm (m); ESI-MS (*m/z*) 1235.1 $[M-10PF_6]^{10+}$ (Calcd. *m/z* = 1235.2), 1388.4 $[M-9PF_6]^{9+}$ (Calcd. *m/z* = 1388.6), 1580.1 $[M-8PF_6]^{8+}$ (Calcd. *m/z* = 1580.4), 1826.7 $[M-7PF_6]^{7+}$ (Calcd. *m/z* = 1826.9), 2155.1 $[M-6PF_6]^{6+}$ (Calcd. *m/z* = 2155.4), 2615.8 $[M-5PF_6]^{5+}$ (Calcd. *m/z* = 2615.6). To obtain **L4M12** with tetra*kis*(perfluorophenyl)borate counterion, potassium tetra*kis*(perfluorophenyl)-borate was used in place of $NH_4PF_6$ yielding (82%); $^1H$ NMR ($CD_3CN$/DMF-$d_7$, 500 MHz, ppm): 9.08 (s, 48H, 3',5'-tpy*H*), 8.74 (d, *J* = 8 Hz, 48H, 3,3"-tpy*H*), 8.17 (d, *J* = 8 Hz, 48H, Ar*H*), 7.73 (d, *J* = 5 Hz, 48H, 6,6"-tpy*H*), 7.61 (dd, $J_1 = J_2 = 8$, 48H, 4,4"-tpy*H*), 7.52 (d, *J* = 8 Hz, 48H, Ar*H*), 7.29 (s, 24H, Ar*H*), 6.82 (m, 48H, 5,5"-tpyH), 4.66 - 4.55 (m), 4.40 - 4.32 (m), 4.18 - 4.10 ppm (m), 4.10 - 4.00 ppm (m)

**Self-assembly of model complex 2** was synthesized and characterized according to the literature.[127] To obtain complex **2** with tetra*kis*(perfluorophenyl)borate counterion, potassium tetrakis(perfluorophenyl)-borate (BARF) was used in place of $NH_4PF_6$ . $^1H$ NMR ($CD_3CN$/DMF-$d_7$, 500 MHz, ppm): 9.08 (s, 12H, 3',5'-tpy*H*), 8.80 (d, *J* = 8 Hz, 12H, 3,3"-tpy*H*), 8.16 (d, *J* = 8 Hz, 12H, Ar*H*), 8.06 (dd, $J_1 = J_2 = 8$ Hz, 12H, 4,4"-tpy*H*), 7.85 (d, *J* = 5 Hz, 12H, 6,6"-tpy*H*), 7.61 (d, *J* = 8, 12H, Ar*H*), 7.32 (dd, $J_1 = 8$ Hz, $J_2 = 5$ Hz, 12H, 5,5"-tpyH), 7.21 (s, 6H, Ar*H*), 4.00 (s, 9H, -O$CH_3$); ESI-MS (*m/z*) 409.1 [M-6BARF]$^{6+}$ (Calcd. *m/z* = 408.7), 626.7 [M-5BARF]$^{5+}$ (Calcd. *m/z* = 626.2), 953.0 [M-4BARF]$^{4+}$ (Calcd. *m/z* = 952.5), 1497.0 [M-3BARF]$^{3+}$ (Calcd. *m/z* = 1496.3).

# CHAPTER IV

# GROUP 8 METALLOTRIANGLES: SYNTHESIS, CHARACTERIZATION, AND STABILITY†

## 4.1 Introduction

Many biomolecular systems used by plants and bacteria to convert solar energy into chemical energy are self-assembled *via* a variety of non-covalent inter- and intra-molecular forces, including van der Waals, hydrogen bonding, ionic, and ligand-based coordination interactions. Use of these forces to construct abiological molecular assemblies is a tenant of supramolecular chemistry, a paradigm for non-covalent materials construction, that was introduced and developed by Lehn, Cram, and Pederson.[6] Metal-ligand-promoted self-assembly utilizing the *N*-heteroaromatic ligand, [2,2':6',2"]terpyridine (tpy), has received increasing attention[170] due to its ability to coordinate with a wide variety of transition metals, thus enabling a range of bonding strengths, properties, and molecular architectures[68] such as, macrocycles[90, 127] and 3D structures.[48, 62, 168] Of particular interest, due to their light absorption in the visible spectrum, are <tpy–$Os^{II}$–tpy> complexes that possess long lived metal-to-ligand charge transfer (MLCT) excitations, photo-reactivity, and structural stability.[68, 195] These characteristics make <tpy–$Os^{II}$-tpy> complexes and structures suitable for a range of

† Parts of this chapter are reprinted with permission from Wiley: J. M. Ludlow III, Z. Guo, A. Schultz, R. Sarkar, C. N. Moorefield, C. Wesdemiotis and G. R. Newkome, *Eur. J. Inorg. Chem* , **2015**, (in press).

functions in artificial photosynthesis including photosensitizers,[195] light harvesting antennae,[196] and the bridging[197] of such components into fully integrated artificial photosynthetic molecular architectures. To date, synthesis and characterization of <tpy–$Os^{II}$–tpy> complexes has been essentially limited to simple, linear systems[68, 83, 195, 198-200] and grids.[58] Incorporation of <tpy–$Os^{II}$–tpy> into 2 and 3-D architectures is largely unexplored.[197, 201, 202] Each of these citations involves the formation of a mononuclear Os complex, followed by subsequent modification to build architecture. Herein, we detail the design, one-step synthesis and characterization of the first homoleptic <tpy–$Os^{II}$-tpy>-based macrocycle. The corresponding <tpy–$Fe^{II}$–tpy>[128] and <tpy–$Ru^{II}$–tpy> macrocycles were studied as well for comparison. Gradient tandem mass spectrometry is utilized to develop an understanding of the relationship between metal type and the stability of these structures. Stability of <tpy–$Os^{II}$–tpy> complexes has not been previously reported.

## 4.2 Results and Discussion

Figure 4.1 shows the synthesis[127] of ligand **1** *via* Suzuki-Miyaura coupling[39] of 1,2-dibromo-4,5-*bis*(methoxy)benzene with (4-([2,2':6',2'-terpyridin]-4'-yl-phenyl)boronic acid, which was prepared *via* the Kröhnke synthesis,[38] as previously reported.[35] This 60° ligand was then self-assembled as shown with respective group 8 metals (Figure 4.1). Each of these $d_6$ metals forms non-labile, octahedral complexes with a pair of terpyridines. Thus, the resultant products are kinetically determined and the cyclic trimers (triangle) subsequently isolated via column chromatography.

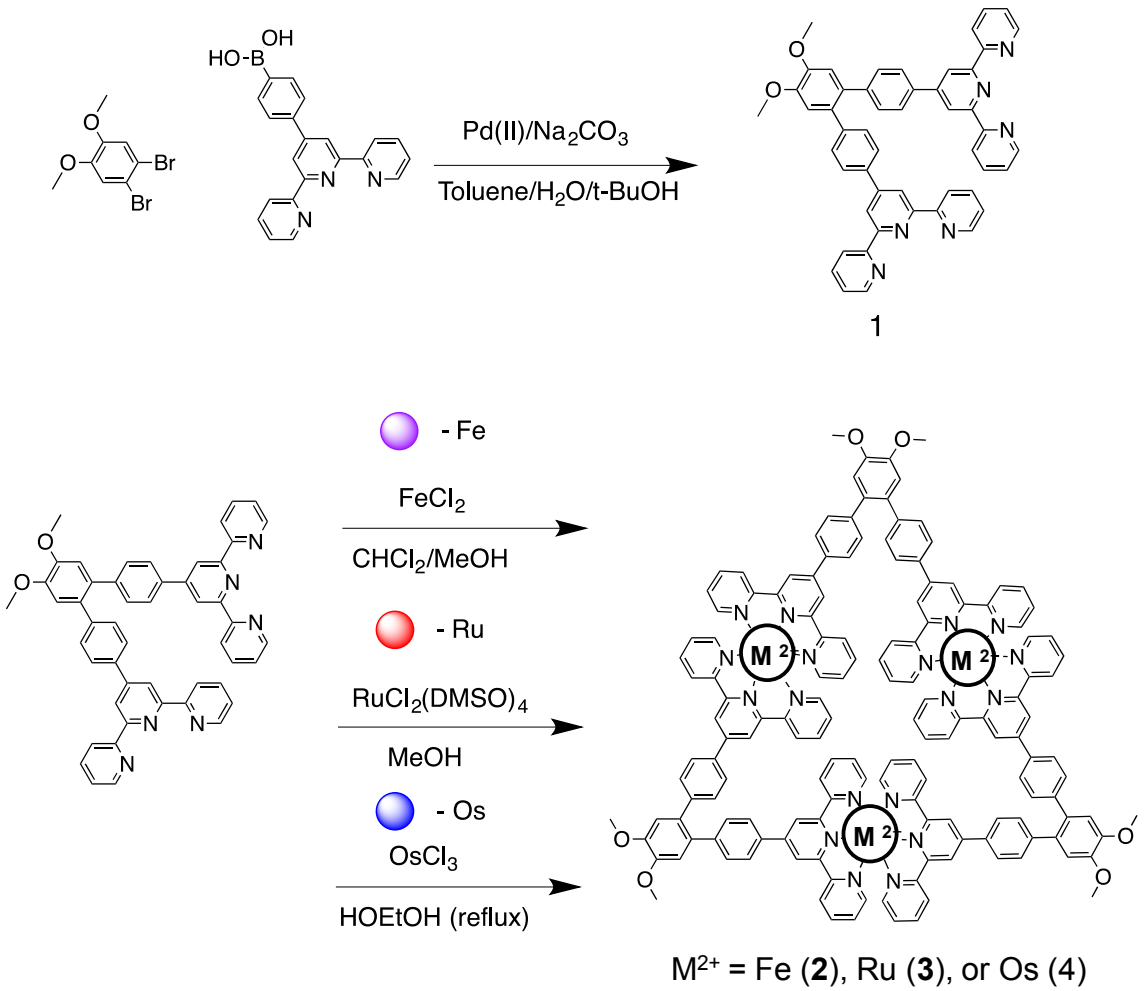


Figure 4.1 Synthesis of ligand **1** *via* Suzuki coupling and its subsequent self-assembly with the Group 8 metals Fe, Ru, and Os in a 1:1 ratio to generate macrocycles **2**, **3**, and **4**, respectively. All were isolated as the $PF_6^-$ salts.

A low yield of **4** (<10%, Os) compared to **2** (29%, Fe) and **3** (24%, Ru) is presumably due to the more severe reaction conditions generally used to synthesize <tpy–$Os^{II}$–tpy> (typically, *ca.* 200 °C). Figure 4.2 shows stacked aromatic region spectra of **1** and the three group 8 metallotriangles, **2**, **3**, and **4**. Each triangle exhibits a single set of fully complexed terpyridine protons. The 6,6" doublet exhibits the expected upfield shift

upon complexation from 8.70 to 7.19, 7.42, and 7.33 ppm, respectively. This is due to the 6,6" protons being projected into the opposing perpendicular ring current upon complexation.[68] Triangles **2**, **3**, and **4** also displayed a marker singlet for the methoxy protons at 4.05, 4.03, and 4.03 ppm.

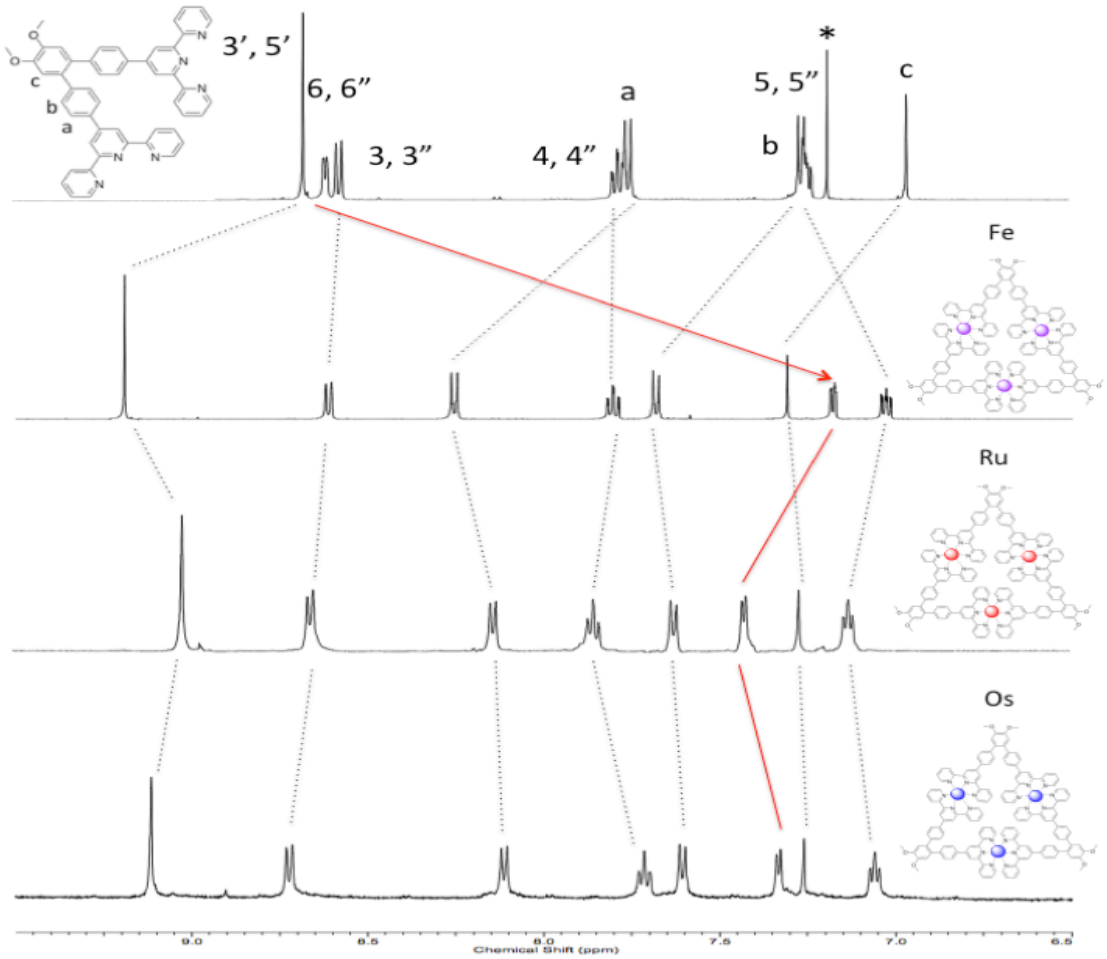


Figure 4.2 Stacked $^{1}$H NMR (500 MHz) aromatic region spectra of **1**, **2**, **3**, and **4**. (Ligand **1**,*$CDCl_3$; **2**, **3**, and **4**, $CD_3CN$).

Table 4.1 shows assigned $^{1}$H NMR peaks for each compound. The relative chemical shifts of Fe and Ru species are similar to previously reported values for such complexes.[128]

Table 4.1 $^{1}$H NMR (500 MHz) chemical shifts (ppm) assigned to **2**, **3**, and **4** in $CD_3CN$.

| Compound | M(II) | 3', 5' | 3, 3" | ArH | 4, 4" | ArH2 | 6, 6" | 5, 5" | OCH3 |
|---|---|---|---|---|---|---|---|---|---|
| **2** | Fe | 9.20 | 8.62 | 8.25, 7.68 | 7.80 | 7.31 | 7.19 | 7.03 | 4.05 |
| **3** | Ru | 9.02 | 8.66 | 8.14, 7.62 | 7.86 | 7.27 | 7.42 | 7.13 | 4.03 |
| **4** | Os | 9.12 | 8.73 | 8.12, 7.61 | 7.71 | 7.26 | 7.33 | 7.06 | 4.03 |

$^{1}$H NMR peak assignments were supported by COSY. The spectrum for **4** is shown in Figure 4.3. The expected cross peaks are observed showing 3,3"-*H* to 4,4"-*H* to 5,5"-*H* to 6,6"-*H* coupling and, likewise between aryl protons a and b.

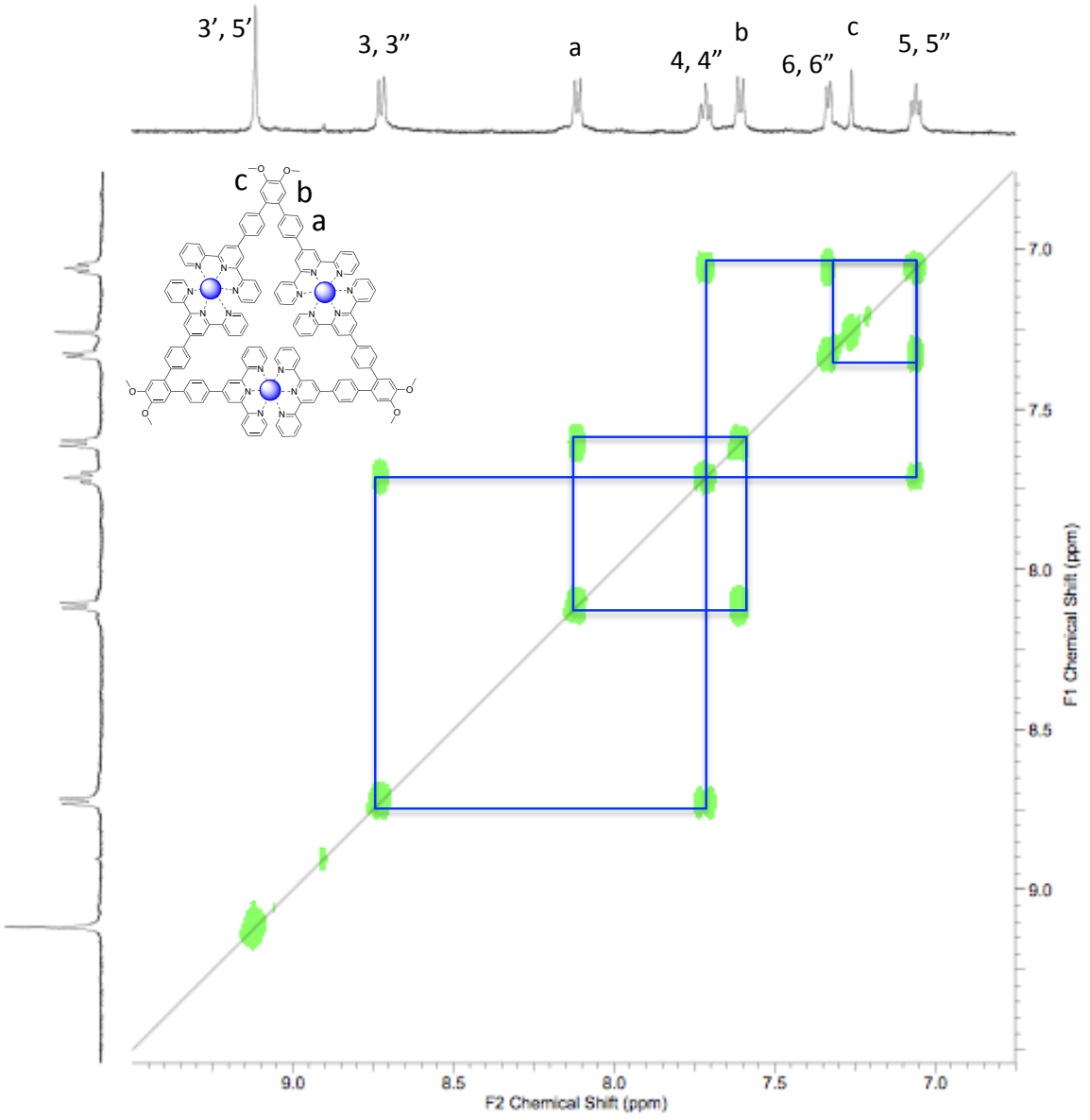


Figure 4.3 COSY spectrum of **4** in $CD_3CN$.

The ESI-MS spectrum[97] (Figure 4.4) of **4** shows a series of peaks corresponding with charge states 3+ through 6+ for the combination of three ligands, three metals and the corresponding number of $PF_6^-$ anions. The inset shows the matching theoretical (calcd) and experimental isotope patterns for the 5+ charge state.

The TWIM-MS spectrum[183] (Figure 4.5) plots m/z against drift time (milliseconds) of **4** shows the expected step pattern corresponding with charge states 3+ through 6+. Each charge state has a narrow drift time distribution showing that no other structural conformers or isomers were detected.

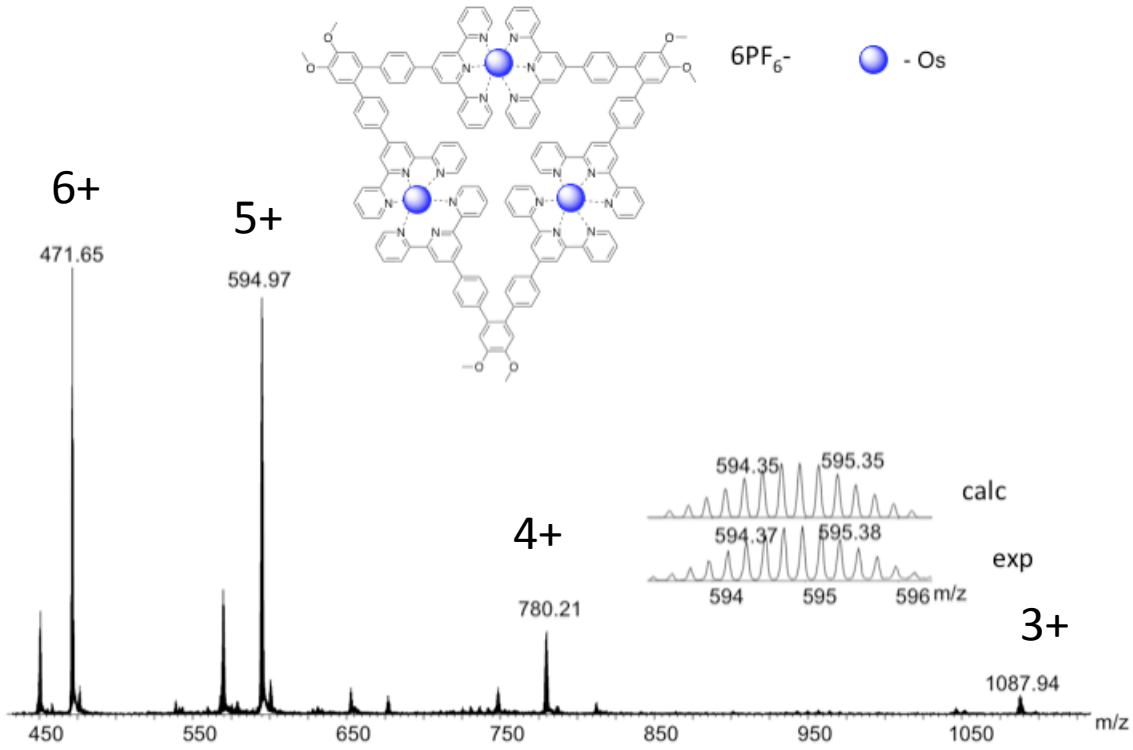


Figure 4.4 ESI-MS spectra of **4** with theoretical and experimental isotope patterns for the 5+ ion.

Previous investigators[150] have looked at relative binding strength of <tpy–$M^{II}$-tpy> complexes using MALDI-TOF. Binding strength by metal was ranked based upon percentage laser intensity required to achieve a fragmentation ratio of 10. Relative complex stability was ranked by metal as Co > Ru > Fe > Ni > Cu > Mn > Cd. However, the study was not quantitative and did not include <tpy–$Os^{II}$-tpy>. Other methods[203] of

estimating relative binding strength of these complexes include thermogravimetric analysis (TGA), however, these studies did not include <tpy–$Os^{II}$-tpy> either.

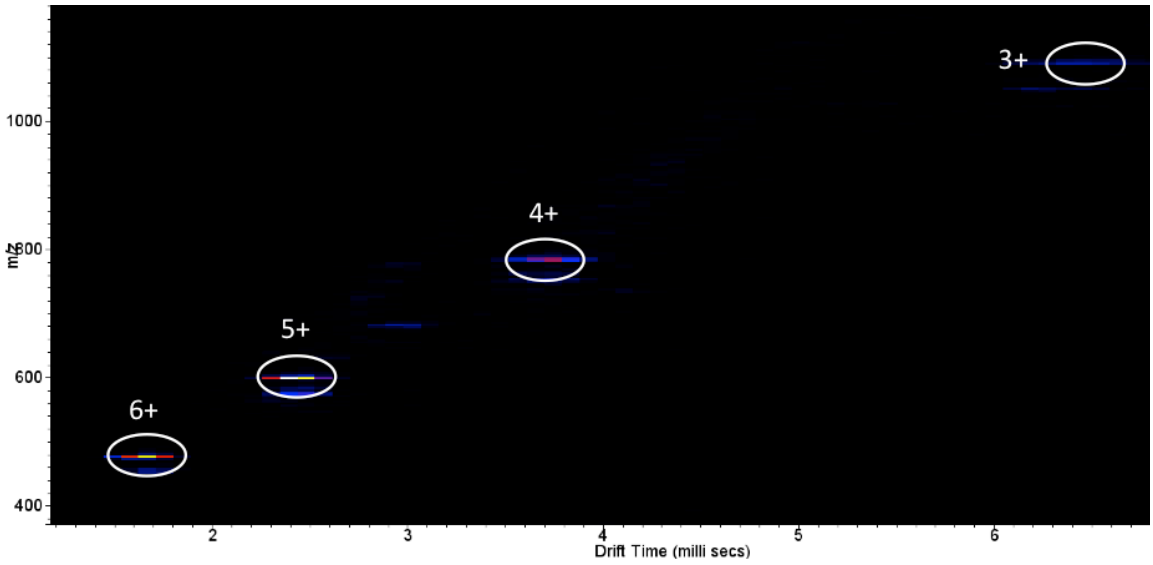


Figure 4.5 TWIM-MS spectra of **4** shows m/z *vs.* drift time (ms).

Gradient $MS^2$ in tandem with TWIM MS was utilized to study[97] the relative stability of **2**, **3**, and **4**. The 5+ charge state was selected and then subjected to collisionally activated dissociation (CAD) in the trap cell, using Ar as the collision gas. The $MS^2$ spectra was obtained across a range of voltages to determine at which point the 5+ ion was fully dissociated. The 2D $MS^2$ spectra are shown for each in Figure 4.6. **2**, **3**, and **4** fully disappeared at 32, 46, and 45V, respectively. The equivalent center-of-mass collision energies ($E_{cm}$) were calculated and were found to be 2.45, 3.35, and 2.96 eV. This result indicates that <tpy–$Ru^{II}$-tpy> has the highest binding strength and that relative binding strength is Ru > Os > Fe. The same trend was observed with charge state 4+. **2**, **3**, and **4** fully disappeared at 34, 49, and 50V, respectively. The equivalent center-of-mass

collision energies ($E_{cm}$) were calculated and were found to be 1.97, 2.71, and 2.53 eV. A previous comparison[128] of Ru versus Fe Dondorff rings (tetramer of ligand **1**) gave 2.31 and 1.77 eV respectively, for a 4+ charge state, indicating a similar trend. The lower values for the tetramers could be related to more ring strain. Note also that, as expected, **2**, **3**, and **4** have essentially identical drift times on the order of 2.5 milli-secs. Investigators[195, 198, 204] of electrochemical behavior of <tpy–$M^{II}$-tpy> systems have reported that Ru is oxidized at much more positive potentials that Os (*e.g.*[198]: 1.30 *vs.* 0.95V). Accordingly, if an electron is more readily removed from $Os^{II}$ compared to $Ru^{II}$, breakup of a coordinative bond to $Os^{II}$ should be more facile, as indeed indicated by the gradient $MS^2$ methodology (Figure 5). Previous studies[64] indicate that the rupture of the coordinative bond is the mechanism by which <tpy-$M^{II}$-tpy> based structures breakup under CAD.

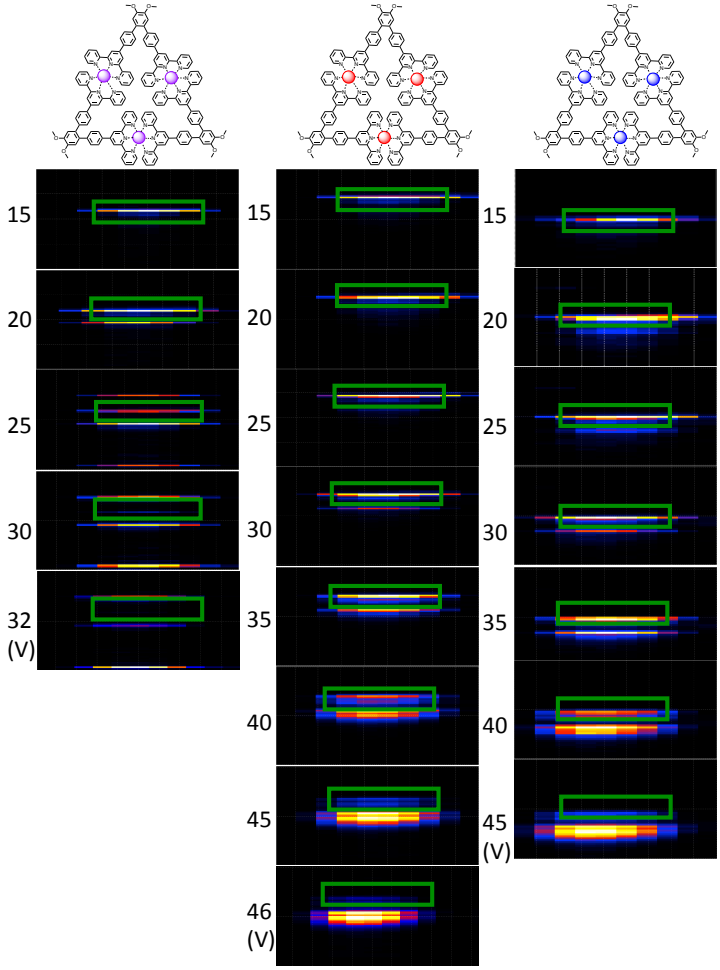


Figure 4.6 Gradient Tandem-MS spectra of the 5+ charge state for **2** (514 m/z), **3** (541 m/z), and **4** (595 m/z) shows m/z vs. drift time (ms). The x-axis range for all is 1.8 to 2.7 *vs.* drift time.

Absorption spectra for **2**, **3**, and **4** are shown in Figure 4.7. The intense bands in the UV region are attributable to ligand centered π-π* transitions. Neat ligand **1** has π-π* bands at 285 and 330nm localized on the tpy-Ph subunits.[128] Upon complexation with $M^{II}$, MLCT bands occur in the visible region. Absorption maxima for **2**, **3**, **4**, and some reference compounds are summarized in Table 4.2. Absorption maxima for the spin allowed d-π $^{1}$MLCT are essentially the same for $Ru^{II}$-**1** and $Os^{II}$-**1** (492 *vs.* 493nm). The

band maxima at 670 nm observed with **4** is attributable to a spin forbidden d-π $^{3}$MLCT. The values are characteristic of previously reported[195, 198] values of <ttpy-Ru$^{II}$-ttpy> and <ttpy-Os$^{II}$-ttpy> complexes (ttpy = 4-(*p*-tolyl)-[2,2':6',2"]terpyridine). Looking at reference compounds, for both Ru and Os, we see that substituent change from tpy to ttpy shifts λ values to lower energy. The Fe$^{II}$-**1** band at 569 nm is characteristic[68, 204] of <tpy-Fe$^{II}$-tpy> complexes.

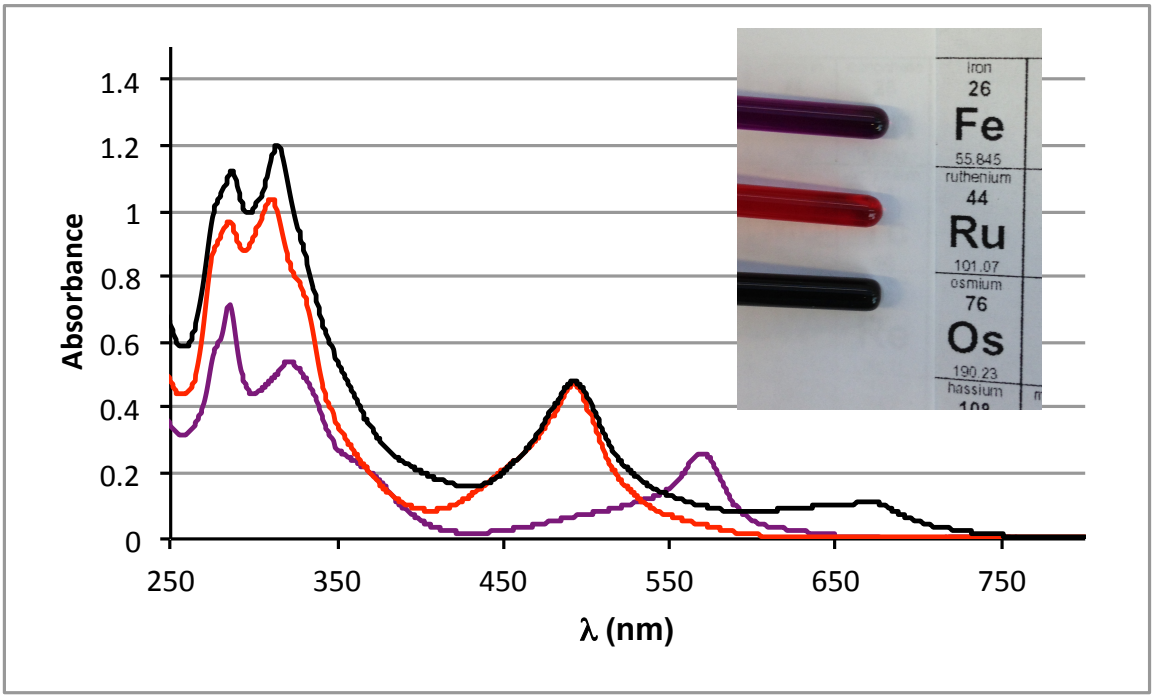


Figure 4.7 UV-Visible absorption spectra of **2** (Fe), **3** (Ru), and **4** (Os) in MeCN.

Table 4.2 Absorption spectra. **2**, **3**, and **4** were measured in MeCN.

| Complex | M(II) | λ [nm], (ε x$10^{-3}$($M^{-1}$ $cm^{-1}$)) | | | Ref |
|---|---|---|---|---|---|
| | | Ligand centered | $^{1}$MLCT | $^{3}$MLCT | |
| **2** | Fe | 285 (143), 321 (36) | 569 (17) | | |
| **3** | Ru | 285 (65), 310 (69) | 492 (31) | | |
| **4** | Os | 286 (74), 314 (80) | 493 (32) | 670 (8) | |
| **Ru(tpy)$_2$** | Ru | 270 (32), 307(52) | 475 (12) | | 198 |
| **Ru(ttpy)$_2$** | Ru | 284 (68), 310 (76) | 490 (29) | | 198 |
| **Os(tpy)$_2$** | Os | 270 (44), 310 (74) | 475 (15) | 656 (4) | 198 |
| **Os(ttpy)$_2$** | Os | 286 (58), 314 (68) | 490 (26) | 667 (7) | 198 |

## 4.3 Conclusions

The <tpy–Os$^{II}$-tpy>-based complexes are of interest in the area of artificial photosynthesis and yet their incorporation into supramolecular structures is largely unexplored. Herein, we report the first one step self-assembly of a homoleptic, <tpy–Os$^{II}$-tpy>-based metallomacrocycle (**4**) using a 60° *bis*terpyridyl ligand **1**. Macrocycle **4** was characterized *via* NMR, ESI-MS, TWIM-MS, gradient tandem-MS, and UV-VIS alongside Fe$^{II}$ and Ru$^{II}$ analogues. Center of mass collision energies derived from Gradient Tandem-MS spectrometry indicates that the Ru$^{II}$ based analogue has the highest stability followed by Os$^{II}$ and Fe$^{II}$. Absorption bands of these complexes are shifted to lower energy λ values relative to reference <tpy-M$^{II}$-tpy> and match closely those of <ttpy-M$^{II}$-ttpy> complexes.

## 4.4 Experimental

See Section 2.4 for general experimental details.

**Synthetic Procedures**

**3,4-*Bis*(4′-[2,2':6',2'']terpyridinyl-*p*-phenyl)-*o*-dimethoxybenzene (1)** was prepared, as described in the literature.[127]

**$(1)_3Fe_3^{+6}[6PF_6]$ (2)** trimer was prepared, as described in the literature;[128] $^1$H NMR (500 MHz, $CD_3CN$): δ (ppm) 9.20 (s, 12H, 3',5'-tpy*H*), 8.62 (d, *J* = 8 Hz, 12H, 3,3"-tpy*H*), 8.25 (d, *J* = 8 Hz, 12H, Ar*H*), 7.80 (dd, $J_1$ = 8 Hz, $J_2$ = 7Hz, 12H, 4,4"-tpy*H*), 7.68 (d, *J* = 8 Hz, 12H, Ar*H*), 7.31 (s, 6H, Ar*H*), 7.19 (d, *J* = 6 Hz, 12H, 6,6"-tpy*H*), 7.03 (dd, $J_1$ = 8 Hz, $J_2$ = 7Hz, 12H, 5,5"-tpy*H*), 4.05 (s, 18H, OC$H_3$; $^{13}$C NMR (125 MHz, $CD_3CN$): δ (ppm) 57.28, 115.68, 122.89, 125.29, 128.73, 128.99, 132.86, 133.52, 136.24, 140.07, 145.31, 150.80, 151.32, 154.42, 159.47, 161.68; ESI-MS (*m/z*) 404.2 $[M\text{-}6PF_6]^{6+}$ (Calcd. *m/z* = 404.1), 514.1 $[M\text{-}5PF_6]^{5+}$ (Calcd. *m/z* = 514.0), 678.8 $[M\text{-}4PF_6]^{4+}$ (Calcd. *m/z* = 678.7), 953.4 $[M\text{-}3PF_6]^{3+}$ (Calcd. *m/z* = 953.3).

**$(1)_3Ru_3^{+6}[6PF_6]$ (3).** To a solution of **1** (203 mg, 270 μmol) in MeOH/$CHCl_3$ solution (v/v,1:1, 270 mL) was added $RuCl_2(DMSO)_4$ (144 mg, 297 μmol). The orange solution was refluxed for 96 h under $N_2$, and precipitated with excess (10X) $NH_4PF_6$. The resultant orange solid was chromatographed on $SiO_2$ eluting with $H_2O$/MeCN/$KNO_{3(aq)}$ (1:17:1; v/v/v) to give (24%) **3**, as an orange solid: 74 mg; $^1$H NMR (500 MHz, $CD_3CN$): δ (ppm) 9.02 (s, 12H, 3',5'-tpy*H*), 8.66 (d, *J* = 8 Hz, 12H, 3,3"-tpy*H*), 8.14 (d, *J* = 8 Hz, 12H, Ar*H*), 7.86 (dd, $J_1$ = 8 Hz, $J_2$ = 7Hz, 12H, 4,4"-tpy*H*), 7.62 (d, *J* = 8 Hz, 12H, Ar*H*), 7.42 (d, *J* = 6 Hz, 12H, 6,6"-tpy*H*), 7.27 (s, 6H, Ar*H*), 7.13 (dd, $J_1$ = 8 Hz, $J_2$ = 7Hz, 12H, 5,5"-tpy*H*), 4.03(s, 18H, OC$H_3$); $^{13}$C NMR (125 MHz, $CD_3CN$): δ (ppm) 57.24, 115.64,

122.90, 125.99, 128.83, 132.74, 133.46, 134.36, 136.31, 139.39, 145.00, 149.14, 150.74, 153.78, 156.83, 159.61; ESI-MS (*m/z*) 427.1 $[M - 6PF_6]^{6+}$ (Calcd. *m/z* = 427.1), 541.5 $[M - 5PF_6]^{5+}$ (Calcd. *m/z* = 541.6), 713.0 $[M - 4PF_6]^{4+}$ (Calcd. *m/z* = 713.2), 999.1 $[M - 3PF_6]^{3+}$ (Calcd. *m/z* = 999.3).

**$(1)_3Os_3^{+6}[6PF_6]$ (4). 1** (100 mg, 133 μmol) and $OsCl_3$ $H_2O$ (39.4 mg, 133 μmol) were added to $HO(CH)_2OH$ (70 mL), the solution was stirred at reflux under $N_2$ for 6 h, cooled, and diluted with 0.4M $NH_4PF_6$ in $H_2O$. A fine black solid was filtered, washed with $H_2O$ and EtOH, dried *in vacuo*, dissolved in MeCN, adsorbed onto $SiO_2$ and chromatographed using $H_2O$/MeCN/$KNO_{3(aq)}$ (1:17.5:1) to isolate crude **4**. Conversion to $PF_6^-$ counterions was achieved by dissolving the complex in MeOH and precipitating with excess $NH_4PF_6$. A black precipitate formed, which was filtered, washed with a mixture of MeOH and $H_2O$, and dried *in vacuo* to give (7.3 %) of **4**: 12 mg; $^1$H NMR (500 MHz, $CD_3CN$): δ (ppm): 9.12 (s, 12H, 3',5'-tpy*H*), 8.73 (d, *J* = 8 Hz, 12H, 3,3"-tpy*H*), 8.12 (d, *J* = 8 Hz, 12H, Ar*H*), 7.71 (dd, $J_1$ = 8 Hz, $J_2$ = 7Hz, 12H, 4,4"-tpy*H*), 7.61 (d, *J* = 8 Hz, 12H, Ar*H*), 7.33 (d, *J* = 6 Hz, 12H, 6,6"-tpy*H*), 7.26 (s, 6H, Ar*H*) 7.06 (dd, $J_1$ = 8 Hz, $J_2$ = 7 Hz, 12H, 5,5"-tpy*H*), 4.03(s, 18H, $OCH_3$; ESI-MS (*m/z*) 471.6 $[M-6PF_6]^{6+}$ (Calcd. *m/z* = 471.6), 594.9 $[M-5PF_6]^{5+}$ (Calcd. *m/z* = 594.9), 780.2 $[M-4PF_6]^{4+}$ (Calcd. *m/z* = 780.0), 1087.9 $[M-3PF_6]^{3+}$ (Calcd. *m/z* = 1088.2).

# CHAPTER V

# AMPHIPHILIC METALLOTRIANGLES: SYNTHESIS, CHARACTERIZATION AND HIERARCHICAL ORDERING

## 5.1 Introduction

Biomolecular systems employ a variety of non-covalent inter- and intramolecular interactions including van der Waals, *H*-bonding, π-π stacking, electrostatic, as well as metal-ligand coordination to achieve macromolecular structure and specific function.[205] Use of these forces to construct synthetic macromolecular assemblies is better known as supramolecular chemistry.[6] Metal-ligand self-assembly with the *N*-heteroaromatic ligands, specifically [2,2':6',2'']terpyridine (tpy) using the directional bonding approach,[48] has expanded the field of metallosupramolecular chemistry[170] and created a collection of interesting new macrocycles[33, 48, 127, 147, 183] and 3D structures.[48, 62, 168]

Various strategies have been utilized to incorporate these well-defined supramolecular structures into larger, macroscopic compositions or materials, including the synthesis of nanoscale macromolecular structures,[68] functionalization of nanoparticles,[133, 146] and attachment to diverse surfaces.[137] There is increasing interest in use of non-covalent forces in second order self-assembly of nanostructures.[138, 139] Investigations into self-ordering of <tpy-$M^{II}$-tpy>-based supramolecular structures using non-covalent intermolecular interactions have been limited, mainly focusing on using ion

pairing[127, 146] to enhance structural stacking. The limited number of investigations is surprising given that biological systems use self-organization *via* non-covalent forces to create structure and function at a variety of scales[206] including not only molecular (*e.g.* enzymes, DNA), but also materials (*e.g.* cell membranes, protein coats). Nature also provides examples for self-assembly of metal complexes into nanostructures, namely, the self-ordering of chlorophyll b (BChl) into rolls of light adsorbing arrays by photosynthetic bacteria.[207] BChl is a macrocyclic metal complex [porphyrin ($Mg^{II}$)] with a long alkyl chain, ranging from C16 to C20.[207] Thus, BChl is amphiphilic; containing both a hydrophilic, ionic metal complex region and a hydrophobic chain. Aromatic π-π stacking interactions have been shown to play a role in recognition and ordering of these biomolecular materials.[208] Such <tpy-$M^{II}$-tpy> complexes also possess ionic and aromatic character. Synthetic amphiphiles including surfactants and amphiphilic block copolymers have been used to create ordered structures[139] and the field of supra-amphiphiles has been pioneered by the Zhang group.[209, 210] Studies of hierarchical ordering of amphiphilic metallocycles is relatively limited to those using to pyridine[138] and bipyridine based ligands.[211] Whereas, the related <tpy-$M^{II}$-tpy>-based systems are unexplored. Can an amphiphile based strategy be used to promote the ordering of <tpy-$M^{II}$-tpy>-based supramolecular structures? Just as the directional bonding approach[48] allows for precise placement and concentration of <tpy-$M^{II}$-tpy> moieties or functionality within a supramolecular architecture, it can also be utilized for positioning the direct termini of intermolecular recognition/self-organization at the material scale.[139] In the field of crystal engineering, such moieties have been termed supramolecular synthons[212] and their location and orientation have been shown to affect self-ordering behavior.[213, 214]

Scheme 5.1 shows the self-assembly of a C16-functionalized *bis*terpyridine to create an amphiphilic <tpy-$M^{II}$-tpy>-based supramolecular structure.

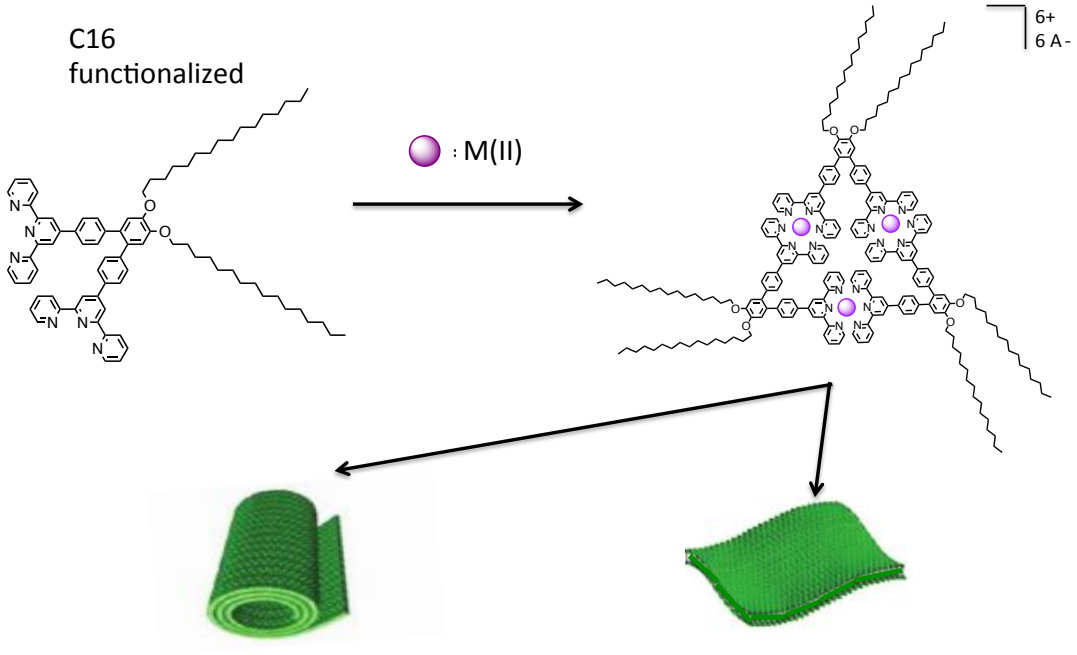


Scheme 5.1 Self-assembly of *bis*-C16 functionalized *bis*terpyridine with $M^{II}$ forming amphiphilic triangles, and its subsequent, proposed ordering into lamella and rod-like structures. [Illustration used with permission of *Acc. Chem. Res.*, **2011**, *44*, 72-82.]

Given the limited information on self-ordering of amphiphilic, terpyridine-based metallosuprastructures, unanswered questions include: does lability of the <tpy-$M^{II}$-tpy> complex affect ordering? How does the introduction of hydrophobic/hydrophilic type interactions impact ordering? Does directionality and location of hydrophobic moieties play a role? Understanding such issues is critical since self-organization will continue to play a critical role in nanotechnology.[215, 216] Also, the use of non-covalent forces in bottom up fabrication of materials is projected to offer potential advantages including economic fabrication, self-healing, stimuli responsiveness, and recyclability.[144]

In this study, we synthesize, characterize, and evaluate self-ordering of a simple series of metallotriangles that include alkylated (C16) and non-alkylated analogues, self-assembled with both labile ($Zn^{II}$) and non-labile ($Fe^{II}$) metals. Also, we include a ′corner′ analogue, synthesized with the non-labile $Ru^{II}$, in order to gauge the effects of structure on aggregation.

## 5.2 Results and Discussion

### Synthesis

Ligand **3** was synthesized in three steps (Figure 5.1): alkylation of catechol with 1-bromohexadecane, followed by bromination, and then Suzuki-Miyaura coupling[39] to yield the desired *bis*-C16 functionalized, 60°, *bis*terpyridine directed monomer in an overall yield of 46%.

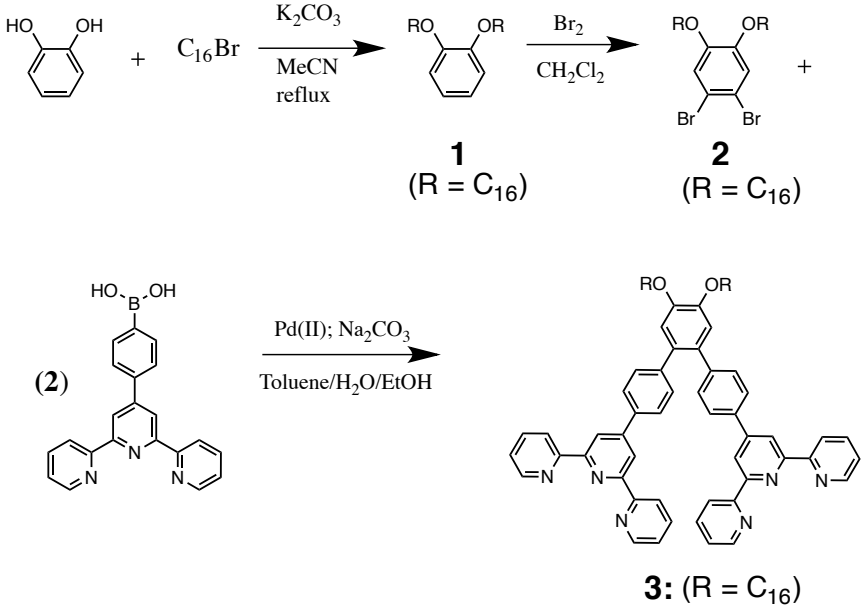


Figure 5.1 Synthesis of C16 *bis*alkylated *bis*terpyridine ligand **3.** (2) = 2 equiv.

The 60° directed monomer **3** was subsequently self-assembled (Figure 5.2) using $Zn^{II}$ to generate the kinetic amphiphilic triangle **4**, which was isolated in 84% and with $Fe^{II}$ non-labile triangle **5**, which was purified by column chromatography. Self-assembly using ligand **6** (Figure 5.2) gave non-amphiphilic, ′control′ triangles **7** and **8**, which were compared to **4** and **5** to gauge the effect of alkylation on self-assembly and resultant morphology.

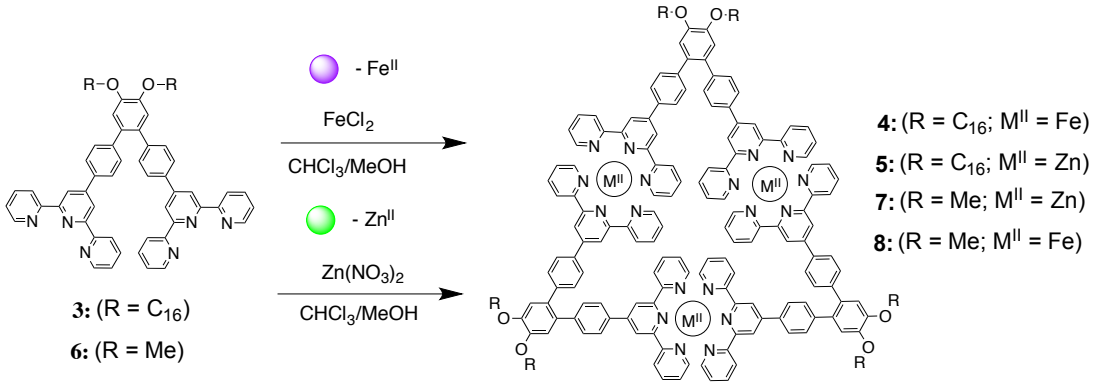


Figure 5.2 Self-assembly of **3** at 1:1 ratio with $Fe^{II}$ and non-labile $Zn^{II}$ forming the amphiphilic triangles **4** and **5**, respectively and of **6** to form non-amphiphilic ′control′ triangles **7** and **8**.

Synthesis of ′corner analogue′ **11** required a two-step synthesis,[195, 217, 218] as shown in Figure 5.3. The $Ru^{III}$ adduct was formed and subsequently reduced at a 2:1 ratio with ligand **3**. Complexes formed with $Ru^{II}$ are non-labile so **11** can be compared to **4** to gauge the effect of the triangular geometry on self-assembly and resultant morphology.

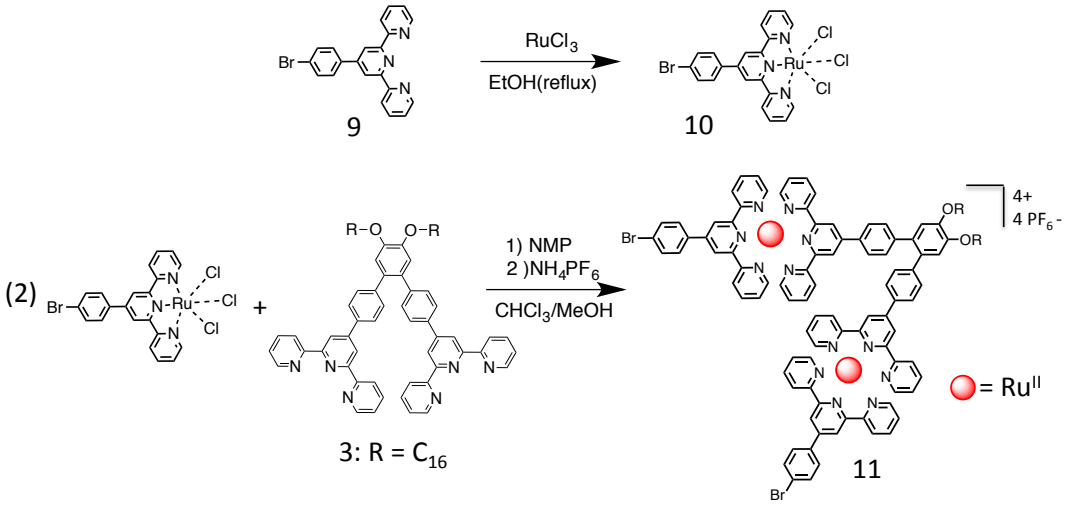


Figure 5.3 Synthesis of a non-labile ($Ru^{II}$) corner analogue (**11**) using a two-step synthesis.

This series of compounds will allow us to gauge the effect of molecular topology on the self-ordering of <tpy-$M^{II}$-tpy>-based structures. The differences between the structures are modeled and represented in Scheme 5.2.

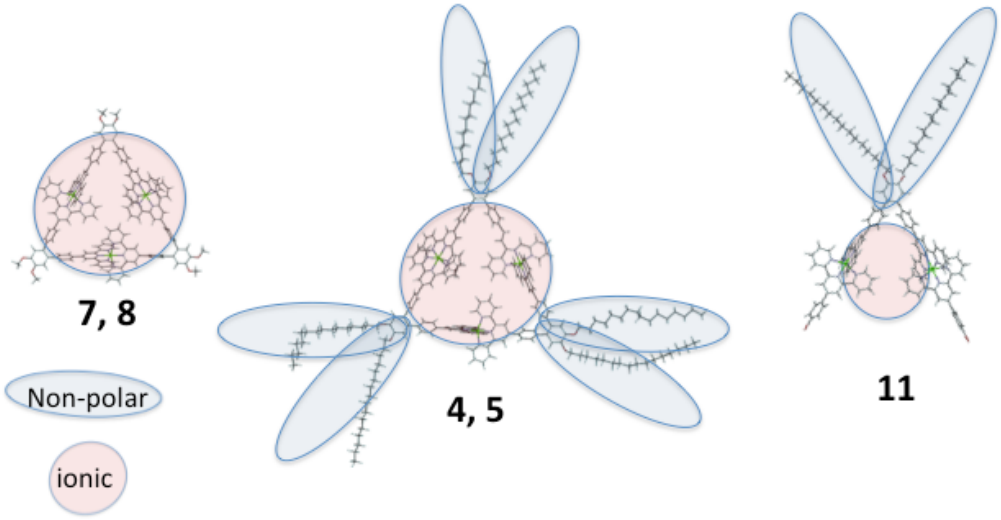


Scheme 5.2 Molecular models and topology of **4**, **5**, **7**, **8**, and **11**.

**NMR Spectroscopy and Mass Spectrometry**

The $^{1}$H NMR of **4** and **5** each reveal a single set of terpyridine proton signals consistent with a fully cyclic structure (Figure 5.4). Compared to the initial ligand **3**, the upfield shift of the 6,6"-tpy*H* signals (8.69 to 7.15 (**4**) and 7.81 (**5**) ppm) supports *bis*terpyridine complexation; no uncomplexed terpyridine was observed. The relative shifts between Fe and Zn complexes, such as the less pronounced 6,6"-tpy*H* shift for Zn complexes and the highly deshielded 3',5"-tpy*H* for the Fe complexes, match well with previously reported systems.[128] Both **4** and **5** show a triplet corresponding to the methoxy protons at 4.13 and 4.19 ppm, respectively. COSY NMR spectroscopy confirmed proton assignments. $^{1}$H NMR shifts for controls **7** and **8** each matched with previous values as well.

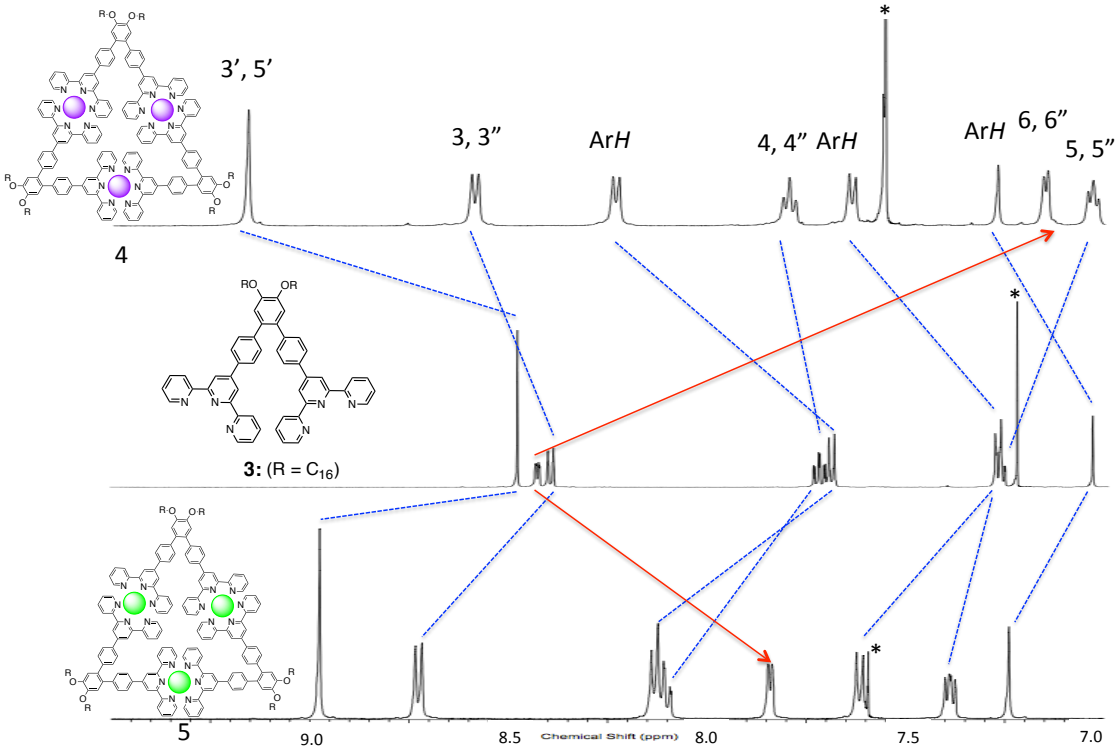


Figure 5.4 $^{1}$H NMR spectrum of ligand (**3**) in $CDCl_3$ and alkylated triangles **4** and **5** in $CD_3CN/CDCl_3$ (5:1) (*-$CHCl_3$).

Table 5.1 $^{1}$H NMR (500MHz) chemical shifts (ppm) assigned to **4**, **5**, **7**, and **8** in $CD_3CN/CDCl_3$ (5:1).

| Compound | 3', 5' | 3, 3" | ArH | 4, 4" | ArH2 | 6, 6" | 5, 5" | OCHn |
|---|---|---|---|---|---|---|---|---|
| **4 (Fe/OC16)** | 9.16 | 8.59 | 8.23, 7.64 | 7.8 | 7.27 | 7.15 | 7.03 | 4.13 |
| **5 (Zn/OC16)** | 8.94 | 8.69 | m(8.04-8.14), 7.58 | m(8.04-8.14) | 7.20 | 7.81 | 7.35 | 4.19 |
| **7 (Zn/OMe)** | 8.99 | 8.73 | 8.14, 7.64 | 8.1 | 7.26 | 7.85 | 7.38 | 4.04 |
| **8 (Fe/OMe)** | 9.2 | 8.62 | 8.25, 7.68 | 7.8 | 7.31 | 7.19 | 7.03 | 4.05 |

The $^{1}$H NMR of **11** (Figure 5.5) shows two distinct sets of terpyridine. Both sets show an upfield shift of the 6,6"-tpy*H*- signals to the multiplet at 7.37-7.40 ppm thereby supporting the *bis*terpyridine complexation; no uncomplexed terpyridine was observed. A triplet corresponding to the alkoxy protons was present at 4.20 ppm. Shift values matched well with previously reported $Ru^{II}$ complexes.[128]

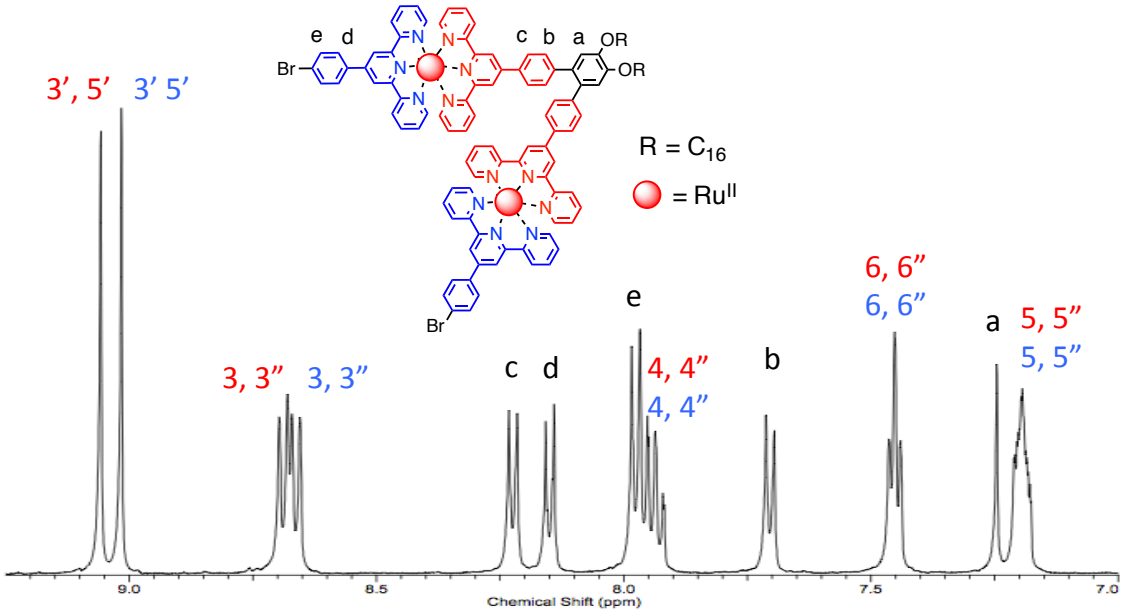


Figure 5.5 $^{1}$H NMR spectrum, aromatic region of corner analogue **11** in $CD_3CN/CDCl_3$ (5:1).

Both COSY and NOESY NMR spectroscopy confirmed proton assignments (Figures 5.6 - 7). With the exception of the 3',5'-*H*s the two sets of terpyridine protons overlap; however, the aryl-*H* doublets b, c, d, and e are all distinct and can be paired based upon coupling cross peaks in the COSY spectra. Full assignment requires NOESY. With the NOESY spectrum we are able to assign the 3',5'-*H*s by tracing the red 3',5'-*H* signals through space interactions with doublet c, which then interacts with signal b to a, which has a cross-peak with the alkoxy protons (triplet) at 4.20 ppm. Similarly, the blue 3',5'-*H* can be traced with doublets d and e. The 3,3" signals are readily assigned as well, while the remaining terpyridine protons are overlappped.

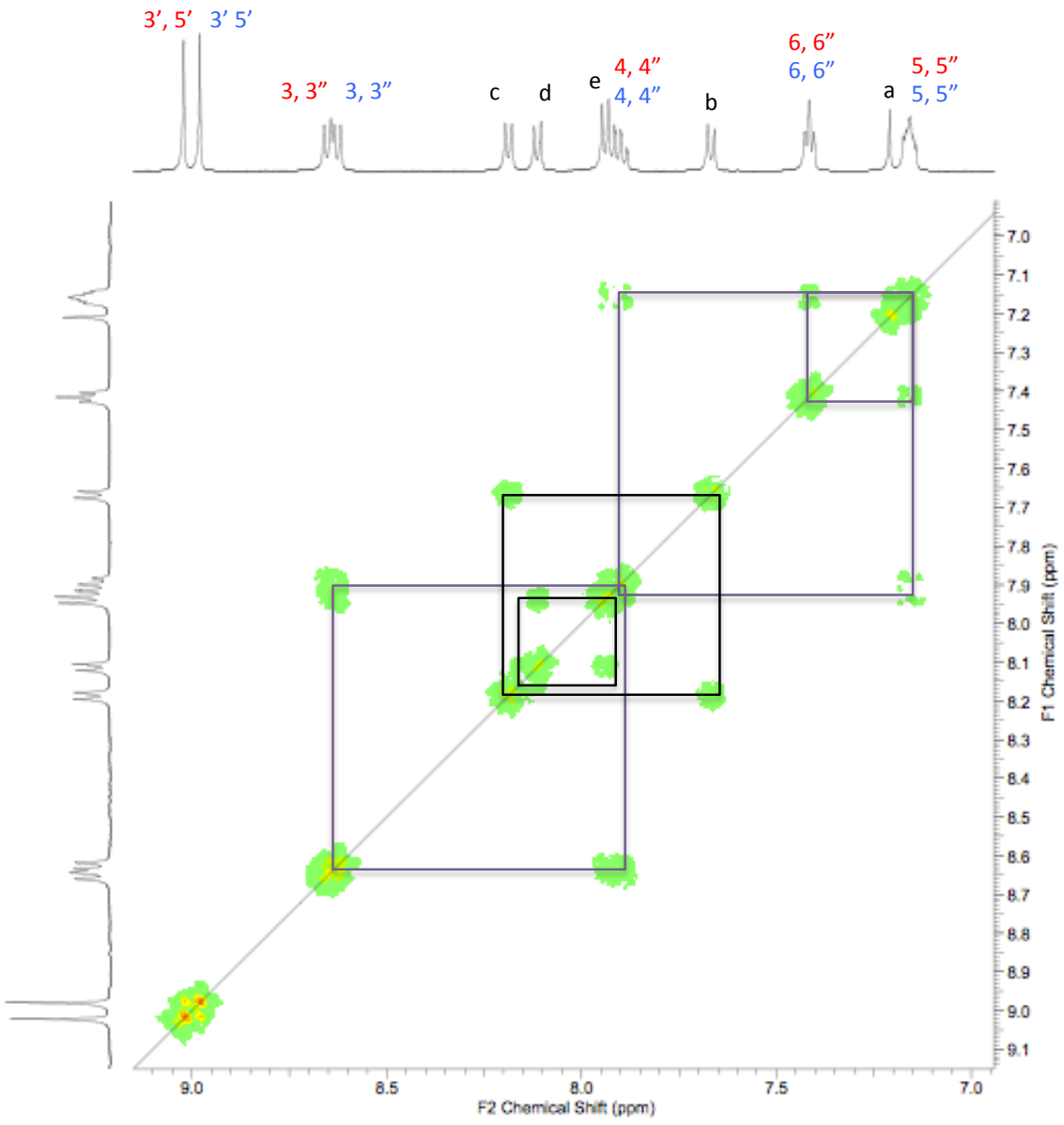


Figure 5.6 COSY NMR spectra, aromatic region of corner analogue **11** in $CD_3CN/CDCl_3$ (5:1).

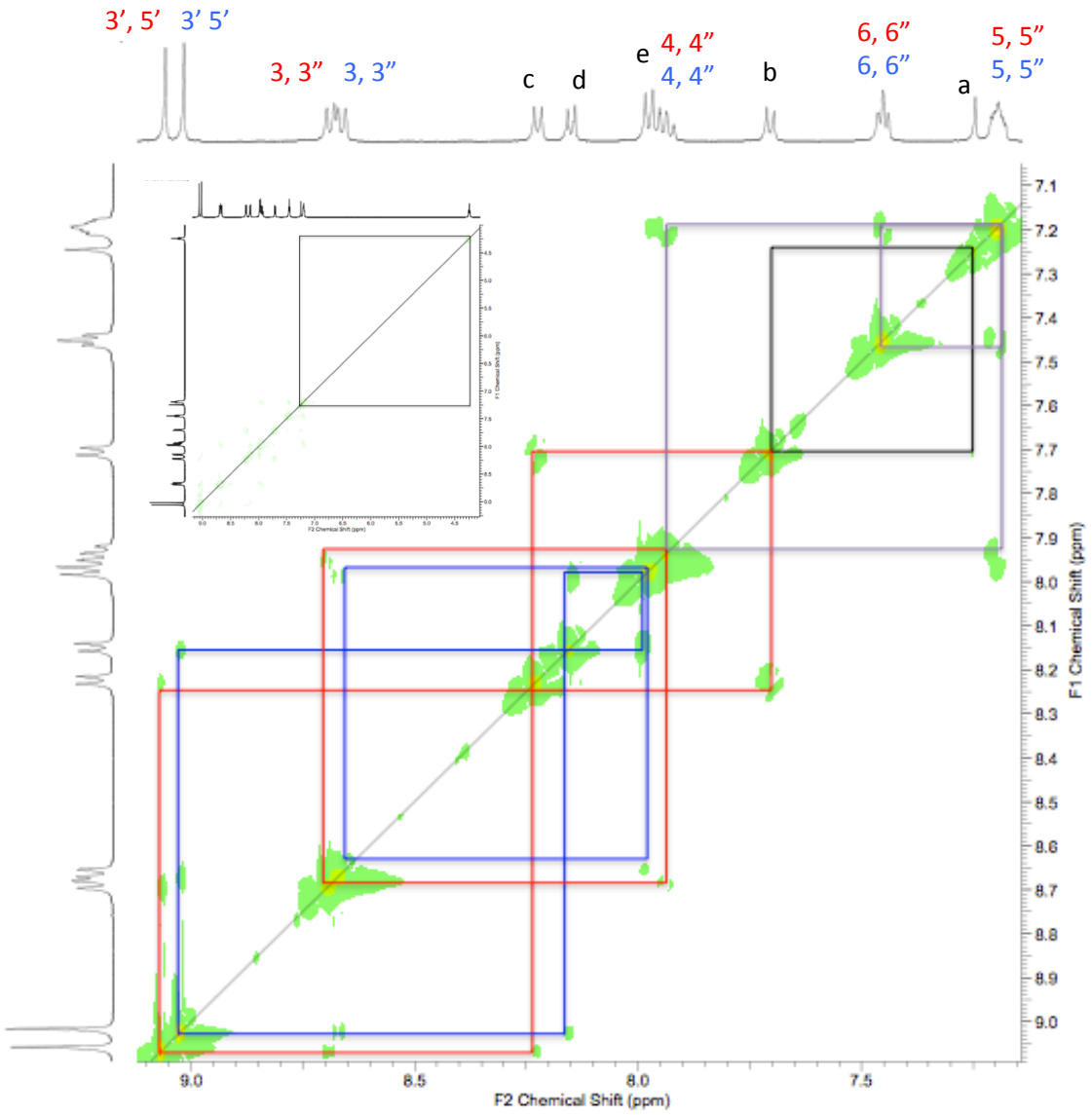


Figure 5.7 NOESY spectra, aromatic region of corner analogue **11** in $CD_3CN/CDCl_3$ (5:1). The inset shows through space interaction between aryl proton A (singlet) and the alkoxy ($CH_2$) protons (triplet).

Triangles **4, 5**, **7**, **8**, and **11** were characterized by ESI-MS. The spectrum of **4** with $Cl^-$ counterion is shown in Figure 5.8. The series of peaks match charge states $3^+$ through $6^+$ corresponding to three ligands, three $Fe^{II}$ atoms, and corresponding number of $Cl^-$ anions.

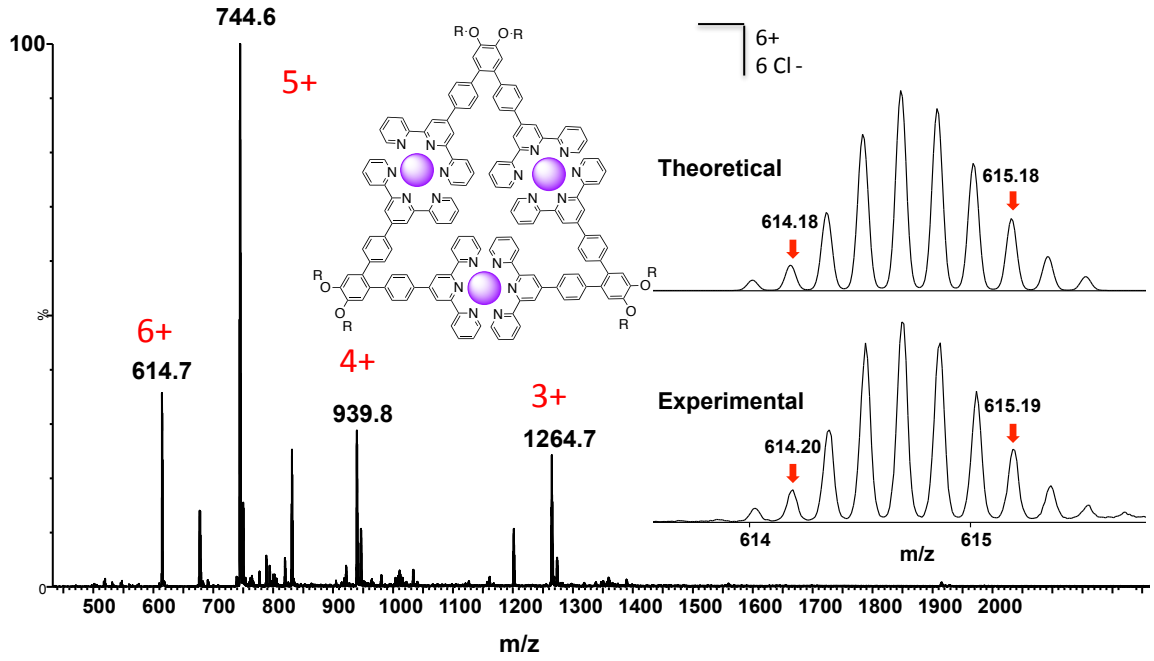


Figure 5.8 ESI-TOF-MS of self assembled triangle $Fe/C_{16}$ (**4**) with chloride counterion. Isotope patterns are for the 6+ charge state. R = $C_{16}$.

## Microscopy

Using TEM, 0.1 μM solutions were cast onto copper grids and viewed to assess the effect of amphiphilicity, metal type, and geometry upon the resultant morphology. These comparisons are represented in Figure 5.9.

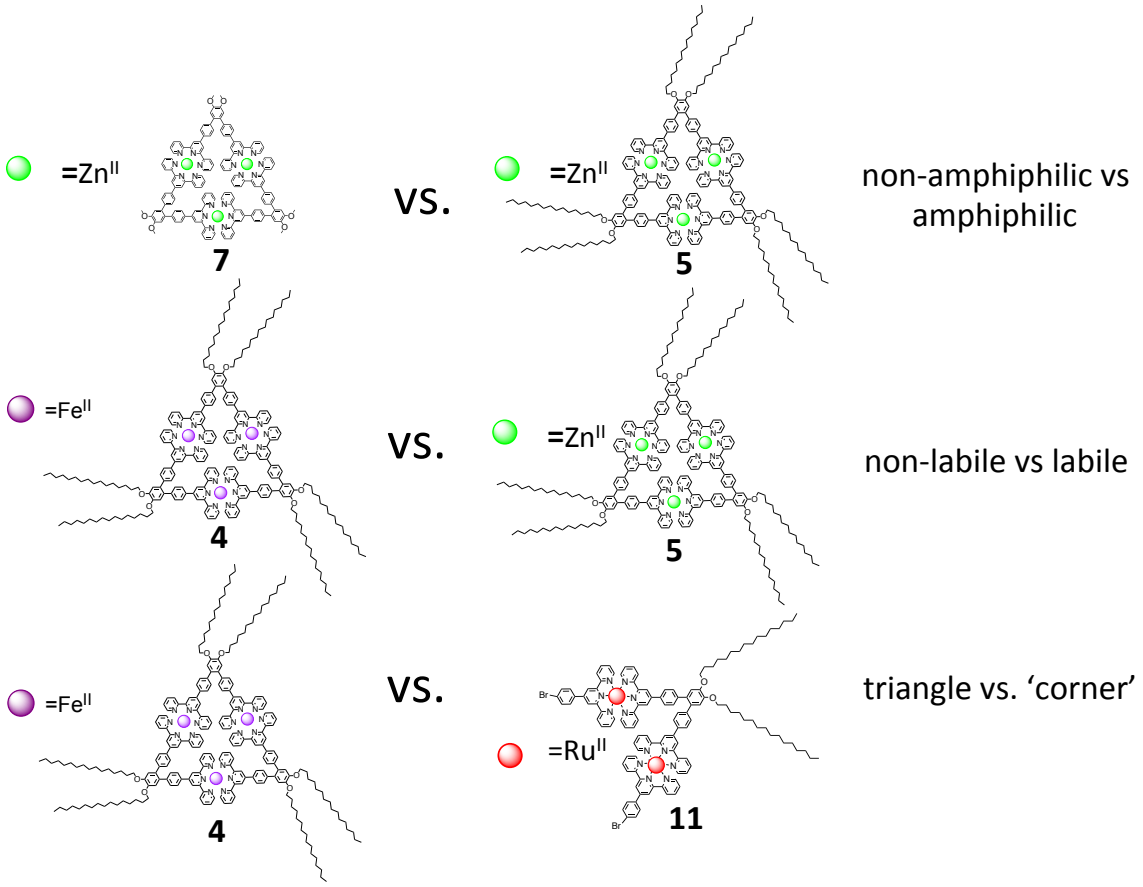


Figure 5.9. Comparisons in TEM study.

Figure 5.10 shows representative pictures of the Zn/OC16 (**5**) *vs*. control Zn/OMe (**7**). Aggregates of **7** are coarse and amorphous; however, those formed by **5** are comprised of extended, rod-like structures with diameters of *ca.* 40 nm, which have bundled. The sharp, uniform edges were likely formed at an interface during the ordering process. Lamellar features are observed suggesting presence of greater surface area during the formation of the amphiphile-based aggregates. The aspect ratio of the resultant structures is consistent with 1D propagation process seen where $\pi - \pi$ stacking can occur.[139]

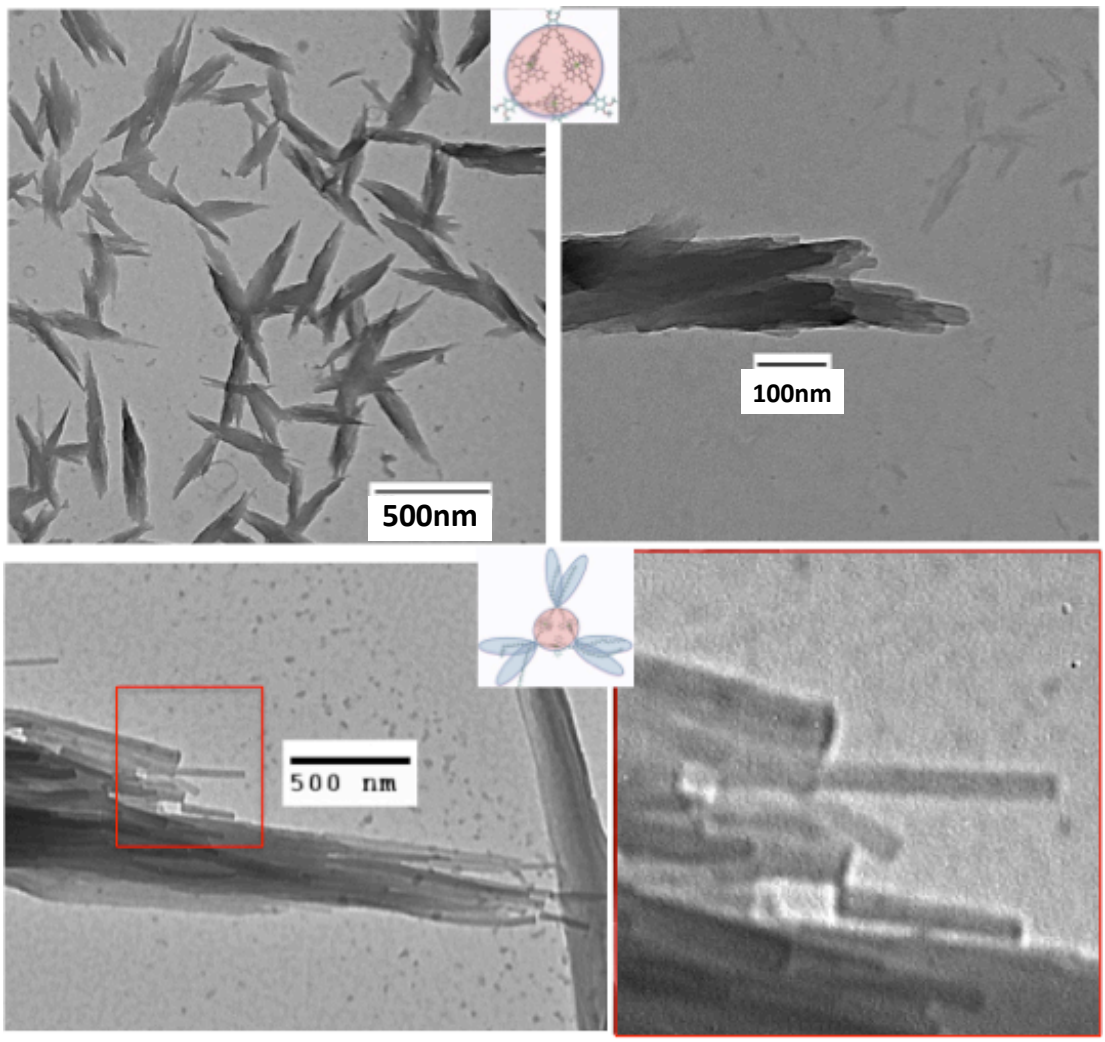


Figure 5.10 TEM images. Aggregates of $Zn^{II}$-based triangles. Top – **7** (control). Bottom – **5**, (C16 functionalized). Cast from 5/1 MeCN/$CHCl_3$.

Figure 5.11 shows a similar comparison for the macrocycles self-assembled using the non-labile metal $Fe^{II}$. Again, the Fe/OMe (**8**) forms coarse, granular structures with no clear nanoscale order. Conversely, the aggregations of Fe/OC16 (**4**) show a combination of highly directional, anisotropic rod-like structures and lamellar regions. Concentration effects on supramolecular structure with labile <tpy-$M^{II}$-tpy> systems have been demonstrated[105, 125] and could potentially affect ordering/morphology under these

conditions. Comparing Zn/OC16 (**5)** to Fe/OC16 (**4)** it is clear that both form more extended structures relative to their respective controls. No major differences between the labile and non-labile based systems were conclusively noted. Possible mechanisms for creation of these rod-like structures include formation of anisotropic lamellae, which subsequently roll, curl, or stack into rod-like structures upon concentration, precipitation, and drying that occurs after casting. Formation of micelles which aggregate to form cylindrical vesicles is another possibility.[139] Constable and Housecroft have studied the effects of alkylation (C8 vs. Me) on ordering/crystallization of metal complexes formed using divergent isomeric terpyridines (*e.g.* – 4,2':6',4"). They reported[219, 220] that the longer alkyl chains promoted enhanced 2D sheet formation and interpenetration and preliminarily attributed the effect to enhanced solubility.

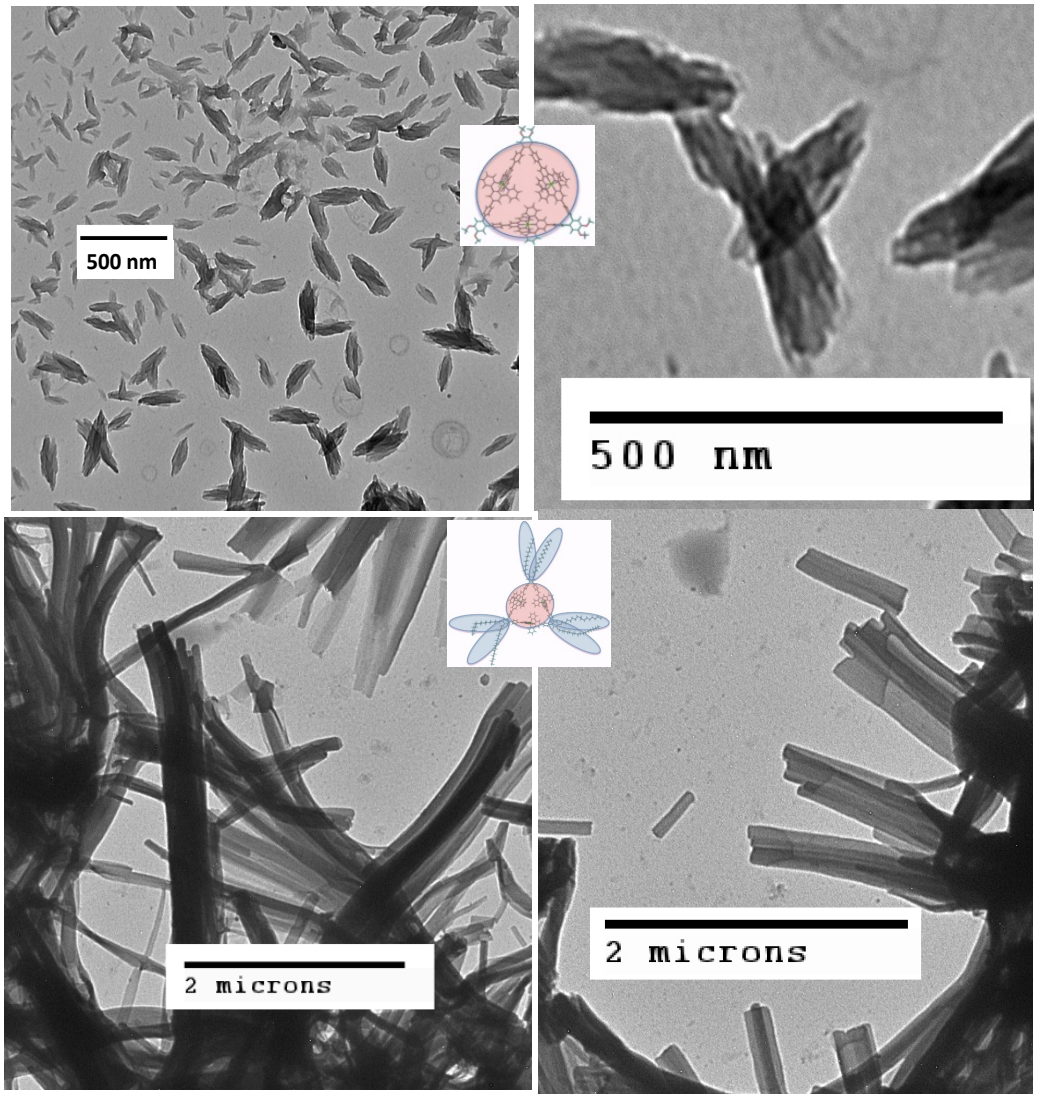


Figure 5.11 TEM images. Aggregates of $Fe^{II}$ based triangles. Top **8** (control), Bottom – **4** (C16 functionalized). Cast from 5/1 MeCN/$CHCl_3$.

Figure 5.12 shows TEMs of the ′corner analogue′ **11**. This material did not form the rod-like structures seen with the alkylated triangles. Directionality and uniformity, are significantly impaired relative to the non-labile, Fe/OC16 (**4)** and the morphology bears more resemblance to Fe/OMe (**8**). Since the rods are not seen, this suggests that the triangular geometry/topology contributes to the ability to form the rod-like structures.

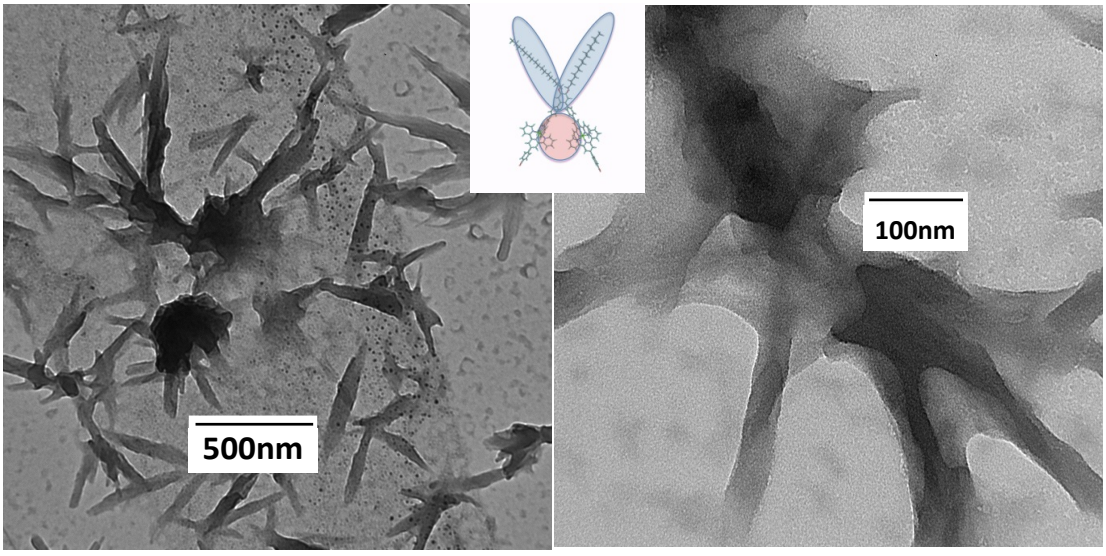


Figure 5.12 TEMs showing aggregations of **11**, $Ru^{II}$-based ′corner analogue′. Cast from 5/1 MeCN/$CHCl_3$.

TEM diffraction was conducted on structures of **4** and **5** to gain insight into molecular packing. Figure 5.13 includes a diffraction pattern for **5**. The streaked pattern is due to some defects and disordered regions within the ribbon-like structure and is commonly observed in stacked, liquid crystalline phases.[146, 221] From the diffraction patterns we were able to estimate two, d-spacing values of 8.9 and 46Å. A proposed 2D packing model, based on these values, is shown. Modeling indicates that to achieve spacing of 8.9Å, very close packing of the triangles is necessary and that intermolecular π-π stacking of the <tpy-$M^{II}$-tpy> would be present and that the stacking corresponds to the longitudinal direction of the structures. π-π stacking has been reported, both intra-[118, 169] and intermolecularly,[170, 222] in <tpy-$M^{II}$-tpy>-based molecules and materials. Diffraction of the $Fe^{II}$ structures gave similar d-spacing values of 8.9 and 48 Å. Previously reported[128] fibers of non-alkylated $Zn^{II}$ triangle using a hexacarboxylate counterion showed similar spacing values of 8.4 and 40 Å and also showed a stacking

direction corresponding to longitudinal direction of the fiber. That report did not make note that a spacing value of 8.4 Å would likely require intermolecular π-π stacking of the complexes. The larger spacing values observed here can be explained by presence of the bulky aliphatic chains. The different counterion could also be a factor. These results support the proposition that <tpy-$M^{II}$-tpy> moieties, due to their ionic and π-π stacking interactions, constitute a crystal engineering motif or synthon.[170] These results suggest that the coalescence promoted by the hydrophobic/hydrophilic interactions facilitates and propagates molecular information sharing and recognition between the molecules/synthons, thus enabling formation of more uniform and extended nanostructures.

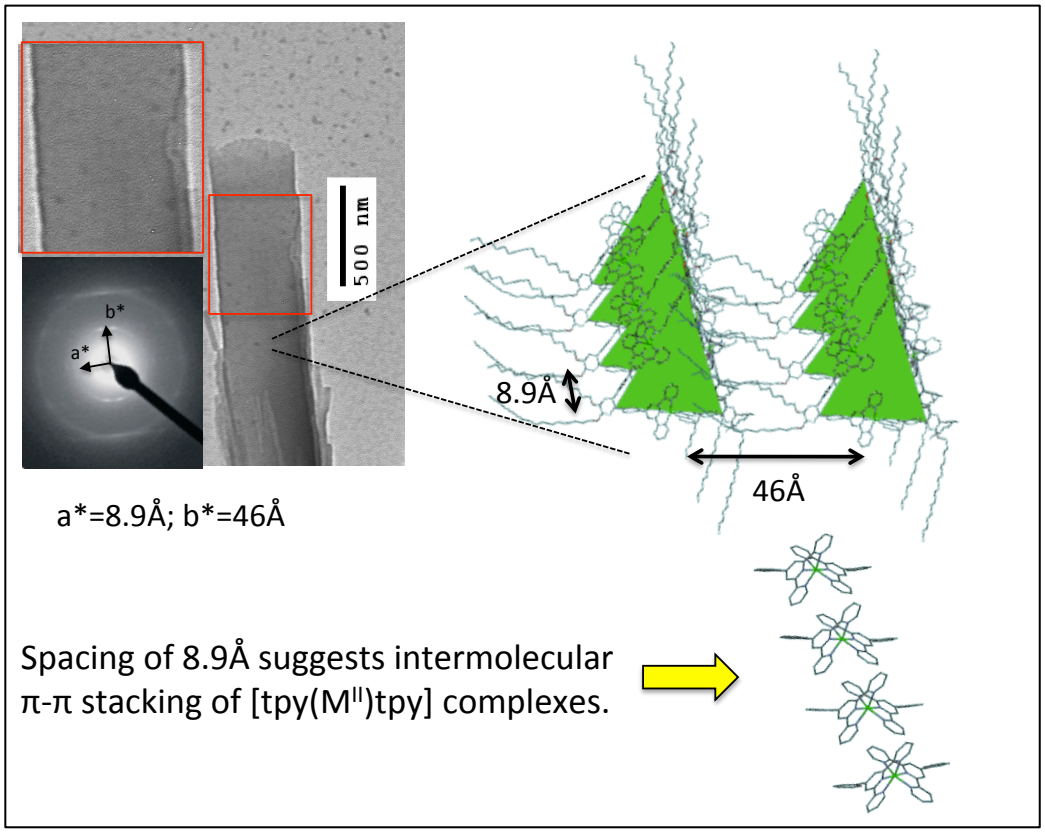


Figure 5.13 TEM of $Zn^{II}$ metallotriangle **5** lamellar region with SAXD pattern and a proposed packing model, based upon two, d-spacing values. The triangular plane in each molecule is highlighted in green to aid in visualization. Lower right corner is a cutaway showing stacks of complexes indicated by the model.

To gauge the effect of counterion and solvent on morphology, **4** ($Cl^-$) was cast from MeCN/$CHCl_3$ (5/1). Disordered lamellae and no rods were observed (Figure 5.14). TEMs of **4** ($Cl^-$) cast from $CHCl_3$/MeOH (2:1) are shown in Figures 5.15 and 5.16, rod-like structures are present with lengths approaching a micron and transverse dimensions sub 50 nm. There are examples of intact rods and ones in varying states of unrolling, twisting, and/or separating. These observations are consistent with lamellar type

structures, which have rolled up, a mechanism that has been described in formation of nanotubes.[26,223]

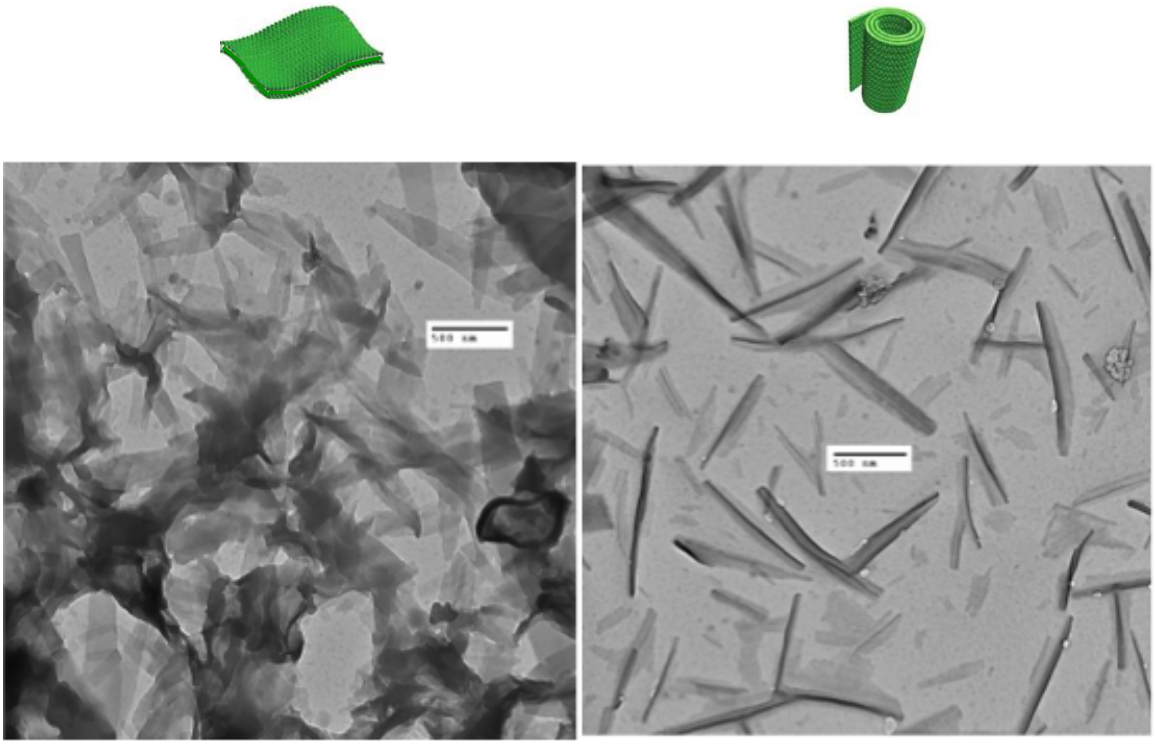

Figure 5.14 – TEM images - **4** with $Cl^-$ counter ion. Left – lamellar strutures (ribbons) when cast from MeCN/$CHCl_3$ (5:1). Right – coiled structures when cast from $CHCl_3$/MeOH (2:1). Scales are 500 nm. [Illustrations used with permission of *Acc. Chem. Res.*, **2011**, *44*, 72-82.]

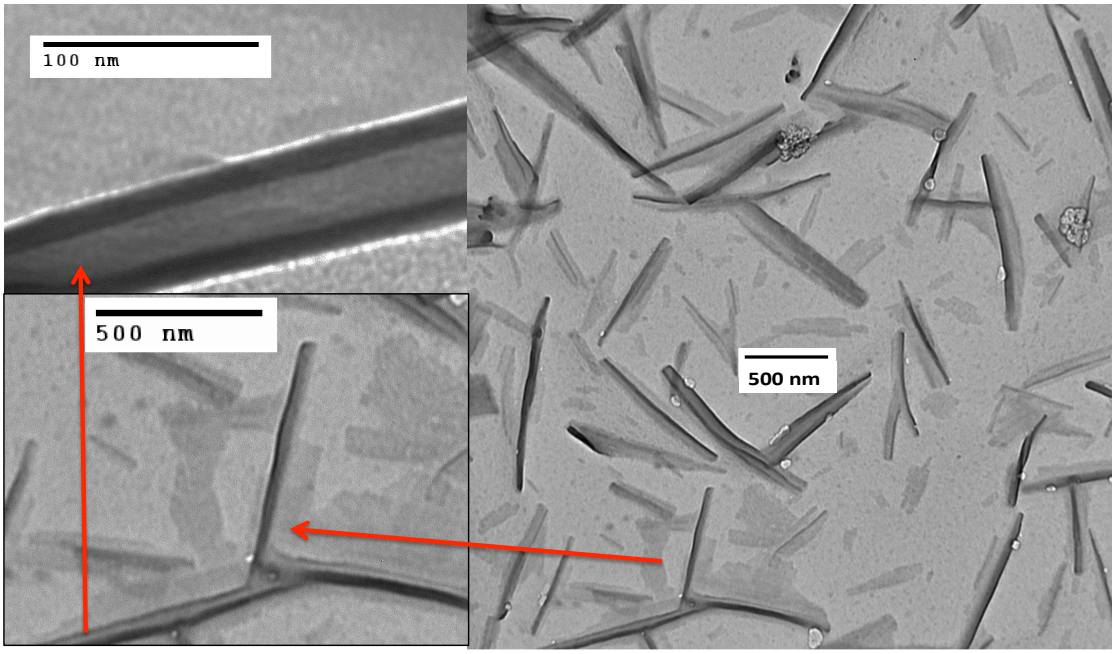


Figure 5.15 Ordering of non-labile, alkylated $Fe^{II}$ triangles ($Cl^-$) from $CHCl_3$/MeOH (2/1). Top-left shows a tube-like structure with overall diameter of *ca.* 40 nm with an outer edge/wall thickness of *ca.* 8 nm.

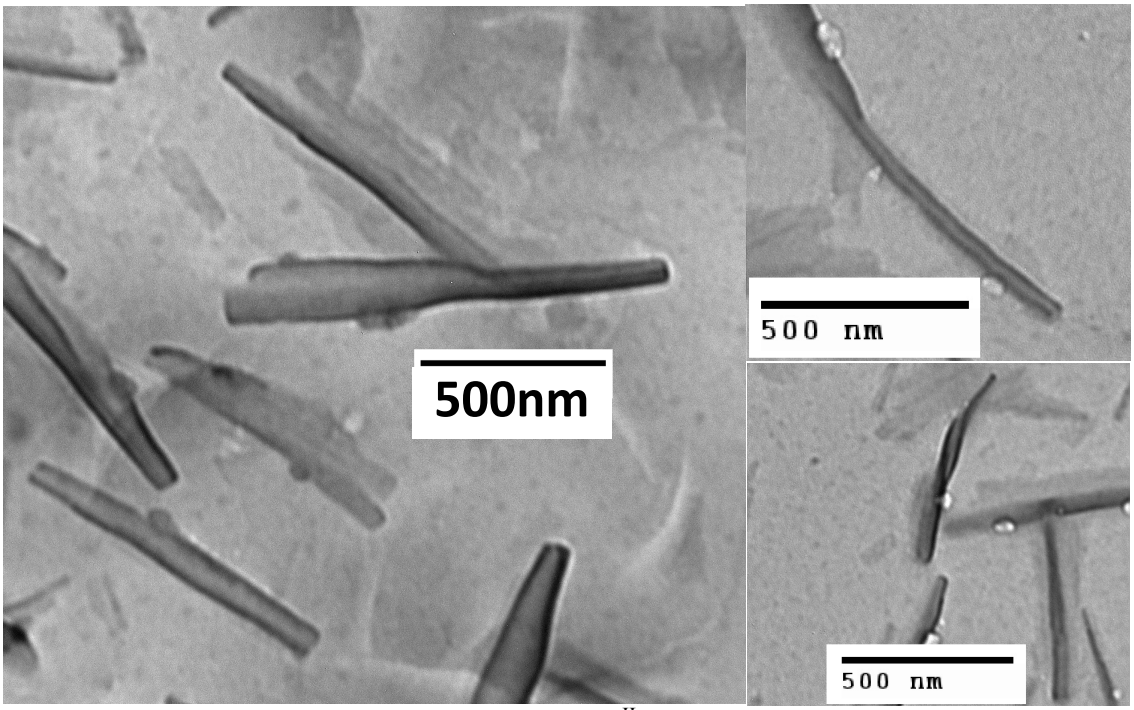


Figure 5.16 Ordering of non-labile, alkylated $Fe^{II}$ triangles ($Cl^-$) from $CHCl_3$/MeOH (2/1) into tube-like structures.

Structures formed by **4** were evaluated by AFM. A 0.1 μM solution was cast onto a glass slide and allowed to dry in a saturated MeCN atmosphere. Height and phase images are shown in Figure 5.17 and confirm the 3D, rod-like character of the structures, which were bundled and entangled. Diameters of the base structures ranged from *ca.* 30 to 90 nm.

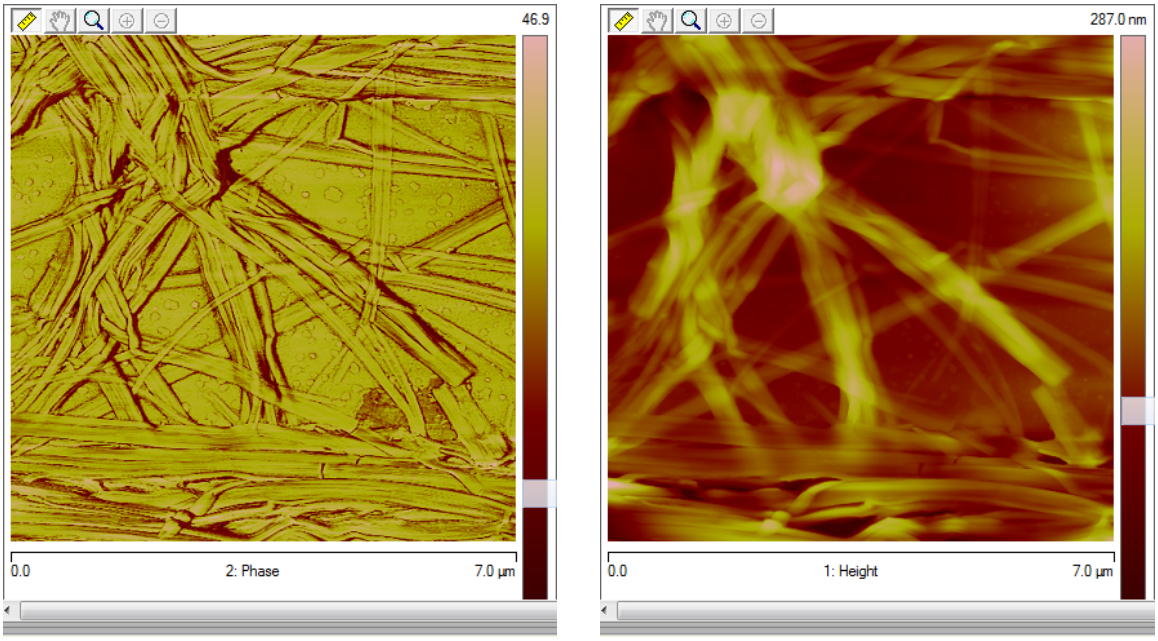


Figure 5.17 – AFM phase and height images of **4** showing entangled rod structures**.**

## 5.3 Conclusions

Novel amphiphilic <tpy-$M^{II}$-tpy> metallotriangles were synthesized using both labile $Zn^{II}$ and non-labile $Fe^{II}$ metals and characterized (1D and 2D NMR, ESI-MS). Aggregate morphology was examined *via* TEM and compared to non-amphiphilic analogues. Ordering was promoted by introduction of amphiphilic character to the metallotriangles. Rod-like structures of uniform diameter (*ca*. 40 nm) and aggregates thereof were present in both the labile and non-labile systems. The D-spacing values were derived using electron diffraction of amphiphilic metallotriangle aggregates. Molecular

modeling is used to propose a 2D packing model and suggests that the d-spacing values would require π-π stacking of the <tpy-$M^{II}$-tpy> complexes. The stacking is in the longitudinal direction of the structures. A 'corner' analogue was included in the study to gauge the effect of molecular geometry on morphology; it showed low uniformity aggregation relative to the amphiphilic triangle, suggesting that the triangular geometry plays a role in their ability to form the rod-like nanostructures. Incorporation of amphiphilic character into the metallocycles, and the resultant hydrophobic/hydrophilic interactions, facilitates cooperative molecular information sharing during hierarchical self assembly, thus enabling formation of nanoscale structures. Therefore, an amphiphile-based strategy combined with the directional bonding approach of metal-ligand supramolecular assembly affords a path towards materials with ordered arrays of <tpy-$M^{II}$-tpy> metal centers *via* hierarchical self assembly.

## 5.4 Experimental

See Section 2.4 for general experimental procedures.

**Microscopy.** For the transmission electron microscopy (TEM) studies, solutions were prepared at 0.1 μM in 5/1 MeCN/$CHCl_3$ or 2/1 $CHCl_3$/MeOH and cast onto carbon-coated copper grids (300 mesh) using a JOEL JEM-1230 transmission electron microscope. AFM height and phase images were obtained on a Nanoscope III multimode microscope from Digital Instruments operating in the tapping mode with aluminum-coated AFM probe from (Nanosensors PPP-NCHR, length 125 mm, width 30 mm, thickness 4 mm, 330 kHz frequency).

**1,2-*Bis*(hexadecyloxy)benzene (1):** To a solution of catechol (721 mg, 6.55 mmol) and 1-bromohexadecane (5 g, 16.37 mmol) in MeCN (200 mL), $K_2CO_3$ (4.32 g, 26.2 mmol) was added. The reaction mixture was refluxed for 2 days. After cooling to 25 °C, the mixture was filtered, dried *in vacuo* to give a solid that was dissolved in $CHCl_3$ and extracted (2X) with water, then washed with a brine solution. After drying ($MgSO_4$), the organic solution was filtered and concentrated *in vacuo* to give a white solid, which was washed with hexane and dried to give (84%) **1**, as a white solid: 3.08 g, mp 51-52°C; $^1$H NMR (500 MHz, $CDCl_3$): δ 6.90 (s, 4H, Ar*H*), 3.92 (t, *J* = 7Hz, 4H, OC$H_2$), 1.82 (m, 4H), 1.48 (br m, 8H), 1.33 (br m, 44 H), 0.89 (t, *J* = 7Hz, 6H); $^{13}$C NMR (125 MHz, $CDCl_3$): δ 14.12, 22.69, 26.06, 29.36, 29.37, 29.45, 29.65, 29.66, 29.67, 29.71, 29.72, 31.93, 69.25, 114.14, 120.99, 149.25; MALDI-ToF MS (m/z): Calcd. $(C_{38}H_{70}O_2+H)^+$: 559.5; Found: 559.5. Calcd. $(C_{38}H_{70}O_2+Na)^+$: 581.5; Found: 581.5.

**1,2-Dibromo-4,5-*bis*(hexadecyloxy)benzene (2):** A solution of 1,2-*Bis*(hexadecyloxy)benzene (2.00 g, 4.0 mmol) in $CH_2Cl_2$ (150 mL) was cooled to 0 °C, then bromine (1.43 g, 8.96 mmol) in $CH_2Cl_2$ (12 mL) was added dropwise over *ca.* 2 h. The stirred mixture was warmed to 25 °C over 12 h, quenched with aqueous sodium metabisulfate, dried ($MgSO_4$), filtered, and concentrated *in vacuo* to give (89%) **2**, as a white solid: 2.58 g, mp 57-58°C; $^1$H NMR (300 MHz, $CDCl_3$): δ 7.07 (s, 2H, Ar-*H*), 3.95 (t, *J* = 7Hz, 4H, OC$H_2$), 1.80 (m, 4H), 1.46 (br m, 8H), 1.29 (br m, 44H), 0.89 (br m, 6H); $^{13}$C NMR (125 MHz, $CDCl_3$): δ 14.12, 22.69, 25.93, 29.05, 29.34, 29.37, 29.59, 29.61, 29.67, 29.69, 29.71, 31.93, 69.62, 114.66, 118.04, 149.04; MALDI-ToF MS (m/z): Calcd. $(C_{38}H_{68}Br_2O_2+Na)^+$: 739.3 Found: 739.4.

**4',4''''-(4',5'-Bis(hexadecyloxy)[1,1':2',1''-terphenyl]-4,4''-diyl)-di[2,2':6',2''-terpyridine] (3):** A mixture of toluene (150 mL), water (150 mL), and EtOH (50 mL) was deaerated with argon for 30 min. 1,2-dibromo-4,5-*bis*(hexadecyloxy)benzene (1.69 g, 2.36 mmol), [4-(2,2':6',2''-terpyridin-4'-yl)phenyl]boronic acid (2.50 g, 7.09 mmol), and $Na_2CO_3$ (3.75 g, 35.4 mmol) were combined in a dry round bottom flask, evacuated *in vacuo* and backfilled with argon (5X), then combined with the solvent mixture. $Pd(PPh_3)_2Cl_2$ (334 mg, 472 μmol) was added under argon and the mixture was refluxed for 48 hr. After cooling to 25 °C, the organic layer was removed. The aqueous layer was extracted with $CH_2Cl_2$ (2X); the organic layers were combined, dried ($MgSO_4$), and filtered. The resultant, pinkish solution was concentrated, dried *in vacuo*, and the resultant solid was recrystallized from EtOAc and hexane to give (62%) **3**, as a white solid: 1.7 g, mp 98 °C; $^1$H NMR (500 MHz, $CDCl_3$): δ 8.75 (s, 4H, 3',5'-tpy*H*), 8.69 (d, *J* = 5Hz, 4H, 6,6''-tpy*H*), 8.65 (d, *J* = 8Hz, 4H, 3,3''-tpy*H*), 7.86 (dd, $J_1$ = 8Hz, $J_2$ = 2Hz, 4H, 4,4''-tpy*H*), 7.82 (d, *J* = 9Hz, 4H, Ar*H*), 7.32 (m, 8H, Ar*H*, 5,5''-tpy*H*), 7.04 (s, 2H), 4.13 (t, *J* = 7Hz, 4H, OC$H_2$), 1.90 (m, 4H), 1.53 (m, 4H), 1.36 (m, 48H), 0.88 (t, *J* = 6Hz, 6H); $^{13}$C NMR [125 MHz, $CDCl_3$]: δ 13.86, 22.40, 25.83, 29.11, 29.21, 29.41, 29.43, 29.47, 29.48, 31.67, 69.32, 76.49, 76.75, 76.95, 77.00, 115.94, 118.50, 121.03, 123.43, 126.71, 130.22, 132.32, 135.96, 136.50, 142.07, 148.46, 148.82, 149.54, 155.60, 156.07; MALDI-ToF MS (m/z): Calcd. $(C_{80}H_{96}N_6O_2+H)^+$: 1173.76; Found: 1173.80.

**$(3)_3Fe_3^{+6}[6PF_6^-]$ (4) or $[6Cl^-]$ (4a)**: To a stirred solution of **3** (181.7 mg, 0.155 μmol) dissolved in $CH_2Cl_2$ (250 mL), MeOH (50 mL) was gradually added. A solution of $FeCl_2 \cdot 4H_2O$ (3.23 mg, 0.163 μmol) in MeOH (20 mL) was added dropwise. The reaction mixture was stirred at 25 °C for 12 h., concentrated and dried *in vacuo* to give a

solid that was chromatographed ($SiO_2$) eluting with $CH_2Cl_2$:MeOH (9:1). A purple solid was obtained (35%) **4a**, (71 mg). Conversion to $PF_6^-$ counterion was achieved by dissolving this solid in $CHCl_3$/MeOH (4:1) and precipitating with excess (ca. 10X) $NH_4PF_6$ affording the desired **4**: mp > 300 °C; $^1$H NMR (500 MHz, $CD_3CN/CDCl_3$ 5:1): δ 9.16 (s, 12H, 3',5'-tpy*H*), 8.59 (d, *J* = 6Hz, 12H, 3,3"-tpy*H*), 8.23 (d, *J* = 8Hz, 12H, Ar*H*), 7.80 (dd, *J* = 8, 12Hz, 4,4"-tpy*H*), 7.64 (d, *J* = 8 Hz, 12H, Ar*H*), 7.27 (s, 6H, Ar*H*), 7.15 (d, *J* = 6Hz, 12H, 6,6"-tpy*H*), 7.03 (dd, *J* = 7Hz, 12H, 5,5"-tpy*H*), 4.13 (t, *J* = 6Hz, 12H, OC$H_2$), 1.90 (m, 12H), 1.59 (m, 12H), 1.46 (m, 132H), 1.28 (m, 12H), 0.88 (m, 18H); $^{13}$C NMR [125 MHz, $CD_3CN/CDCl_3$ (5:1)]: δ 13.80, 22.56, 26.11, 29.26, 29.38, 29.42, 29.56, 29.59, 29.61, 29.63, 29.65, 31.83, 69.83, 104.99, 116.23, 121.39, 124.20, 127.60, 131.32, 132.49, 134.11, 138.79, 144.01, 149.23, 150.87, 152.44, 157.89, 159.99; ESI **4a** (*m/z*): 1264.7 $[M-3Cl]^{3+}$ (Calcd. *m/z* = 1263.8), 939.8 $[M-4Cl]^{4+}$ (Calcd. *m/z* = 939.1), 744.6 $[M-5Cl]^{5+}$ (Calcd. *m/z* = 744.3) and 614.7 $[M-6Cl]^{6+}$ (Calcd. *m/z* = 614.4); ESI **4** (*m/z*): 1374.2 $[M-3PF_6]^{3+}$ (Calcd. *m/z* = 1373.7), 994.4 $[M-4PF_6]^{4+}$ (Calcd *m/z* = 994.1), 766.5 $[M-5PF_6]^{5+}$ (Calcd. *m/z* = 766.2) and 614.4 $[M-6PF_6]^{6+}$ (Calcd. *m/z* = 614.4)

**$(3)_3Zn_3^{+6}[6PF_6]$** (**5**): To a stirred mixture of **3** (10 mg, 8.52 μmol) in $CH_2Cl_2$:MeOH (4:1, 12.5 mL), a solution of $Zn(NO_3)_2 \cdot 6H_2O$ (2.53 mg, 8.52 μmol) in MeOH (536 μL) was added. The solution turned yellow and was stirred for 30 min. and $NH_4PF_6$ (80 mg) was added. After stirring for an additional 15 min., MeOH (2.5 mL) was added. A light yellow solid was filtered, and washed sequentially with MeOH, water, and MeOH. The solid was dried *in vacuo* to give (84%) **5**: 11 mg, mp > 300 °C; $^1$H NMR [500 MHz, $CD_3CN/CDCl_3$ (5:1)]: δ 8.94 (s, 12H, 3',5'-tpy*H*), 8.69 (d, *J* = 8Hz, 12H, 3,3"-tpy), 8.04 - 8.14 (m, 24H, 4,4"-tpy*H*, Ar*H*), 7.81 (d, *J* = 5Hz, 12H, 6,6"-tpy*H*), 7.58 (d, *J*

= 8Hz, 12H, Ar*H*), 7.35 (dd, $J_1$ = 8, $J_2$ = 5 Hz, 12H, 5,5"-tpy*H*), 7.20 (s, 6H, Ar*H*), 4.19 (t, *J* = 6Hz, 12H, OC$H_2$), 1.84 - 1.92 (m, 12H), 1.57 (m, 12H), 1.41 - 1.49 (m, 12H), 1.19 - 1.41 (m, 132H), 0.84 - 0.92 (m, 18H); $^{13}$C NMR [125 MHz, $CD_3CN/CDCl_3$ (5:1)]: δ 14.93, 23.89, 27.41, 30.58, 30.64, 30.67, 30.86, 30.87, 30.92, 30.93, 30.94, 33.15, 70.83, 106.44, 122.72, 124.69, 129.01, 129.18, 132.75, 133.46, 135.57, 142.66, 145.87, 149.29, 149.39, 150.72, 151.21, 157.28; ESI (*m/z*): 1383.7 $[M\text{-}3PF_6]^{3+}$ (Calcd. *m/z* = 1382.7), 1001.5 $[M\text{-}4PF_6]^{4+}$ (Calcd. *m/z* = 1000.8), 772.2 $[M\text{-}5PF_6]^{5+}$ (Calcd. *m/z* = 771.6) and 618.4 $[M\text{-}6PF_6]^{6+}$ (Calcd. *m/z* = 618.9).

**3,4-*Bis*(4′-terpyridyl-*p*-phenyl)-*o*-dimethoxybenzene (6)** was prepared as described.[127]

**$(6)_3Zn_3^{+6}[6PF_6]$ (7)** was prepared as described.[127]

**$(6)_3Fe_3^{+6}[6PF_6]$ (8)** was prepared as described:[128] mp > 300 °C; $^1$H NMR (500 MHz, $CD_3CN$) δ (ppm): 9.20 (s, 12H, 3',5'-tpy*H*), 8.62 (d, *J* = 8 Hz, 12H, 3,3"-tpy*H*), 8.25 (d, *J* = 8 Hz, 12H, Ar*H*), 7.80 (dd, $J_1$ = 8 Hz, $J_2$ = 7Hz, 4,4"-tpy*H*), 7.68 (d, *J* = 8 Hz, 12H, Ar*H*), 7.31 (s, 6H, Ar*H*), 7.19 (d, *J* = 6 Hz, 12H, 6,6"-tpy*H*), 7.03 (dd, $J_1$ = 8 Hz, $J_2$ = 7Hz, 5,5"-tpy*H*), 4.05 (s, 18H, OC$H_3$; $^{13}$C NMR [125 MHz, $CD_3CN$]: δ 57.27, 115.68, 122.90, 125.30, 128.73, 129.00, 132.86, 133.51, 136.24, 140.07, 145.31, 150.79, 151.31, 154.42, 159.47, 161.67; ESI-MS (*m/z*) 404.2 $[M\text{-}6PF_6]^{6+}$ (Calcd. *m/z* = 404.1), 514.1 $[M\text{-}5PF_6]^{5+}$ (Calcd. *m/z* = 514.0), 678.8 $[M\text{-}4PF_6]^{4+}$ (Calcd. *m/z* = 678.7), 953.4 $[M\text{-}3PF_6]^{3+}$ (Calcd. *m/z* = 953.3).

(**10**): A mixture of 4'-(4-bromophenyl)[2,2':6',2"]terpyridine (**9**) (1 g, 2.6 mmol) and $RuCl_3 \cdot 3H_2O$ (740 mg, 2.8 mmol) were combined in EtOH (300 mL), then refluxed overnight. The solid was filtered and washed with EtOH, sonicated in $CHCl_3$, filtered,

and washed with EtOH and $CHCl_3$, and dried *in vacuo* to give (85%) **10**, as a brown solid: 1.32 g. The solid was used without further purification.

**(6)$Ru_2^{+4}$(9)$_2$[4$PF_6$] (11):** To a stirred mixture of **3** (310 mg, 264 μmol) in $CHCl_3$/MeOH (3:2, 100 mL), **10** (345 mg, 580 μmol), and 5 drops of *N*-ethyl morpholine were added. After refluxing for 2 days, the mixture was concentrated *in vacuo* to give a red solid, which was chromatographed ($SiO_2$) eluting with a solution of $H_2O$/satd $KNO_3$/MeCN (1:1:44). The desired red fractions were combined, concentrated *in vacuo* to give a solid that was washed with $H_2O$. Conversion to $PF_6^-$ counterion was achieved by dissolving this solid in $CHCl_3$/MeOH (4:1) and precipitating with $NH_4PF_6$. The resultant red solid was washed with $H_2O$ and MeOH to give (37%) **11**: 266 mg; mp > 300°C; $^1$H NMR [500 MHz, $CD_3CN/CDCl_3$ (5/1): δ 9.02 (s, 4H, 3',5'-tpy*H*), 8.98 (s, 4H, 3',5'-tpy*H*), 8.60 - 8.68 (m, 8H, 3,3", 3,3"-tpy*H*), 8.19 (d, *J* = 8 Hz, 4H, Ar*H*$^c$), 8.12 (d, *J* = 8 Hz, 4H, Ar*H*$^d$), 7.86 - 7.98 (m, 12H, 4,4", 4,4"-tpy*H*, Ar*H*$^e$,), 7.67 (d, *J* = 8 Hz, 4H, Ar*H*$^b$), 7.37 - 7.46 (m, 8H, 6,6", 6,6"-tpy*H*), 7.21 (s, 2H, Ar*H*$^a$), 7.12 - 7.19 (m, 8H, 5,5", 5,5"-tpy*H*), 4.20 (t, *J* = 6.0 Hz, 4H, OC*H*$_2$), 1.83 - 1.92 (m, 4H), 1.53 - 1.63 (m, 4H), 1.41 - 1.51 (m, 4H), 1.28 (br. s., 44H), 0.84 - 0.92 (m, 6H); $^{13}$C NMR [125 MHz, $CD_3CN/CDCl_3$ (5:1)] δ (ppm); 14.81, 23.79, 27.31, 30.48, 30.54, 30.56, 30.77, 30.88, 30.83, 30.84, 33.05, 70.65, 71.52, 117.74, 122.61, 122.88, 125.77, 125.95, 128.76, 128.85, 128.88, 130.99, 132.64, 133.48, 134.07, 136.05, 137.36, 139.38, 139.44, 145.20, 148.38, 149.00, 150.41, 153.74, 153.79, 156.77, 156.90, 159.46, 159.50; ESI (*m/z*): 765.8 [M-3$PF_6$]$^{3+}$ (Calcd. *m/z* = 765.2), 538.1 [M-4$PF_6$]$^{4+}$ (Calcd. *m/z* = 537.7).

# CHAPTER VI

## SUMMARY

A series of carborane-functionalized macrocycles were synthesized including a novel dimeric structure containing stacked <tpy-$M^{II}$-tpy> complexes with intramolecular π-π interactions. The macrocycles were formed under both thermodynamic and kinetic control using $Zn^{II}$ and $Fe^{II}$, respectively. Characterization was achieved by NMR, ESI-MS and ESI-TWIM-MS, and molecular modeling. Under thermodynamic control, dynamic interconversion between the metallosupramolecular structures was demonstrated and characterized. Under adequate entropic driving force the system was shown to form exclusively the dimeric structure; however, under kinetic control, the predominant cyclic product was trimeric and the dimeric structure was a minor product (<5%).

*Ab initio* design of a metallosupramolecular tetrahedron was demonstrated. The design and synthesis of a novel hexa*kis*terpyridine ligand containing a trio of 60°-directed *bis*ligands connected by crown ether vertices and its self-assembly into a tetrahedral structure under thermodynamic control was accomplished. The combination of a flexible vertex with 60° directionality allowed a controlled extension into a discrete 3D structure facilitated by intramolecular interactions (*π*-*π*). Molecular modeling and NMR data were used to demonstrate the presence of parallel (*π*-*π*) and T-shaped (CH-*π*) interactions in the close-packed tpy complexes. Variable temperature NMR experiments support this model and, using $^{19}F$ NMR experiments, the presence of counter anions within the

supramolecular cavity was indicated. DOSY, TEM, and ESI-TWIM-MS were used to further characterize the structure.

The first one-step self-assembly of a homoleptic, <tpy–$Os^{II}$-tpy> based metallomacrocycle was shown using a 60° *bis*terpyridine ligand. The structure was characterized *via* NMR, ESI-MS, TWIM-MS, gradient tandem-MS, and UV-VIS alongside $Fe^{II}$ and $Ru^{II}$ analogues. Center of mass collision energies derived from Gradient Tandem-MS spectrometry indicated that the $Ru^{II}$ based analogue has the highest stability followed by $Os^{II}$ and $Fe^{II}$. This work establishes where <tpy-$Os^{II}$-tpy> lie with the spectrum of bonding strengths obtainable with terpyridine-based systems.

An amphiphile-based strategy with <tpy-$M^{II}$-tpy>-based macrocycles demonstrated that conversion of metallotriangles into directional amphiphiles dramatically enhanced their self-ordering characteristics, enabling the formation of nanoscale structures. Long chain (C16) alkylated metallotriangles were synthesized and characterized *via* NMR and ESI-MS. Ordered aggregation of these amphiphiles was studied *via* TEM to gauge morphology and nanoscale structure as related to the effects of molecular topology, solvent, counterion, and metal center(s). Labile ($Zn^{II}$) and non-labile ($Fe^{II}$) systems were compared. SAXD suggests intramolecular π-π stacking. The results indicate that an amphiphile-based strategy combined with the directional bonding approach of metal-ligand supramolecular assembly affords a path towards materials with ordered arrays of <tpy-$M^{II}$-tpy> metal centers *via* hierarchical self-assembly.

REFERENCES


1. P. J. Flory, *Principles of Polymer Chemistry*, Cornell University Press, Ithaca, New York, **1953**.

2. H. Staudinger, Macromolecular chemistry; Nobel Lecture, December 11, **1953**.

3. J. D. Watson and F. H. Crick, *Nature*, **1953**, *171*, 737-738.

4. D. T. Zallen, *Nature*, **2003**, *425*, 15-15.

5. P. D. Frischmann, K. Mahata and F. Würthner, *Chem. Soc. Rev.*, **2013**, *42*, 1847-1870.

6. J.-M. Lehn, *Supramolecular Chemistry*, John Wiley & Sons, Ltd, **2009**.

7. C. J. Pedersen, *J. Am. Chem. Soc.*, **1967**, *89*, 7017-7036.

8. D. J. Cram, *Angew. Chem. Int. Ed.*, **1988**, *27*, 1009-1020.

9. J.-M. Lehn, *Angew. Chem. Int. Ed.*, **1988**, *27*, 89-112.

10. F. Grimm, N. Ulm, F. Gröhn, J. Düring and A. Hirsch, *Chem. Eur. J.*, **2011**, *17*, 9478-9488.

11. P. P. Kapadia, L. R. Ditzler, J. Baltrusaitis, D. C. Swenson, A. V. Tivanski and F. C. Pigge, *J. Am. Chem. Soc.*, **2011**, *133*, 8490-8493.

12. C. Carpanese, S. Ferley, N. Kyritsakas, M. Henry and M. W. Hosseini, *Chem. Commun.*, **2009**, 6786-6788.

13. J. Xia, L. Chen, J. Chen, H. Tian, F. Li, X. Zhu, G. Li and X. Chen, *Macromol. Biosci.*, **2011**, *11*, 211-218.

14. D. Türp, M. Wagner, V. Enkelmann and K. Müllen, *Angew. Chem. Int. Ed.*, **2011**, *50*, 4962-4965.

15. I. N. Kurniasih, H. Liang, J. P. Rabe and R. Haag, *Macromol. Rapid Commun.*, **2010**, *31*, 1516-1520.

16. F. Wurm, J. Nieberle and H. Frey, *Macromolecules*, **2008**, *41*, 1184-1188.

17. H.-Y. Kim, J. Song, S.-H. Kim, E. Lee, J. K. Lee, W.-C. Zin and B.-K. Cho, *Chem. Eur. J.*, **2009**, *15*, 8683-8686.

18. M. Ruben, J. Rojo, F. J. Romero-Salguero, L. H. Uppadine and J.-M. Lehn, *Angew. Chem. Int. Ed.*, **2004**, *43*, 3644-3662.

19. A. R. Stefankiewicz, G. Rogez, J. Harrowfield, M. Drillon and J.-M. Lehn, *Dalton Trans.*, **2009**, 5787-5802.

20. A.-M. Stadler, F. Puntoriero, F. Nastasi, S. Campagna and J.-M. Lehn, *Chem. Eur. J.*, **2010**, *16*, 5645-5660.

21. A. Marquis, V. Smith, J. Harrowfield, J.-M. Lehn, H. Herschbach, R. Sanvito, E. Leize-Wagner and A. Van Dorsselaer, *Chem. Eur. J.*, **2006**, *12*, 5632-5641.

22. N. Takeda, K. Umemoto, K. Yamaguchi and M. Fujita, *Nature*, **1999**, *398*, 794-796.

23. S. Sato, J. Iida, K. Suzuki, M. Kawano, T. Ozeki and M. Fujita, *Science*, **2006**, *313*, 1273.

24. Q. F. Sun, J. Iwasa, D. Ogawa, Y. Ishido, S. Sato, T. Ozeki, Y. Sei, K. Yamaguchi and M. Fujita, *Science*, **2010**, *328*, 1144-1147.

25. M. Fujita, M. Tominaga, A. Hori and B. Therrien, *Acc. Chem. Res.*, **2005**, *38*, 371-380.

26. B. H. Northrop, H.-B. Yang and P. J. Stang, *Chem. Commun.*, **2008**, 5896-5908.

27. B. H. Northrop, Y. R. Zheng, K. W. Chi and P. J. Stang, *Acc. Chem. Res.*, **2009**, *42*, 1554-1563.

28. J. Lee, K. Ghosh and P. J. Stang, *J. Am. Chem. Soc.*, **2009**, *131*, 12028-12029.

29. B. Olenyuk, A. Fechtenkötter and P. J. Stang, *J. Chem. Soc., Dalton Trans.*, **1998**, 1707-1728.

30. M. Schmittel, V. Kalsani, R. S. K. Kishore, H. Cölfen and J. W. Bats, *J. Am. Chem. Soc.*, **2005**, *127*, 11544-11545.

31. M. Schmittel and P. Mal, *Chem. Commun.*, **2008**, 960-962.

32. M. Schmittel and B. He, *Chem.Commun.*, **2008**, 4723-4725.

33. Y.-T. Chan, X. Li, C. N. Moorefield, C. Wesdemiotis and G. R. Newkome, *Chem. Eur. J.*, **2011**, *17*, 7750-7754.

34. G. R. Newkome, P. Wang, C. N. Moorefield, T. J. Cho, P. Mohapatra, S. Li, S.-H. Hwang, O. Lukoyanova, L. Echegoyen, J. A. Palagallo, V. Iancu and S.-W. Hla, *Science*, **2006**, *312*, 1782-1785.

35. A. Schultz, X. Li, B. Barkakaty, C. N. Moorefield, C. Wesdemiotis and G. R. Newkome, *J. Am. Chem. Soc.*, **2012**, *134*, 7672−7675.

36. S.-H. Hwang, C. N. Moorefield, F. R. Fronczek, O. Lukoyanova, L. Echegoyen and G. R. Newkome, *Chem. Commun.*, **2005**, 713-715.

37. S. G. Morgan and F. H. Burstall, *J. Chem. Soc.*, **1932**, 20-30.

38. F. Kröhnke, *Synthesis*, **1976**, 1 – 24.

39. N. Miyaura, T. Yanagi and A. Suzuki, *Synth. Commun.*, **1981**, *11*, 513-519.

40. K. Sonogashira, Y. Tohda and N. Hagihara, *Tetrahedron Lett.*, **1975**, *16*, 4467-4470.

41. A. Wild, A. Winter, F. Schlütter and U. S. Schubert, *Chem. Soc. Rev.*, **2011**, *40*, 1459-1511.

42. C. Wang, X.-Q. Hao, M. Wang, C. Guo, B. Xu, E. N. Tan, Y.-Y. Zhang, Y. Yu, Z.-Y. Li, H.-B. Yang, M.-P. Song and X. Li, *Chem. Sci.*, **2014**, *5*, 1221-1226.

43. T.-Z. Xie, K. Guo, Z. Guo, W.-Y. Gao, L. Wojtas, G.-H. Ning, M. Huang, X. Lu, J.-Y. Li, S.-Y. Liao, Y.-S. Chen, C. N. Moorefield, M. J. Saunders, S. Z. D. Cheng, C. Wesdemiotis and G. R. Newkome, *Angew. Chem. Int. Ed.*, **2015**, *54*, 9224-9229.

44. T.-Z. Xie, K. Guo, M. Huang, X. Lu, S.-Y. Liao, R. Sarkar, C. N. Moorefield, S. Z. D. Cheng, C. Wesdemiotis and G. R. Newkome, *Chem. Eur. J.*, **2014**, *20*, 11291-11294.

45. T. Schröder, R. Brodbeck, M. C. Letzel, A. Mix, B. Shnatwinkel, M. Tonigold, D. Volkmer and J. Mattay, *Tetrahedron Lett.*, **2009**, *49*, 5939-5942.

46. W. R. McWhinnie and J. D. Miller, *Adv. Inorg. Chem. Radiochem.*, **1969**, *11*, 135-215.

47. U. S. Schubert, H. Hofmeier and G. R. Newkome, *Modern Terpyridine Chemistry*, Wiley-VCH, Weinheim, **2006**.

48. R. Chakrabarty, P. S. Mukherjee and P. J. Stang, *Chem. Rev.*, **2011**, *111*, 6810-6918.

49. E. C. Constable and A. M. W. C. Thompson, *J. Chem. Soc., Dalton Trans.*, **1995**, 1615-1627.

50. E. C. Constable, A. M. W. C. Thompson, P. Harveson, L. Macko and M. Zehnder, *Chem. Eur. J.*, **1995**, *1*, 360-367.

51. M. Osawa, M. Hoshino, S. Horiuchi and Y. Wakatsuki, *Organometallics*, **1999**, *18*, 112-114.

52. J.-L. Wang, Y.-T. Chan, C. N. Moorefield, J. Pei, D. A. Modarelli, N. C. Romano and G. R. Newkome, *Macromol. Rapid Commun.*, **2010**, *31*, 850-855.

53. E. C. Constable and E. Schofield, *Chem. Commun.*, **1998**, 403-404.

54. F. M. Romero, R. Ziessel, A. Dupont-Gervais and A. Van Dorsselaer, *Chem. Commun.*, **1996**, 551-553.

55. G. R. Newkome, T. J. Cho, C. N. Moorefield, P. P. Mohapatra and L. A. Godínez, *Chem. Eur. J.*, **2004**, *10*, 1493-1500.

56. G. S. Hanan, C. R. Arana, J.-M. Lehn and D. Fenske, *Angew.Chem., Int. Ed.*, **1995**, *34*, 1122-1124.

57. G. S. Hanan, U. S. Schubert, D. Volkmer, E. Rivière, J.-M. Lehn, N. Kyritsakas and J. Fischer, *Can. J. Chem.*, **1997**, *75*, 169-182.

58. D. M. Bassani, J.-M. Lehn, K. Fromm and D. Fenske, *Angew. Chem. Int. Ed.*, **1998**, *37*, 2364-2367.

59. D. M. Bassani, J.-M. Lehn, S. Serroni, F. Puntoriero and S. Campagna, *Chem. Eur. J.*, **2003**, *9*, 5936-5946.

60. M. Barboiu, G. Vaughan, R. Graff and J.-M. Lehn, *J. Am. Chem. Soc.*, **2003**, *125*, 10257-10265.

61. T. Schröder, R. Brodbeck, M. C. Letzel, A. Mix, B. Schnatwinkel, M. Tonigold, D. Volkmer and J. Mattay, *Tetrahedron Lett.*, **2008**, *49*, 5939.

62. J. M. Ludlow III, T. Xie, Z. Guo, K. Guo, M. J. Saunders, C. N. Moorefield, C. Wesdemiotis and G. R. Newkome, *Chem. Commun.*, **2015**, *51*, 3820-3823.

63. T.-Z. Xie, S.-Y. Liao, K. Guo, X. Lu, X. Dong, M. Huang, C. N. Moorefield, S. Z. D. Cheng, X. Liu, C. Wesdemiotis and G. R. Newkome, *J. Am. Chem. Soc.*, **2014**, *136*, 8165-8168.

64. K. Guo, Z. Guo, J. M. Ludlow III, T. Xie, S. Liao, G. R. Newkome and C. Wesdemiotis, *Macromol. Rapid Commun.*, **2015**, *36*, 1539-1552.

65. J. Fenn, M. Mann, C. Meng, S. Wong and C. Whitehouse, *Science*, **1989**, *246*, 64-71.

66. K. Tanaka, H. Waki, Y. Ido, S. Akita, Y. Yoshida, T. Yoshida and T. Matsuo, *Rapid Commun. Mass Spectrom.*, **1988**, *2*, 151-153.

67. M. Karas and F. Hillenkamp, *Anal. Chem.*, **1988**, *60*, 2299-2301.

68. U. S. Schubert, A. Winter and G. R. Newkome, *Terpyridine-based Materials - For Catalytic, Optoelectronic, and Life Science Applications*, Wiley-VCH, Weinheim, Germany, **2011**.

69. W. Kubo, A. Sakamoto, T. Kitamura, Y. Wada and S. Yanagida, *J. Photochem. Photobiol., A*, **2004**, *164*, 33-39.

70. S. A. Sapp, C. M. Elliott, C. Contado, S. Caramori and C.-A. Bignozzi, *J. Am. Chem. Soc.*, **2002**, *124*, 11215-11222.

71. K. Y. K. Man, H. L. Wong, W. K. Chan, A. B. Djurišic, E. Beach and S. Rozveld, *Langmuir*, **2006**, *22*, 3368-3375.

72. S.-H. Hwang, P. Wang, C. N. Moorefield, J.-C. Jung, J.-Y. Kim, S.-W. Lee and G. R. Newkome, *Macromol. Rapid Commun.*, **2006**, *27*, 1809-1813.

73. Y.-Y. Chen and H.-C. Lin, *J. Polym. Sci., Part A: Polym. Chem.*, **2007**, *15*, 3255.

74. Y.-Y. Chen, Y.-T. Tao and H.-C. Lin, *Macromolecules*, **2006**, *39*, 8559-8566.

75. A. Winter, G. R. Newkome and U. S. Schubert, *ChemCatChem*, **2011**, *3*, 1384-1406.

76. D. J. Wasylenko, C. Ganesamoorthy, M. A. Henderson, B. D. Koivisto, H. D. Osthoff and C. P. Berlinguette, *J. Am. Chem. Soc.*, **2010**, *132*, 16094-16106.

77. C. Baffert, S. Romain, A. Richardot, B. Lefebvre, A. Deronzier and M. N. Collomb, *J. Am. Chem. Soc.*, **2005**, *127*, 13694-13704.

78. R. Zong and R. P. Thummel, *J. Am. Chem. Soc.*, **2005**, *127*, 12802-12803.

79. A. Winter, C. Friebe, M. Chiper, M. D. Hager and U. S. Schubert, *J. Polym. Sci., Part A: Polym.Chem.*, **2009**, *47*, 4083-4098.

80. J. Zheng, C. W. Zhang and R. M. Dickson, *Phys. Rev. Lett.*, **2004**, *93*, 077402-077401-077402-077404.

81. B. Song, G. Wang, M. Tan and J. Yuan, *J. Am. Chem. Soc.*, **2006**, *128*, 13442-13450.

82. E. Coronado, J. R. Galan-Mascaros, C. Marti-Gastaldo, E. Palomares, J. R. Durrant, R. Vilar, M. Gratzel and M. Nazeeruddin, *J. Am. Chem. Soc.*, **2005**, *127*, 12351-12356.

83. D. Maity, C. Bhaumik, D. Mondal and S. Baitalik, *Inorg. Chem.*, **2013**, *52*, 13941-13955.

84. J. Du, Z. Huang, X.-Q. Yu and L. Pu, *Chem. Commun.*, **2013**, *49*, 5399-5401.

85. D.-L. Ma, T. Y.-T. Shum, F. Zhang, C.-M. Che and M. Yang, *Chem. Commun.*, **2005**, 4675-4677.

86. K. Karidi, A. Garoufis, A. Tsipis, N. Hadjiliadis, H. den Dulk and J. Reedijk, *Dalton Trans.*, **2005**, 1176-1187.

87. I. Eryazici, C. N. Moorefield and G. R. Newkome, *Chem. Rev.*, **2008**, *108*, 1834-1895.

88. J.-M. Lehn, *Science*, **2002**, *295*, 2400-2403.

89. X. Lu, X. Li, J.-L. Wang, C. N. Moorefield, C. Wesdemiotis and G. R. Newkome, *Chem. Commun.*, **2012**, *48*, 9873-9875.

90. J.-L. Wang, X. Li, X. Lu, I.-F. Hsieh, Y. Cao, C. N. Moorefield, C. Wesdemiotis, S. Z. D. Cheng and G. R. Newkome, *J. Am. Chem. Soc.*, **2011**, *133*, 11450-11453.

91. R. Sarkar, K. Guo, C. N. Moorefield, M. J. Saunders, C. Wesdemiotis and G. R. Newkome, *Angew. Chem. Int. Ed.*, **2014**, *53*, 12182-12185.

92. I. Eryazici and G. R. Newkome, *New J. Chem.*, **2009**, *33*, 345-357.

93. G. R. Newkome, T. J. Cho, C. N. Moorefield, G. R. Baker, M. J. Saunders, R. Cush and P. S. Russo, *Angew. Chem. Int. Ed.*, **1999**, *38*, 3717-3721.

94. Y.-P. Liang, Y.-J. He, Y.-H. Lee and Y.-T. Chan, *Dalton Trans.*, **2015**, *44*, 5139-5145.

95. M. Wang, C. Wang, X.-Q. Hao, J. Liu, X. Li, C. Xu, A. Lopez, L. Sun, M.-P. Song, H.-B. Yang and X. Li, *J. Am. Chem. Soc.*, **2014**, *136*, 6664-6671.

96. Y.-T. Chan, X. Li, M. Soler, J.-L. Wang, C. Wesdemiotis and G. R. Newkome, *J. Am. Chem. Soc.*, **2009**, *131*, 16395-16397.

97. X. Li, Y.-T. Chan, M. Casiano-Maldonado, J. Yu, G. A. Carri, G. R. Newkome and C. Wesdemiotis, *Anal. Chem.*, **2011**, *83*, 6667-6674.

98. P. Wang, C. N. Moorefield and G. R. Newkome, *Angew. Chem. Int. Ed.*, **2005**, *44*, 1679-1683.

99. S.-H. Hwang, P. Wang, C. N. Moorefield, L. A. Godínez, J. Manríquez, E. Bustos and G. R. Newkome, *Chem. Commun.*, **2005**, 4672-4674.

100. Y. Gao, T. He, P. Hu, T. M. Koh, H. Sun and A. C. Grimsdale, *Macromol. Chem. Phys.*, **2014**, *215*, 753-762.

101. Q.-F. Sun, T. Murase, S. Sato and M. Fujita, *Angew. Chem. Int. Ed.*, **2011**, *50*, 10318-10321.

102. A. K. Pal, B. Laramee-Milette and G. S. Hanan, *RSC Advances*, **2014**, *4*, 21262-21266.

103. T. R. Cook and P. J. Stang, *Chem. Rev.*, **2015**, *115*, 7001-7045.

104. J.-J. Liu, Y.-J. Lin and G.-X. Jin, *Organometallics*, **2014**, *33*, 1283-1290.

105. J. M. Ludlow III, M. Tominaga, Y. Chujo, A. Schultz, X. Lu, T. Xie, K. Guo, C. N. Moorefield, C. Wesdemiotis and G. R. Newkome, *Dalton Trans.*, **2014**, *43*, 9604-9611.

106. J. H. Fu, Y. H. Lee, Y. J. He and Y. T. Chan, *Angew. Chem. Int. Ed.*, **2015**, *54*, 6231-6235.

107. J. M. Grimes, J. N. Burroughs, P. Gouet, J. M. Diprose, R. Malby, S. Zientara, P. P. C. Mertens and D. I. Stuart, *Nature*, **1998**, *395*, 470-478.

108. C. M. S. Fabry, M. Rosa-Calatrava, J. F. Conway, C. Zubieta, S. Cusack, R. W. H. Ruigrok and G. Schoehn, *EMBO J*, **2005**, *24*, 1645-1654.

109. K. Harris, D. Fujita and M. Fujita, *Chem. Commun.*, **2013**, *49*, 6703-6712.

110. F. Hof, S. L. Craig, C. Nuckolls and J. Rebek, Jr., *Angew. Chem. Int. Ed.*, **2002**, *41*, 1488-1508.

111. L. R. MacGillivray and J. L. Atwood, *Angew. Chem. Int. Ed.*, **1999**, *38*, 1018-1033.

112. B. Olenyuk, J. A. Whiteford, A. Fechtenkötter and P. J. Stang, *Nature*, **1999**, *398*, 796-799.

113. A. Winter, J. Hummel and N. Risch, *J. Org. Chem.*, **2006**, *71*, 4862-4871.

114. M. Schmittel, B. He and P. Mal, *Org. Lett.*, **2008**, *10*, 2513-2516.

115. T.-Z. Xie, S.-Y. Liao, K. Guo, X. Lu, X. Dong, M. Huang, C. N. Moorefield, S. Z. D. Cheng, X. Liu, C. Wesdemiotis and G. R. Newkome, *J. Am. Chem. Soc.*, **2014**, *136*, 8165-8168.

116. E. C. Constable, C. E. Housecroft and C. B. Smith, *Inorg. Chem. Commun.*, **2003**, *6*, 1011-1013.

117. P. R. Andres and U. S. Schubert, *Synthesis*, **2004**, 1229-1238.

118. E. C. Constable, C. E. Housecroft, M. Neuburger, S. Schaffner and C. B. Smith, *Dalton Trans.*, **2005**, 2259-2267.

119. H. S. Chow, E. C. Constable, C. E. Housecroft, M. Neuberger and S. Schaffner, *Polyhedron*, **2006**, *25*, 1831-1843.

120. T. J. Cho, C. N. Moorefield, S.-H. Hwang, P. Wang, L. A. Godínez, E. Bustos and G. R. Newkome, *Eur. J. Org. Chem.*, **2006**, 4193-4200.

121. R. Ziessel, *Synthesis*, **1999**, *11*, 1839-1865.

122. C. B. Caputo, V. N. Vukotic, N. M. Sirizzotti and S. J. Loeb, *Chem. Commun.*, **2011**, 8545.

123. P. Knops, N. Sendhoff, H.-B. Mekelburger and F. Vögtle, *Top. Curr. Chem.*, **1991**, *161*, 1-36.

124. G. R. Newkome, K. S. Yoo and C. N. Moorefield, *Chem. Commun.*, **2002**, 2164-2165.

125. X. Lu, X. Li, K. Guo, T. Z. Xie, C. N. Moorefield, C. Wesdemiotis and G. R. Newkome, *J Am Chem Soc*, 2014, **136**, 18149-18155.

126. X. Lu, X. Li, Y. Cao, A. Schultz, J.-L. Wang, C. N. Moorefield, C. Wesdemiotis, S. Z. D. Cheng and G. R. Newkome, *Angew. Chem. Int. Ed.*, **2013**, *52*, 7728-7731.

127. A. Schultz, Y. Cao, M. Huang, S. Z. D. Cheng, X. Li, C. N. Moorefield, C. Wesdemiotis and G. R. Newkome, *Dalton Trans.*, **2012**, *41*, 11573-11575.

128. A. Schultz, X. Li, C. E. McCusker, C. N. Moorefield, F. N. Castellano, C. Wesdemiotis and G. R. Newkome, *Chem. Eur. J.*, **2012**, *18*, 11569-11572.

129. A. Schultz, X. Li, C. N. Moorefield, C. Wesdemiotis and G. R. Newkome, *Eur. J. Inorg. Chem.*, **2013**, 2492-2497.

130. Y. Li, Z. Jiang, J. Yuan, D. Liu, T. Wu, C. N. Moorefield, G. R. Newkome and P. Wang, *Chem. Commun.*, **2015**, *51*, 5766-5769.

131. V. Duprez, M. Biancardo, H. Spanggaard and F. C. Krebs, *Macromolecules*, **2005**, *38*, 10436-10448.

132. A. M. Breul, J. Schafer, C. Friebe, F. Schlütter, R. M. Paulus, G. Festag, M. D. Hager, A. Winter, B. Dietzek, J. Popp and U. S. Schubert, *Macromol. Chem. Phys.*, **2012**, *213*, 808-819.

133. A. Winter, M. D. Hager, G. R. Newkome and U. S. Schubert, *Adv. Mater.*, **2011**, *23*, 5728-5748.

134. P. Wang, C. N. Moorefield, S. Li, C. D. Shreiner, S.-H. Hwang and G. R. Newkome, *Chem. Commun.*, **2006**, 1091-1093.

135. S.-H. Hwang, C. N. Moorefield, L. Dai and G. R. Newkome, *Chem. Mater.*, **2006**, *18*, 4019-4024.

136. E. W. McQueen and J. I. Goldsmith, *J. Am. Chem. Soc.*, **2009**, *131*, 17554-17556.

137. A. Winter, S. Hoeppener, G. R. Newkome and U. S. Schubert, *Adv. Mater.*, **2011**, *23*, 3484-3498.

138. N.-W. Wu, L.-J. Chen, C. Wang, Y.-Y. Ren, X. Li, L. Xu and H.-B. Yang, *Chem. Commun.*, **2014**, *50*, 4231-4233.

139. X. Yan, S. Li, T. R. Cook, X. Ji, Y. Yao, J. B. Pollock, Y. Shi, G. Yu, J. Li, F. Huang and P. J. Stang, *J. Am. Chem. Soc.*, **2013**, *135*, 14036-14039.

140. X. Yan, T. R. Cook, J. B. Pollack, P. Wei, Y. Zhang, Y. Yu, F. Huang and P. J. Stang, *J. Am. Chem. Soc.*, **2014**, *136*, 4460-4463.

141. V. Balzani, S. Campagna, G. Denti, A. Juris, S. Serroni and M. Venturi, *Coord. Chem. Rev.*, **1994**, *132*, 1-13.

142. O. Crespo-Biel, B. Dordi, D. N. Reinhoudt and J. Huskens, *J. Am. Chem. Soc.*, **2005**, *127*, 7594-7600.

143. V. Balzani, A. Credi, S. Silvi and M. Venturi, *Chem. Soc. Rev.*, **2006**, *35*, 1135-1149.

144. B. Rybtchinski, *ACS Nano*, **2011**, *5*, 6791-6818.

145. P. Wei, T. R. Cook, X. Yan, F. Huang and P. J. Stang, *J. Am. Chem. Soc.*, **2014**, *136*, 15497-15500.

146. P. Wang, C. N. Moorefield, K.-U. Jeong, S.-H. Hwang, S. Li, S. Z. D. Cheng and G. R. Newkome, *Adv. Mater.*, **2008**, *20*, 1381-1385.

147. Y.-T. Chan, C. N. Moorefield, M. Soler and G. R. Newkome, *Chem. Eur. J.*, **2010**, *16*, 1768-1771.

148. J. M. Ludlow III, M. J. Saunders, M. Huang, K. Guo, Z. Guo, C. N. Moorefield, S. Z. D. Cheng, C. Wesdemiotis and G. R. Newkome, **2015** (to be submitted).

149. P. Wang, C. N. Moorefield and G. R. Newkome, *Org. Lett.*, **2004**, *6*, 1197-1200.

150. M. A. R. Meier, B. G. G. Lohmeijer and U. S. Schubert, *J. Mass Spectrom.*, **2003**, *38*, 510-516.

151. Z. Zheng, L. Opilik, F. Schiffmann, W. Liu, G. Bergamini, P. Ceroni, L.-T. Lee, A. Schütz, J. Sakamoto, R. Zenobi, J. VandeVondele and A. D. Schlüter, *J. Am. Chem. Soc.*, **2014**, *136*, 6103-6110.

152. A. Fermi, G. Bergamini, M. Roy, M. Gingras and P. Ceroni, *J. Am. Chem. Soc.*, **2014**, *136*, 6395-6400.

153. W. Jiang, C. B. Knobler, M. D. Mortimer and M. F. Hawthorne, *Angew. Chem. Int. Ed.*, **1995**, *35*, 1332-1334.

154. K. Kokado and Y. Chujo, *Dalton Trans.*, **2011**, *40*, 1919-1923.

155. A. Herzog, A. Maderna, G. N. Harakas, C. B. Knobler and M. F. Hawthorne, *Chem. Eur. J.*, **1999**, *5*, 1212-1217.

156. M. F. Hawthorne, *Angew. Chem. Int. Ed.*, **1993**, *32*, 950-984.

157. R. F. Barth, A. H. Soloway and R. G. Fairchild, *Cancer Res.*, **1990**, *50*, 1061-1070.

158. G. R. Newkome, C. N. Moorefield, J. M. Keith, G. R. Baker and G. H. Escamilla, *Agew. Chem. Int. Ed.*, **1994**, *33*, 666-668.

159. C. B. Gorman, B. L. Parkhurst, W. Y. Su and K.-Y. Chen, *J. Am. Chem. Soc.*, **1997**, *119*, 1141-1142.

160. R. Djeda, J. Ruiz, D. Astruc, R. Satapathy, B. P. Dash and N. S. Hosmane, *Inorg. Chem.*, **2010**, *49*, 10702-10709.

161. B. P. Dash, R. Satapathy, B. P. Bode, C. T. Reidl, J. W. Sawicki, A. J. Mason, J. A. Maguire and N. S. Hosmane, *Organometallics*, **2012**, *31*, 2931-2935.

162. A. G. Campo, C. Vinas, F. Teixodor, R. Nunez, R. Sillanpää and R. Kivekäs, *Macromolecules*, **2007**, *40*, 5644-5652.

163. N. S. Hosmane, Z. Yinghuai, J. A. Maguire, W. Kaim and M. Takagaki, *J. Organomet. Chem.*, **2009**, *694*, 1690-1697.

164. B. H. Northrop, H.-B. Yang and P. J. Stang, *Chem. Commun.*, **2008**, *45*, 5896-5908.

165. H. Jude, H. Disteldorf, S. Fischer, T. Wedge, A. M. Hawkridge, A. M. Arif, M. F. Hawthorne, D. C. Muddiman and P. J. Stang, *J. Am. Chem. Soc.*, **2005**, *127*, 12131-12139.

166. N. Das, P. J. Stang, A. M. Arif and C. F. Campana, *J. Org. Chem.*, **2005**, *70*, 10440-10446.

167. Z.-J. Yao, W.-B. Yu, Y.-J. Lin, S.-L. Huang, Z.-H. Li and G.-X. Jin, *J. Am. Chem. Soc.*, **2014**, *136*, 2825-2832.

168. X. Lu, X. Li, Y. Cao, A. Schultz, J.-L. Wang, C. N. Moorefield, C. Wesdemiotis, S. Z. D. Cheng and G. R. Newkome, *Angew. Chem. Int. Ed.*, **2013**, *52*, 7728 – 7731.

169. I. Eryazici, P. Wang, C. N. Moorefield, M. Panzer, S. Durmus, C. D. Shreiner and G. R. Newkome, *Dalton Trans.*, **2007**, 626-628.

170. E. C. Constable, *Chem. Soc. Rev.*, **2007**, *36*, 246-253.

171. E. C. Constable, *Coord. Chem. Rev.*, **2008**, *252*, 842-855.

172. M. A. Fox, J. A. K. Howard, J. A. H. MacBride, A. Mackinnon and K. Wade, *J. Organomet. Chem.*, **2003**, *680*, 155-164.

173. M. Schweiger, S. R. Seidel, A. M. Arif and P. J. Stang, *Inorg. Chem.*, **2002**, *41*, 2556–2559.

174. M. Ferrer, M. Mounir, O. Rossell, E. Ruiz and M. A. Maestro, *Inorg. Chem.*, **2003**, *42*, 5890–5899.

175. A. Sautter, D. G. Schmid, G. Jung and F. Würthner, *J. Am. Chem. Soc.*, **2001**, *123*, 4524–5430.

176. C. A. Schalley, T. Müller, P. Linnartz, M. Witt, M. Schäfer and A. Lützen, *Chem. Eur. J.*, **2002**, *8*, 3538 – 3551.

177. T. Weilandt, R. W. Troff, H. Saxell, K. Rissanen and C. A. Schalley, *Inorg. Chem.*, **2008**, *47*, 7588-7598.

178. M. Fujita, O. Sasaki, T. Mitsuhashi, T. Fujita, J. Yazaki, K. Yamaguchi and K. Ogura, *Chem. Commun.*, **1996**, 1535-1536.

179. M. Fujita, M. Aoyagi and K. Ogura, *Inorg. Chim. Acta*, **1996**, *246*, 53-57.

180. J. Thiel, D. Yang, M. N. Rosnes, X. Liu, C. Yvon, S. E. Kelly, Y.-F. Song, D.-L. Long and L. Cronin, *Angew. Chem. Int. Ed.*, **2011**, *50*, 8871-8875.

181. M. T. Bowers, P. R. Kemper, G. v. Helden and P. A. M. v. Koppen, *Science,* **1993**, *260*, 1446-1451.

182. E. R. Brocker, S. E. Anderson, B. H. Northrop, P. J. Stang and M. T. Bowers, *J. Am. Chem. Soc.*, **2010**, *132*, 13486-13494.

183. Y.-T. Chan, X. Li, J. Yu, G. A. Carri, C. N. Moorefield, G. R. Newkome and C. Wesdemiotis, *J. Am. Chem. Soc.*, **2011**, *133*, 11967-11976.

184. J. Ujma, M. D. Cecco, O. Chepelin, H. Levene, C. Moffat, S. J. Pike, P. J. Lusby and P. E. Barran, *Chem. Commun.*, **2012**, *48*, 4423 – 4425.

185. J. D. Roberts and M. C. Caserio, *Basic Principles of Organic Chemistry*, Benjamin, Inc., Menlo Park, CA, **1977**.

186. S. Tsuzuki, K. Honda, T. Uchimaru, M. Mikami and K. Tanabe, *J. Am. Chem. Soc.*, **2001**, *124*, 104-112.

187. L. Weber, J. Kahlert, L. Bohling, A. Brockhinke, H.-G. Stammler, B. Neumann, R. A. Harder, P. J. Low and M. A. Fox, *Dalton Trans.*, **2013**, *42*, 2266-2281.

188. G. R. Hilton, A. T. Jackson, K. Thalassinos and J. H. Scrivens, *Anal. Chem.*, **2008**, *80*, 9720-9725.

189. A. Peuronen, S. Forsblom and M. Lahtinen, *Chem. Commun.*, **2014**, *50*, 5469-5472.

190. M. D. Ward, *Chem. Commun.*, **2009**, 4487-4499.

191. Q. Chen, F. Jiang, D. Yuan, L. Chen, G. Lyu and M. Hong, *Chem. Commun.*, **2013**, *49*, 719-721.

192. S. J. Cantrill, M. C. T. Fyfe, A. M. Heiss, J. F. Stoddart, A. J. P. White and D. J. Williams, *Org. Lett.*, **1999**, *2*, 61-64.

193. S. Mecozzi and J. J. Rebek, *Chem. Eur. J.*, **1998**, *4*, 1016-1022.

194. R. Custelcean, *Chem. Soc. Rev.*, **2014**, *43*, 1813-1824.

195. J. P. Sauvage, J. P. Collin, J. C. Chambron, S. Guillerez, C. Coudret, V. Balzani, F. Barigelletti, L. De Cola and L. Flamigni, *Chem. Rev.*, **1994**, *94*, 993-1019.

196. Y. Miyake, K. Nakajima, K. Sasaki, R. Saito, H. Nakanishi and Y. Nishibayashi, *Organometallics*, **2009**, *28*, 5240-5243.

197. S.-S. Sun and A. J. Lees, *Inorg. Chem.*, **2001**, *40*, 3154-3160.

198. F. Barigelletti, L. Flamigni, V. Balzani, J.-P. Collin, J.-P. Sauvage, A. Sour, E. C. Constable and A. M. W. C. Thompson, *J. Am. Chem. Soc.*, **1994**, *116*, 7692-7699.

199. E. C. Constable, C. E. Housecroft, A. C. Thompson, P. Passaniti, S. Silvi, M. Maestri and A. Credi, *Inorg. Chim. Acta*, **2007**, *360*, 1102-1110.

200. R. Siebert, A. Winter, B. Dietzek, U. S. Schubert and J. Popp, *Macromol. Rapid Commun.*, **2010**, *31*, 883-888.

201. E. C. Constable, R. W. Handel, C. E. Housecroft, A. Farràn Morales, B. Ventura, L. Flamigni and F. Barigelletti, *Chem. Eur. J.*, **2005**, *11*, 4024-4034.

202. J. Otsuki, A. Imai, K. Sato, D.-M. Li, M. Hosoda, M. Owa, T. Akasaka, I. Yoshikawa, K. Araki, T. Suenobu and S. Fukuzumi, *Chem. Eur. J.*, **2008**, *14*, 2709-2718.

203. U. S. Schubert, C. Eschbaumer, Q. An and T. Salditt, *J. Inclusion Phenom.*, **1999**, *35*, 35-43.

204. E. C. Constable, E. Figgemeier, C. E. Housecroft, J. Olsson and Y. C. Zimmermann, *Dalton Trans.*, **2004**, 1918-1927.

205. D. Philp and J. F. Stoddart, *Angew. Chem. Int. Ed.*, **1996**, *35*, 1154-1196.

206. G. M. Whitesides and B. Grzybowski, *Science*, **2002**, *295*, 2418-2421.

207. G. Oostergetel, H. van Amerongen and E. Boekema, *Photosynth. Res.*, **2010**, *104*, 245-255.

208. Y. Wang and X. Hu, *J. Chem. Phys.*, **2002**, *117*, 1-4.

209. C. Wang, Z. Wang and X. Zhang, *Acc. Chem. Res.*, **2012**, *45*, 608-618.

210. K. Liu, Y. Yao, C. Wang, Y. Liu, Z. Li and X. Zhang, *Chem. Eur. J.*, **2012**, *18*, 8622-8628.

211. Y. He, Z. Bian, C. Kang and L. Gao, *Chem. Commun.*, **2011**, *47*, 1589-1591.

212. G. R. Desiraju, *Angew. Chem. Int. Ed.*, **1995**, *34*, 2311-2327.

213. G. M. Whitesides, J. P. Mathias and C. T. Seto, *Science*, **1991**, *254*, 1312-1319.

214. T. Shimizu, M. Masuda and H. Minamikawa, *Chem. Rev.*, **2005**, *105*, 1401-1444.

215. G. R. Desiraju, *J. Mol. Struct.*, **2003**, *656*, 5-15.

216. G. Golubkov, H. Weissman, E. Shirman, S. G. Wolf, I. Pinkas and B. Rybtchinski, *Angew. Chem. Int. Ed.*, **2009**, *48*, 926-930.

217. M. Beley, J. P. Collin, R. Louis, B. Metz and J. P. Sauvage, *J. Am. Chem. Soc.*, **1991**, *113*, 8521-8522.

218. E. C. Constable, A. M. W. C. Thompson, D. A. Tocher and M. A. M. Daniels, *New J. Chem.*, **1992**, *16*, 855-867.

219. E. C. Constable, C. E. Housecroft, S. Vujovic and J. A. Zampese, *CrystEngComm*, **2014**, *16*, 3494-3497.

220. Y. Maximilian Klein, E. C. Constable, C. E. Housecroft and A. Prescimone, *CrystEngComm*, **2015**, *17*, 2070-2073.

221. C. Xue, S. Jin, X. Weng, J. J. Ge, Z. Shen, H. Shen, M. J. Graham, K.-U. Jeong, H. Huang, D. Zhang, M. Guo, F. W. Harris, S. Z. D. Cheng, C. Y. Li and L. Zhu, *Chem. Mater.*, **2004**, *16*, 1014-1025.

222. M. L. Scudder, H. A. Goodwin and I. G. Dance, *New J. Chem.*, **1999**, *23*, 695-705.

223. H.-J. Kim, T. Kim and M. Lee, *Acc. Chem. Res.*, **2011**, *44*, 72-82.

# APPENDIX

## PUBLICATIONS

1. J. M. Ludlow III, M. Tominaga, Y. Chujo, A. Schultz, X. Lu, T. Xie, K. Guo, C. N. Moorefield, C. Wesdemiotis and G. R. Newkome, *Dalton Trans.*, **2014**, *43*, 9604-9611.

2. J. M. Ludlow III, T. Xie, Z. Guo, K. Guo, M. J. Saunders, C. N. Moorefield, C. Wesdemiotis and G. R. Newkome, *Chem. Commun.*, **2015**, *51*, 3820-3823.

3. K. Guo, Z. Guo, J. M. Ludlow III, T. Xie, S. Liao, G. R. Newkome and C. Wesdemiotis, *Macromol. Rapid Commun.*, **2015**, *36*, 1539-1552.

4. J. M. Ludlow III, Z. Guo, A. Schultz, R. Sarkar, C. N. Moorefield, C. Wesdemiotis and G. R. Newkome, *Eur. J. Inorg. Chem* , **2015**, (in press).

5. J. M. Ludlow III, M. J. Saunders, M. Huang, K. Guo, Z. Guo, C. N. Moorefield, S. Z. D. Cheng, C. Wesdemiotis and G. R. Newkome, 2015. (to be submitted).